

Study on Amino Acid and Lipid Metabolism Accountable for Food Flavor

(食品香気に寄与するアミノ酸代謝および脂質代謝に関する研究)

Takuya Teshima

Graduate School of Sciences and Technology for Innovation

YAMAGUCHI UNIVERSITY

March 2023

Contents

Abstract

Chapter 1

Suppressed Methionine γ -Lyase Expression Causes Hyperaccumulation of
S-Methylmethionine in Soybean Seeds

- 1.1 Introduction
- 1.2 Results
- 1.3 Discussion
- 1.4 Materials and Methods
- 1.5 References
- 1.6 Acknowledgment

Chapter 2

Coprinopsis cinerea Dioxygenase is an Oxygenase Forming
10(*S*)-Hydroperoxide of Linoleic Acid, Essential for Mushroom Alcohol,
1-Octen-3-ol, Synthesis

- 2.1 Introduction
- 2.2 Results
- 2.3 Discussion
- 2.4 Materials and Methods
- 2.5 References
- 2.6 Acknowledgment

Abstract

Not only taste but also flavor has a significant impact on the "deliciousness" of food as perceived by people. Flavor characteristics of food have a significant impact on its palatability and influence the qualitative value of the food itself. In this study, the molecular mechanisms of biosynthesis of flavor compounds derived from amino acids in soybean (*Glycine max*) and fatty acids in mushrooms were elucidated.

In Chapter 1, I identified the characteristic aromatic properties of soybean due to sulfur-containing amino acids. Several soybean germplasms, such as Nishiyamahitashi 98-5 (NH) among local varieties in Nagano Prefecture, have an intense seaweed-like flavor after cooking because of their high seed *S*-methylmethionine (SMM) content. In this study, I compared the amounts of amino acids in the phloem sap, leaves, pods, and seeds between NH and the common soybean cultivar Fukuyutaka. This revealed a comparably higher SMM content alongside a higher free L-methionine (L-Met) content in NH seeds, suggesting that the SMM-hyperaccumulation phenotype of NH soybean was related to L-Met metabolism in seeds. To investigate the molecular mechanism behind SMM hyperaccumulation, I examined the phenotype-associated gene locus in NH plants. Analyses of the quantitative trait loci in segregated offspring of the cross between NH and the common soybean cultivar Williams 82 indicated that one locus on chromosome 10 explains 71.4% of SMM hyperaccumulation. Subsequent fine-mapping revealed that a transposon of about 6 kbp insertion into the intron of a gene, *Glyma.10g172700*, is associated with the SMM-hyperaccumulation phenotype. The *Glyma.10g172700*-encoded recombinant protein showed Met- γ -lyase (MGL) activity in vitro, and the transposon-insertion mutation in NH efficiently suppressed *Glyma.10g172700* expression in developing seeds. Exogenous administration of L-Met to sections of developing soybean seeds resulted in transient increases in L-Met levels, followed by continuous increases in SMM concentrations, which was likely caused by L-Met methyltransferase activity in the seeds. Accordingly, I propose that the SMM-hyperaccumulation phenotype is caused by suppressed MGL expression in developing soybean seeds, resulting in transient accumulation of L-Met, which is converted into SMM to avoid the harmful effects caused by excess free L-Met.

In Chapter 2, I studied the biosynthesis mechanism of 1-octen-3-ol, the main volatile component of mushrooms. 1-Octen-3-ol is a volatile oxylipin found ubiquitously in Basidiomycota and Ascomycota. As 1-octen-3-ol attracts mosquitoes and flies, its involvement in emitter–receiver ecological communication has been proposed. Although

the biosynthetic pathway to form 1-octen-3-ol from linoleic acid through linoleic acid 10(*S*)-hydroperoxide has been proposed in mushrooms, the enzymes involved in this pathway have not been identified. I determined that the *Coprinopsis cinerea* dioxygenase 1 and 2 (CcDOX1 and CcDOX2) genes in the mushroom *C. cinerea* contains an N-terminal cyclooxygenase-like heme peroxidase domain and a C-terminal cytochrome P450-related domain. Through analysis of products formed from linoleic acid by the recombinant CcDOX1 and CcDOX2 proteins, I found that CcDOX1 preferentially catalyzes to form the 10(*S*)-hydroperoxide of linoleic acid (10*S*-HPODE), meanwhile CcDOX2 form the 8-hydroperoxide of linoleic acid. Moreover, disruption of *Ccdox1* in *C. cinerea* ($\Delta Ccdox1$) mycelia suppressed 1-octen-3-ol synthesis. Administration of the 10*S*-HPODE to the microsomes fraction prepared from mycelia resulted in the efficient production of 1-octen-3-ol. Together, these results indicate that CcDOX1 is essential for the biosynthesis of 1-octen-3-ol as the oxygenase that forms 10*S*-HPODE, followed by the cleavage enzyme.

I studied physiological and ecological significance of 1-octen-3-ol of mushroom. $\Delta Ccdox1$ was less attractive to fruit fly larvae, while the feeding behavior of fungus gnats on $\Delta Ccdox1$ mycelia showed little difference from that on the mycelia of the wild-type strain. The proliferation of fungivorous nematodes on $\Delta Ccdox1$ mycelia was similar to or slightly worse than that on wild-type mycelia. Thus, 1-octen-3-ol seems to be an attractive compound for some animals that interact with mushrooms.

CHAPTER 1

**Suppressed Methionine γ -Lyase Expression
Causes Hyperaccumulation of
S-Methylmethionine in Soybean Seeds**

1.1 Introduction

Importance of L-Methionine in Soybean

Soybeans (*Glycine max*) have been cultivated in East Asia for 3,000 to 5,000 years and have long been consumed in Japan as a basic ingredient in traditional Japanese foods such as tofu, soy sauce, and miso. In the 2017/2018 market year, 346.2 million tons of soybean were produced (Food and Agriculture Organization Corporate Statistical Database [FAOSTAT]; <http://www.fao.org/faostat/en/#home>). This large amount of soybean production was driven by the high oil and protein contents of the plant. Soybean meal is widely used as animal feed and has high protein contents and a well-balanced amino acid profile. However, its nutritional value for monogastric animals could be improved by increasing its L-cysteine (L-Cys) and L-Met contents. Accordingly, the regulatory mechanisms relating to L-Met and L-Cys biosynthesis in soybean have been investigated extensively [1-4]. However, methionine biosynthesis is strictly regulated because L-Met is essential not only as a protein constituent but also for C1 metabolism through *S*-adenosylmethionine (SAM), and is also involved in the metabolism of sulfur containing compounds such as glutathione that regulate the redox state of cells. Therefore, it is impossible to increase L-Met production in plants simply by increasing L-Met biosynthetic enzyme activity, and it is necessary to clarify the detailed regulatory mechanisms of each step in the L-Met metabolic pathway.

L-Met metabolism in plants

L-Met is a biosynthetic member of the aspartic acid family (Asp family; Fig. 1) [2, 4]. Cystathionine γ -synthase (CGS) performs the crucial regulatory step in L-Met biosynthesis and determines the rate of L-Met production from *O*-phosphohomoserine [2]. Free L-Met is used to form proteins, but a portion of L-Met is converted to SAM by a SAM synthetase. Another portion of free L-Met accepts a methyl group from SAM through methionine *S*-methyltransferase (MMT) and is converted into SMM. Homocysteine methyltransferase (HMT) converts SMM back to L-Met. MMT and HMT constitute the SMM cycle, which seems to operate throughout plant tissues, including reproductive tissues of various plant species [5]. In several flowering plants, SMM is produced in the leaves by MMT and is transported through the phloem toward the reproductive organs, where it is reconverted to L-Met by HMT [6, 7]. With developing

seeds of *Medicago truncatula*, SMM is converted back to L-Met via HMT in seed coats, and L-Met released into the seed apoplast is taken up by seeds [8]. Both the in situ formation of L-Met through Asp family enzymes and the biosynthesis of SMM in the leaves following phloem transport likely regulate L-Met contents simultaneously in the seeds [4,7]. L-Met catabolism also controls L-Met levels in plant tissues. Met γ -lyase (MGL) is a pyridoxal phosphate (PLP)-dependent enzyme that metabolizes L-Met into 2-ketobutyric acid (2KB), methanethiol, and ammonia [9]. 2KB can be metabolized to form L-isoleucine (L-Ile) even though this pathway is auxiliary to the major L-Ile biosynthetic pathway through L-threonine (L-Thr) deaminase [10].

Seeds also have a high requirement for L-Met because they accumulate large amounts of seed storage proteins. Many sulfur sources absorbed from the roots as sulfate ions are reductively assimilated in the leaves to form L-Cys, which is further converted to methionine in the plastids. During the vegetative stage, these sulfur-containing amino acids and their metabolites are translocated to the seed through sieve tubes [6]. L-Met accumulated in young *Arabidopsis* (*Arabidopsis thaliana*) rosette leaves decreases with the onset of reproductive growth, accompanied by an increase in methionine in seeds [11-13]. SMM is thought to contribute to this transport from trophic to reproductive tissues; SMM is synthesized by MMT from methionine and *S*-adenosylmethionine (SAM). HMT transfers the methyl group of SMM to homocysteine, producing two molecules of methionine. The simultaneous presence of these two enzymes results in a small metabolic circuit (called the SMM cycle) that only moves methionine and SMM back and forth (Fig. 2). This cycle is thought to be a system that delivers the right amount of leaf methionine to the seed at the right time, a transport system that can be actively regulated using ATP molecules [14]. Suppression of CGS expression in *Arabidopsis* seeds enhances SMM synthesis in leaves, resulting in more SMM being transported through sieve tubes [15]. This suggests that the degree of seed methionine requirement is transmitted to the leaves and that long-distance transport through the SMM cycle is highly regulated through remote signaling.

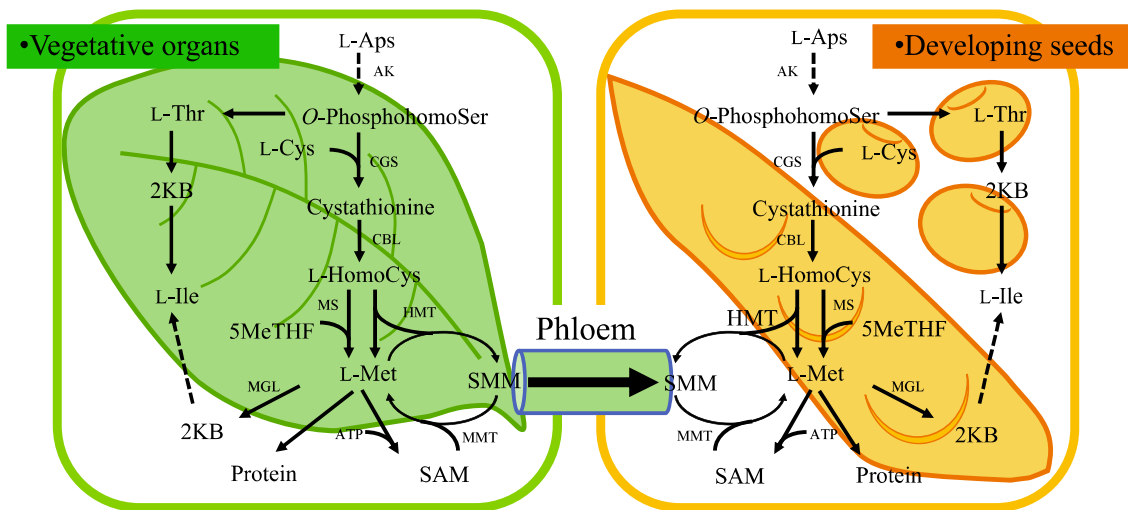


Fig 1. Schematic representation of L-Met metabolism in plants. The pathways mentioned in this study are highlighted. Solid arrows represent one metabolic step, while dashed arrows represent several metabolic steps. The enzyme names are underlined. The canonical Asp family pathway is shown with gray background. The *S*-methylmethionine cycle is shown with striped background. Asp, aspartic acid; CGS, cystathionine γ -synthase; Cys, cysteine; HMT, homocysteine methyltransferase; L-HomoCys, L-homocysteine; L-Ile, L-isoleucine; 2KB, 2-ketobutyric acid; L-Met, L-methionine; MGL, methionine γ -lyase; MMT, methionine methyltransferase; MS, methionine synthase; 5MeTHF, 5-methyltetrahydrofolate; *O*-PhosphohomoSer, *O*-phosphohomoserine; SAM, *S*-adenosylmethionine; SMM, *S*-methylmethionine; L-Thr, L-threonine.

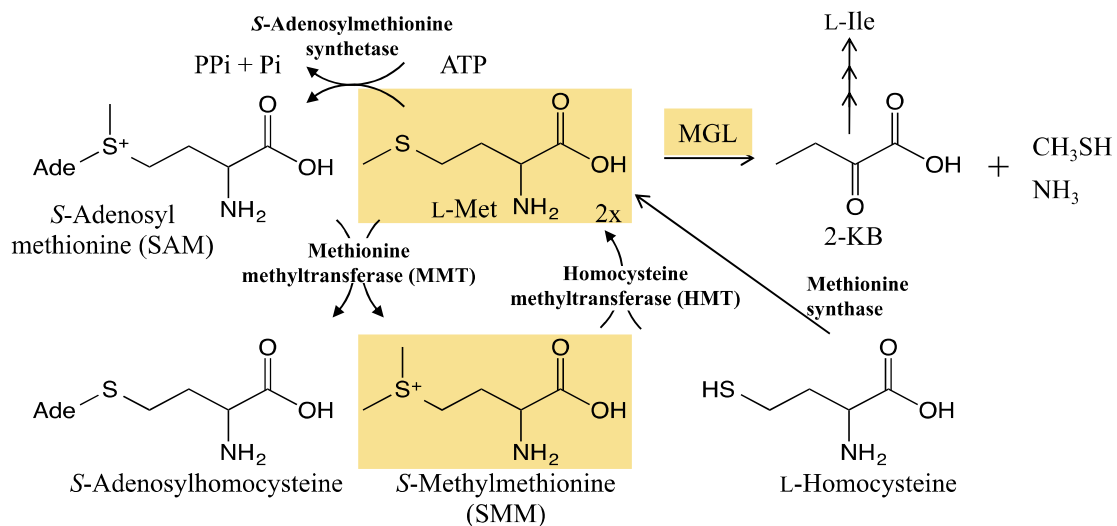


Fig 2. The SMM cycle in plants. The pathways mentioned in this study are highlighted, and L-Met, SMM, and MGL are shown with orange background.

Generation of L-Met Hyperaccumulator Plants

Based on accumulating studies of L-Met regulation in plant tissues, numerous attempts to improve L-Met levels in crops have been made through genetic engineering particularly of the Asp family pathway [4, 14, 16-19]. Acceleration of SMM transport from nonseed tissues to seeds was also attempted to increase L-Met levels in seeds [7, 20]. As such, attempts to increase seed L-Met levels are becoming more successful but are sometimes disturbed by abnormal phenotypes of the plants [4, 21]. Severe growth retardation was observed in potato (*Solanum tuberosum*) plants overexpressing the feedback-insensitive CGS to form more L-Met and β -zein to store L-Met [22]. Tobacco (*Nicotiana tabacum*) plants overexpressing CGS and with elevated free L-Met levels also had increased sensitivity to oxidative stress [23]. In addition, Arabidopsis (*Arabidopsis thaliana*) seeds overexpressing a mutant CGS accumulated L-Met to 2.5-fold higher levels, and these conditions were associated with increased expression of stress-related transcripts [18, 24]. These studies suggest that L-Met levels are tightly controlled in plant tissues and that excessive free L-Met is deleterious to plant health. Yet, the mechanisms by which L-Met levels are regulated in some tissues remain poorly understood.

Aim of This Work

In the central region of Japan, specific soybean seeds have been cultivated for their seaweed odor, which is strongly related to dimethyl sulfide. Dimethyl sulfide is formed spontaneously from SMM during heating of the seeds for cooking (Fig. 3) [25]. In a representative cultivar, Nishiyamahitashi 98-5 (NH), the SMM level in the seeds is more than 100-fold higher than in common soybean cultivars, such as Fukuyutaka (FY) [25]. Because SMM is a direct product of L-Met metabolism by methionine methyltransferase (MMT), it is assumed that the cultivars with higher SMM content are likely to metabolize L-Met and its derivatives via mechanisms that are distinctive from that in ordinary soybean cultivars.

The soybean SMM-hyperaccumulation phenotype, like that of NH, was assumed to be attributable to a genotype related to L-Met metabolism in seeds. We investigated the genotype of SMM-hyperaccumulating soybean plants and identified the gene that is responsible for SMM accumulation in soybean. Through analyses of gene function and NH phenotypes, we propose a mechanism underlying SMM hyperaccumulation.

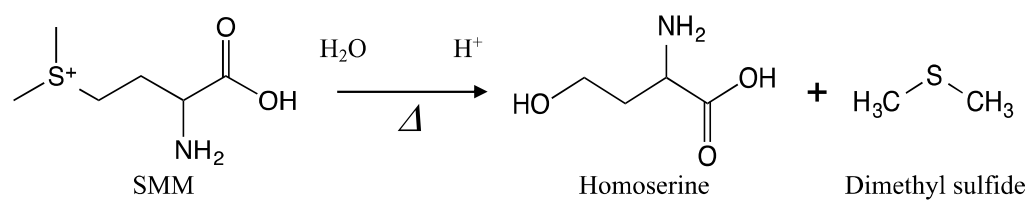


Fig 3. The formation of dimethyl sulfide from thermal degradation of SMM.

1.2 Results

SMM and Free L-Met Levels

The quantities of SMM and free L-Met were determined in the leaves, pods, and seeds of two soybean cultivars, FY and NH, at the flowering stage, immature green seed stage, mature green seed stage, and in dry seeds (Fig. 4). The seed coats were removed from the other parts of seeds (i.e., cotyledons, plumules, and radicles) before analyses to avoid mixing tissues of maternal genotype (i.e., seed coats) and those of offspring genotypes (cotyledons, plumules, and radicles). The contents of SMM and free L-Met were low in the leaves, and no significant differences were identified between FY and NH. The SMM level in the pods seemed to be a little higher than that found in the leaves, but a statistically significant difference in its level between FY and NH was hardly detected. The free L-Met level in the NH pods at the immature green stage was significantly lower than that of FY, but the level in the FY pods lowered at the mature green stage to the level found in the NH pods. The levels of SMM in the NH seeds were eightfold and 15.6-fold higher at the immature and mature green stage, respectively, than those found in the FY seeds. A substantial amount of SMM was detected in dry NH seeds, whereas it was under the detection limit in the dry FY seeds. The levels of free L-Met in the NH seeds were significantly higher at the mature green stage and in dry seeds than those found in the FY seeds.

The SMM level in the phloem exudate collected through a cut petiole of NH at the seed-developing stage was significantly higher than that found for FY, whereas the level of free L-Met was lower than that found for FY (Table 1). The levels of SMM and free L-Met in phloem exudate collected using the same procedure through *Arabidopsis* petioles at the seed-filling stage were more than 93-fold higher than those found for NH and FY.

The free amino acid contents of mature seeds were mostly similar between FY and NH, yet the L-histidine (L-His), L-phenylalanine (L-Phe), L-Met, L-Thr, and homoserine contents were significantly higher in NH than in FY seeds (Fig. 5). Homocysteine was under the detection level (4.2 mg g^{-1}) in both NH and FY. The total protein contents, protein profiles examined using Coomassie Brilliant Blue staining after SDS-PAGE (Fig. 6), and total amino acid contents showed no significant differences between the FY and NH seeds (Table 2).

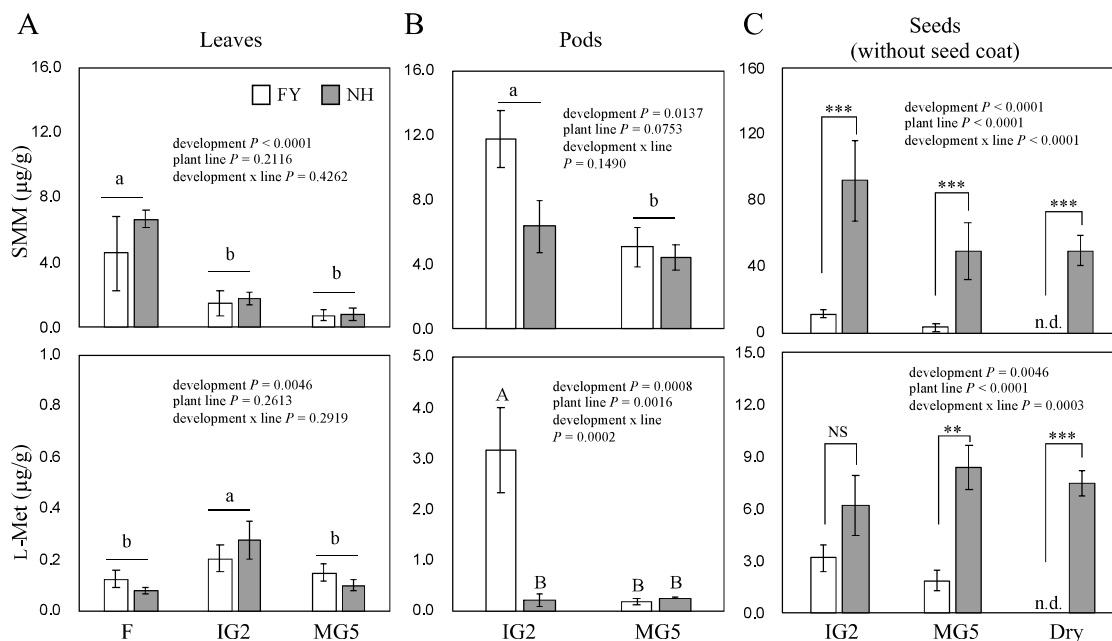


Fig 4. S-Methylmethionine (SMM) (upper panels) and L-methionine (L-Met) (lower panels) contents in the leaves (A), pods (B), and seeds (without seed coats) (C) harvested at the flowering stage (F), the immature green seed stage (IG; corresponding to stage two in Fig. 16), and the mature green seed stage (MG; corresponding to stage five in Fig. 16). Data are shown as means \pm standard errors (SE) of four replicates. Significant differences were identified using a two-way analysis of variance (ANOVA) after Box-Cox transformation and Fisher's least significant difference test (LSD; $P < 0.05$). Different lowercase letters indicate significant differences between the developing stages ($P < 0.05$, Tukey's HSD test after two-way ANOVA). Different capital letters indicate significant differences between all treatments ($P < 0.05$, Tukey's HSD test after two-way ANOVA). ***: $P < 0.001$, **: $0.001 < P < 0.01$, NS: $0.05 < P$ (simple main effect test after two-way ANOVA).

Table 1. Level of SMM and L-Met in soybean and Arabidopsis phloem exudates.

		SMM (nmol g ⁻¹ leaf DW)	L-Met (nmol g ⁻¹ leaf DW)
Soybean	NH	3.40 ± 1.06 *	0.063 ± 0.032 †
	FY	0.63 ± 0.23	0.203 ± 0.033
Arabidopsis (Ws-0)		990 ± 150	18.8 ± 5.2

*: *t*-test after Box-Cox transformation (between soybean NH and FY) $P = 0.0163$

†: *t*-test after Box-Cox transformation (between soybean NH and FY) $P = 0.0292$

To all the values of L-Met was added before Box-Cox transformation to avoid the values of 0.

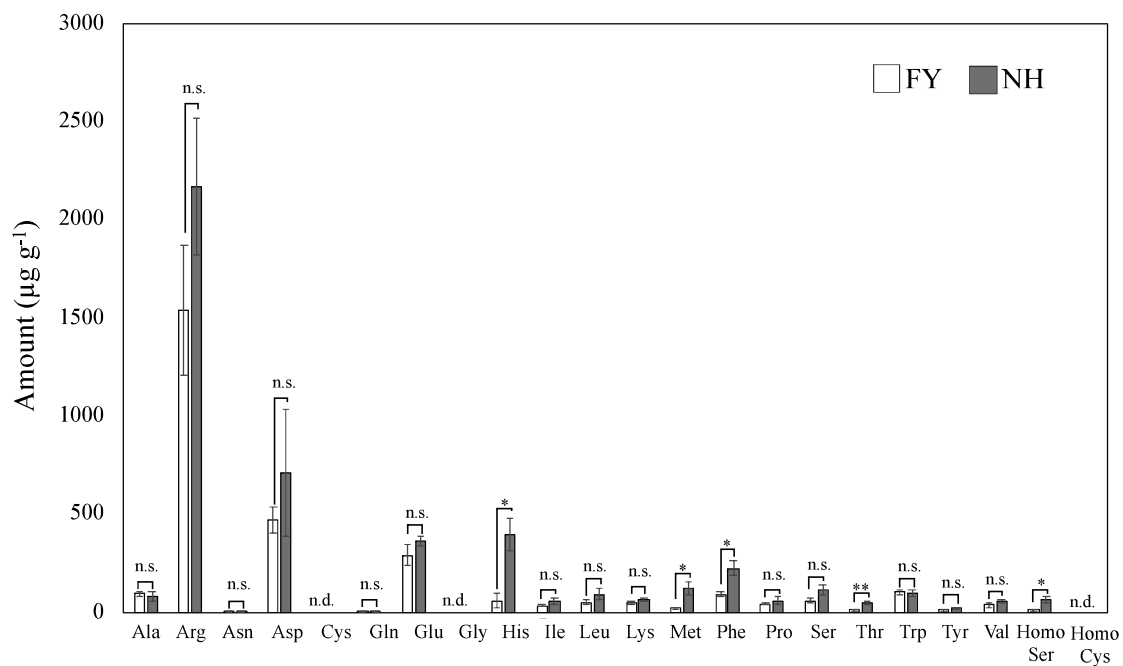


Fig 5. Quantities of free amino acids in high-performance liquid chromatography-tandem mass spectrometry (HPLC-MS/MS) analyses of dry matured seeds of Fukuyutaka (FY; white bar) and Nishiyamahitashi 98-5 (NH; gray bar) varieties. The amounts are shown as µg per g of mature dry seeds. The data are shown as means ± SE of three replicates. Significant differences were identified using Student's *t*-test after Box-Cox transformation (**: $P < 0.01$, *: $0.01 < P < 0.05$, n.s.: $0.05 < P$). HomoSer: homoserine, HomoCys: homocysteine, n.d.: not detected.

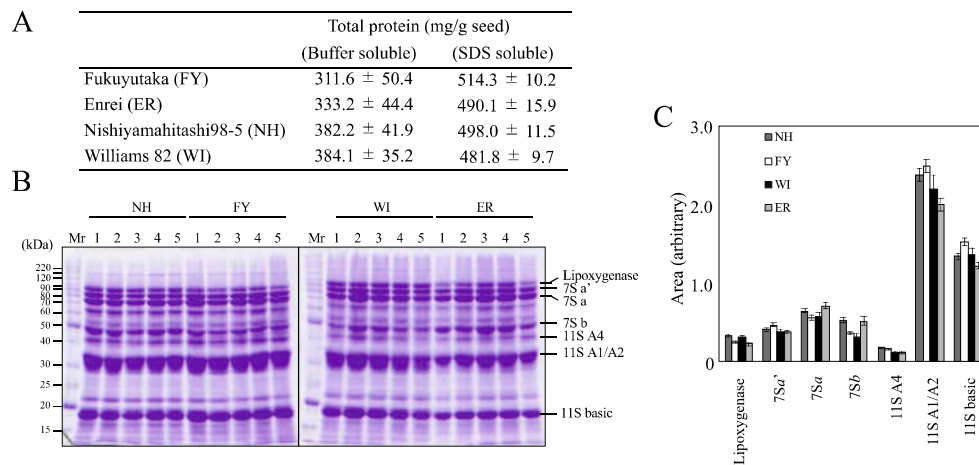


Fig 6. Protein contents and profile of soybean varieties used in this study. **A.** Contents of buffer- and SDS-soluble proteins extracted from dry matured seeds of FY, NH, WI, and Enrei (ER) varieties. Data shown are means \pm SE of three replicates. **B.** SDS-PAGE analyses of SDS-soluble protein extracted from soybean seeds. For each variety, five independent seeds were used. Proteins were tentatively assigned using previous reports. **C.** Intensity of each protein band. The protein bands shown in panel B were quantified using Image J. Data are means \pm SE of five replicates.

Table 2. Total amino acid content in NH and FY dry seeds.

L-Cys was measured as cysteic acid and L-Met as L-Met sulfone. Data are presented as mean \pm SE of 5 replicates. Significant differences were determined by Student's *t*-test ($P < 0.05$).

Amino acid ($\mu\text{mol/g seed}$)	FY	NH
Gly	167.7 \pm 4.68	146.9 \pm 42.12
Ala	140.5 \pm 3.58	122.1 \pm 29.23
Val	126.1 \pm 2.19	111.1 \pm 19.81
Leu	60.9 \pm 1.25	52.4 \pm 11.77
Ile	75.5 \pm 1.45	63.8 \pm 13.73
Pro	121.1 \pm 2.16	103.6 \pm 16.12
Ser	112.6 \pm 2.78	93.1 \pm 22.83
Thr	89.4 \pm 2.47	75.4 \pm 20.64
Cys	65.1 \pm 3.11	61.8 \pm 3.46
Met	47.5 \pm 1.31	47.2 \pm 0.67
Asp	319.6 \pm 10.59	284.7 \pm 91.25
Glu	351.9 \pm 7.67	277.3 \pm 58.34
Arg	145.8 \pm 3.59	126.8 \pm 28.81
Lys	110.1 \pm 2.78	93.1 \pm 22.83
His	41.1 \pm 1.17	35.4 \pm 9.82
Phe	63.1 \pm 1.40	53.6 \pm 11.46
Tyr	47.3 \pm 1.10	39.6 \pm 9.60

Positional Cloning of the Gene Responsible for Hyperaccumulation of SMM

The contents of SMM and free L-Met were determined with four F1 seeds after reciprocal crossing of the FY and NH cultivars. The hyperaccumulation of SMM was only evident in self-pollinated NH seeds, and the maternal and paternal genotypes did not play a significant role in the accumulation of SMM in seeds (Fig. 7). Moreover, F2 seeds of the FY × NH cross were segregated into high SMM: low SMM at a ratio of 3:17 with a consistent segregation ratio of 1:3 (χ^2 test, $P = 0.3$; Fig. 8A). These data indicate that hyperaccumulation of SMM is essentially regulated by a single recessive allele. In order to identify the gene responsible for hyperaccumulation of SMM, we cross-bred NH to the Williams 82 (WI) cultivar. WI was used because the SMM contents in WI seeds were as low as those in FY seeds (see below) and because the reference genome sequence was produced with WI [26]. A total of 156 F5 recombinant inbred lines (RILs) were generated from the cross between NH and WI, and SMM levels in their mature seeds were determined (Fig. 8B). Quantitative trait locus (QTL) analyses with molecular markers indicated that an allele near a simple sequence repeat marker (Satt477) on chromosome 10 explained 71.4% of the phenotypic variation (Fig. 9A). No other QTL with a significant influence on the hyperaccumulation of SMM was detected. Finemapping of the allele responsible for the hyperaccumulation of SMM in F6 and F7 residual heterozygous lines narrowed down this region to a 12 kb sequence on chromosome 10 (Fig. 9B). Furthermore, examination of the Phytozome soybean genome sequence database (<https://phytozome.jgi.doe.gov/pz/portal.html>) revealed only one open reading frame (ORF) of *Glyma.10g172700* in this region. *Glyma.10g172700* comprises two exons flanking a single intron. Finally, sequence analyses of *Glyma.10g172700* in NH (GenBank accession no. MK887190) indicated that a *copia*-type retrotransposon (AB370254) [27] was inserted into the intron.

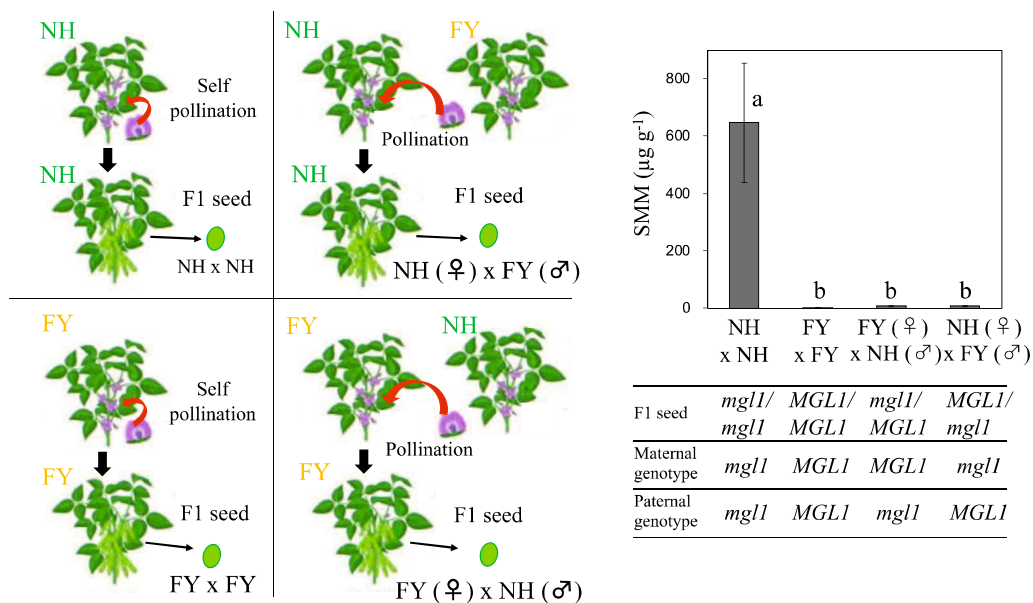


Fig 7. Inheritance of hyperaccumulation of SMM ; Concentrations of SMM in F₁ progenies that were generated by reciprocal crossing of Fukuyutaka (FY) (*MGL1*) and Nishiyamahitashi 98-5 (NH) (*mgll*) soybean strains; data are shown as means \pm SE of three replicates. Significant differences between plant lines in SMM were identified using Tukey's HSD tests after Box-Cox transformation ($P < 0.05$).

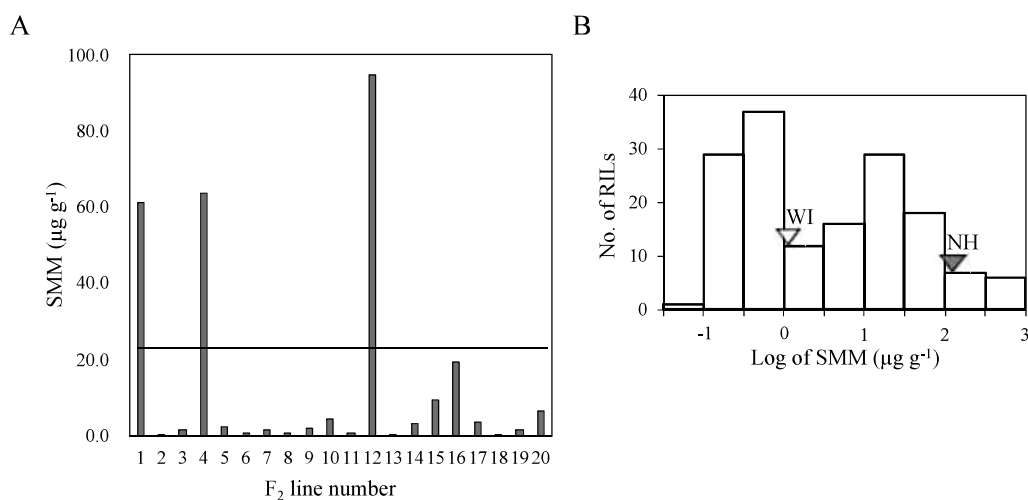


Fig 8. (A) *S*-Methylmethionine (SMM) contents in soybean seeds in self-pollinated F₂ progeny of F₁ individuals from the cross of Fukuyutaka (FY) and Nishiyamahitashi 98-5 (NH) varieties. The horizontal line indicates the boundary between high and low SMM (at 25 $\mu\text{g g}^{-1}$). (B) Distribution of the SMM-hyperaccumulation phenotype among 156 F₅ recombinant inbred lines (RILs) from the NH and Williams 82 (WI) strains. SMM concentrations in WI and NH are indicated by triangles.

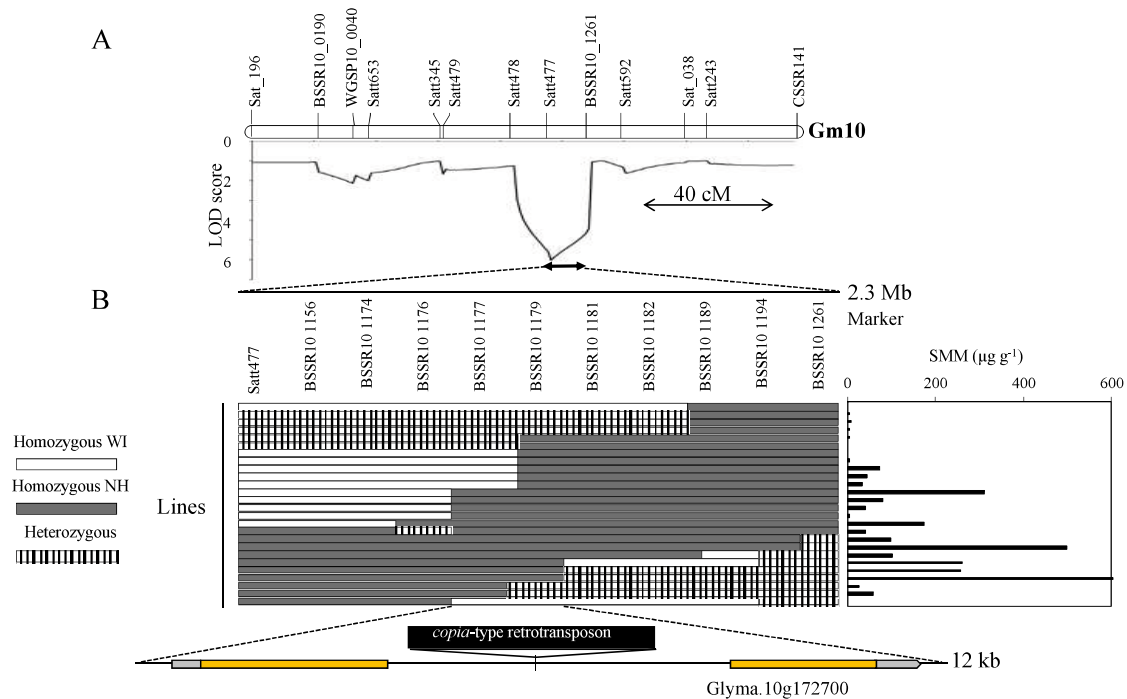


Fig 9. Map-based cloning of the allele responsible for the hyperaccumulation of SMM in soybean. (A) QTL-regions detected in chromosome 10 of soybean. (B) Graphical genotypes of 26 F₆ and F₇ residual heterozygous lines determined with markers are shown (WI: Williams 82, NH: Nishiyamahitashi 98-5). The amounts of SMM in the respective lines are shown in the bar graph on the right. After delimiting the region, only one open reading frame (*Glyma.10g172700*) was identified. *Glyma.10g172700* was tentatively assigned as the gene encoding Met γ -lyase and comprises two exons flanking one intron. The DNA sequencing of genes from NH and WI strains showed a *copia*-type retrotransposon inserted into the intron of the gene in the NH strain only.

Hyperaccumulation of SMM Correlates Well with Transposon Insertion in the *Glyma.10g172700* Gene

We collected local soybean cultivars in Nagano Prefecture, Japan. These were previously shown to have differing SMM levels [25]. I extracted genomic DNA and then amplified the *Glyma.10g172700* gene using primers for 5' and 3' termini of its deduced ORF. In normal soybean cultivars, such as FY and WI, the resulting DNA fragment was 2,885 bp, as expected from genome sequences in the Phytozome database. The *Glyma.10g172700* gene length was the same in five of the 10 local cultivars as that detected in normal cultivars, but it was longer in the other five cultivars and was similar in length to that amplified from NH (approximately 9 kb; Fig. 10A). Therefore, it was expected that these latter five soybean cultivars carry an inserted transposon in the *Glyma.10g172700* gene of the same size as the inserted transposon in NH. Determinations of SMM levels in seeds of these cultivars showed higher SMM levels in cultivars harboring the *Glyma.10g172700* gene with the transposon insertion than in those without the transposon insertion (Fig. 10B). Free L-Met levels were higher in some seeds having the transposon insertion in *Glyma.10g172700* than in those without the insertion, but the correlation was not always evident. Reverse transcription quantitative PCR (RT-qPCR) analyses of RNA extracted from maturing seeds showed that the lower levels of transcript derived from *Glyma.10g172700* were detected with cultivars that had the transposon insertion in *Glyma.10g172700* (Fig. 10C). The product sizes obtained with RT-PCR with NH and FY seeds with excess amplification cycles using primers for the 5' and 3' termini of *GmMGL1* ORF were the same (Fig. 11), and no sign of alternative splicing was detected.

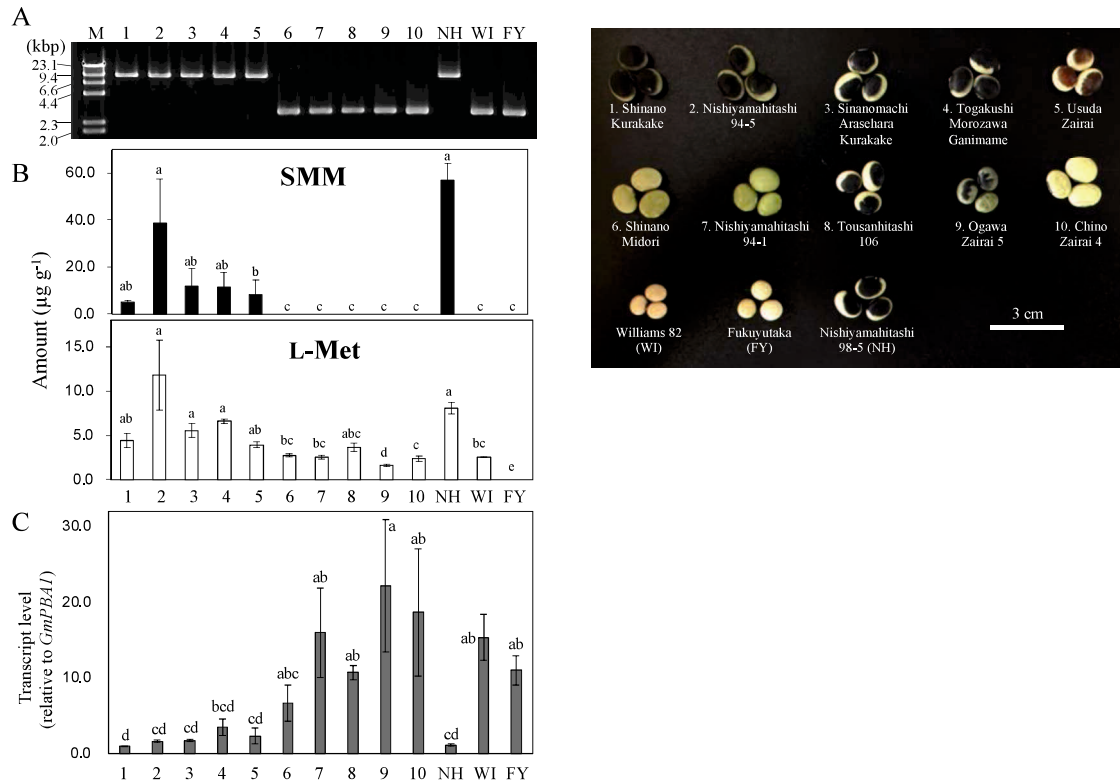


Fig. 10. Hyperaccumulation of *S*-methylmethionine (SMM) correlates with the insertion of a transposon into the *GmMGL1* gene. (A) Sizes of DNA fragments that were amplified with primers for the full-length coding sequence of *Glyma.10g172700*; M: molecular weight marker (*I/Hind* III digests), 1: Shinano-Kurakake, 2: Nishiyamahitashi 94-5, 3: Sinanomachi Arasehara Kurakake, 4: Togakushi Morozawa Ganimame, 5: Usuda Zairai, 6: Shinano Midori, 7: Nishiyamahitashi 94-1, 8: Tousanhitashi 106, 9: Ogawa Zairai 5, 10: Chino Zairai 4. NH: Nishiyamahitashi 98-5, WI: Williams 82, FY: Fukuyutaka. (B) Quantities of SMM (upper panel: black bars) and Met (lower panel: white bars) in dry matured seeds of each soybean line. Data are shown as means \pm SE of three replicates. (C) Expression levels of *Glyma.10g172700* in seeds at the green mature stage (stage five in Fig. 10). The *Glycine max* 20S proteasome subunit (*Glyma.06g078500*) was used as an internal control in RT-PCR analyses. Transcript levels relative to the internal control are shown as multiples of the lowest value of 1. Data are presented as means \pm SE ($n = 3$). Significant differences were identified using Tukey's HSD tests after Box-Cox transformation ($P < 0.05$).

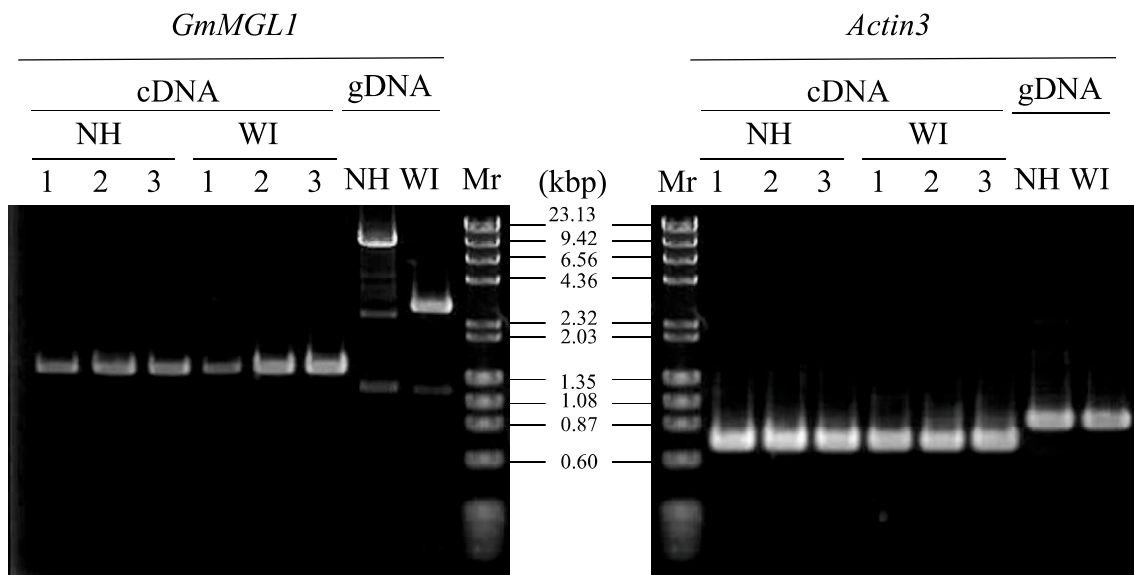


Fig 11. Polymerase chain reactions (PCRs) with cDNA that was prepared from developing Nishiyamahitashi 98-5 (NH) and Williams 82 (WI) seeds and with genomic DNA (gDNA) that was isolated from the two varieties; expression levels of the *actin3* gene are also shown. Mr: molecular weight marker (*lambda* DNA *Hind*III digest + phi X174 DNA *Hae*III digest).

***Glyma.10g172700* Encodes a Functional Met γ -Lyase**

The ORF of *Glyma.10g172700* encodes a protein of 48,069 Da, yet the deduced protein sequence had no predictable targeting signal in TargetP analyses (<http://www.cbs.dtu.dk/services/TargetP/>), suggesting a cytosolic location of the protein. The *Glyma.10g172700* gene was tentatively assigned as a gene encoding an MGL, and the deduced protein sequence had 77.2% and 78.6% identities with Arabidopsis MGL (Q9SGU9, AEE34271.1) and melon (*Cucumis melo*) MGL (M1NFB7, NP_001315378.1), respectively (Fig. 12) [28, 29]. Moreover, the protein sequence has a motif (Ser-237-Xaa-Xaa-Lys-240) that is conserved in PLP enzymes of the γ subfamily and associates with the cofactor PLP (Fig. 12) [30, 31]. Tyr-142, Asp-216, and Arg-410 residues are also involved in substrate binding and catalysis at appropriate positions [32], and Gly-144 is conserved as in Arabidopsis and melon MGLs that retain restricted substrate specificity for L-Met (Fig. 12) [29].

Glyma.10g172700 cDNA was cloned using RNA that was extracted from developing WI seeds. I expressed the recombinant protein as an N-terminal His-tagged protein and purified it using Ni²⁺-affinity chromatography (Fig. 13A). Subsequently, L-Met reacted with the recombinant protein in the presence of PLP, and the products were converted into their 3-methyl-2-benzothiazolinone hydrazone derivatives. This derivatization resulted in increased absorption at 320 nm (Fig. 13B), suggesting the formation of an aliphatic carbonyl compound [33, 34]. To confirm its structure, the reaction product that was extracted using ethyl acetate was reacted with N,O-bis(trimethylsilyl)trifluoroacetamide and was then analyzed using gas chromatography-mass spectrometry (GC-MS). A peak at the retention time of 9.5 min was assigned as trimethylsilylated 2KB by comparing its MS profile and retention time with that prepared from a standard compound (Fig. 13, C and D). Accordingly, we concluded that *Glyma.10g172700* encodes MGL that catalyzes γ -elimination of L-Met. We denoted the gene *GmMGL1*. This reaction had optimal activity at pH 7 and followed Michaelis-Menten kinetics, with *K_m* and *V_{max}* values of 7.72 mM and 0.55 mmol mg⁻¹ min⁻¹, respectively (Fig. 14).

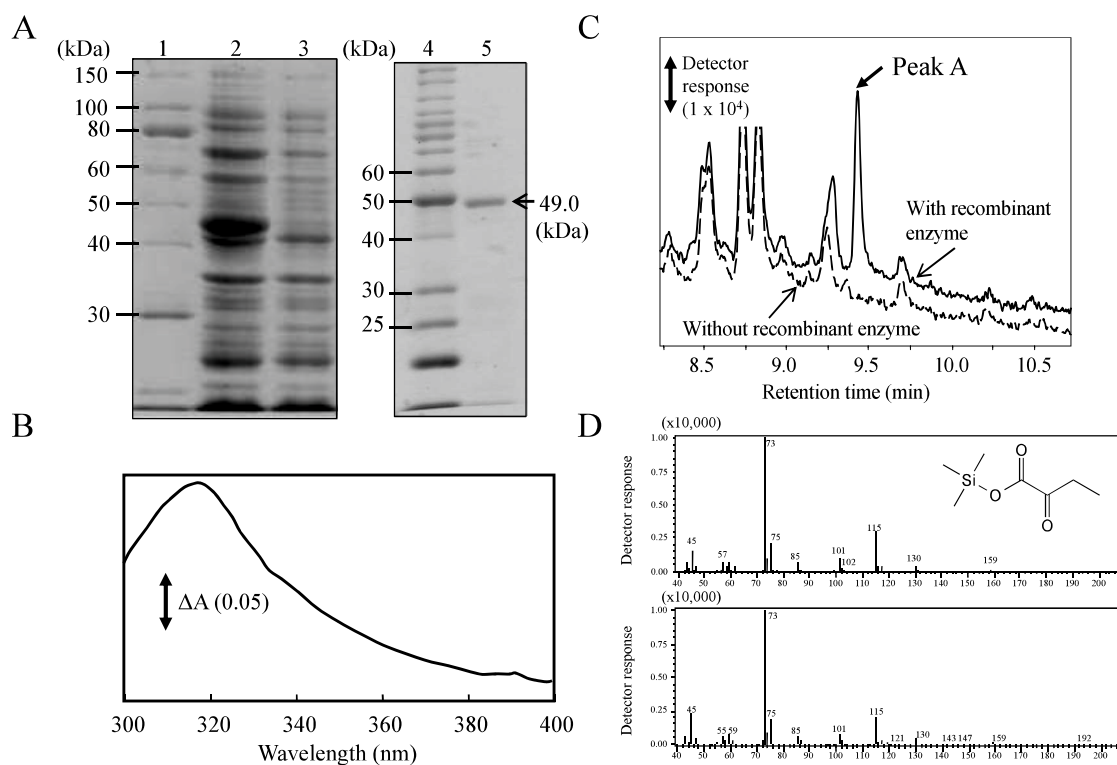


Fig 13. *Glyma.10g172700* encodes a functional MGL

A, sodium dodecyl sulfate-polyacrylamide gel electrophoresis (SDS-PAGE) analysis of the recombinant soybean MGL1 protein with an N-terminal His-tag; lanes 1 and 4, molecular weight marker; lane 2, *E. coli* lysate expressing recombinant GmMGL1 protein; lane 3, *E. coli* lysate with the empty vector (a negative control); lane 5, purified recombinant GmMGL1. B, absorption spectra of 3-methyl-2-benzothiazolinone hydrazone derivatives of the product formed during metabolism of L-Met by recombinant GmMGL1; C, chromatograms of trimethylsilylated products of recombinant GmMGL1 and L-Met from retention times of 8.25–10.75 min; the solid line represents chromatograms from experiments with the recombinant enzyme, and the broken line shows those without enzyme (negative control). The peak specifically found with the product formed with recombinant enzyme is shown with arrow (peak A); D, mass spectra obtained with authentic trimethylsilylated 2KB (upper panel) and with peak A (lower panel).

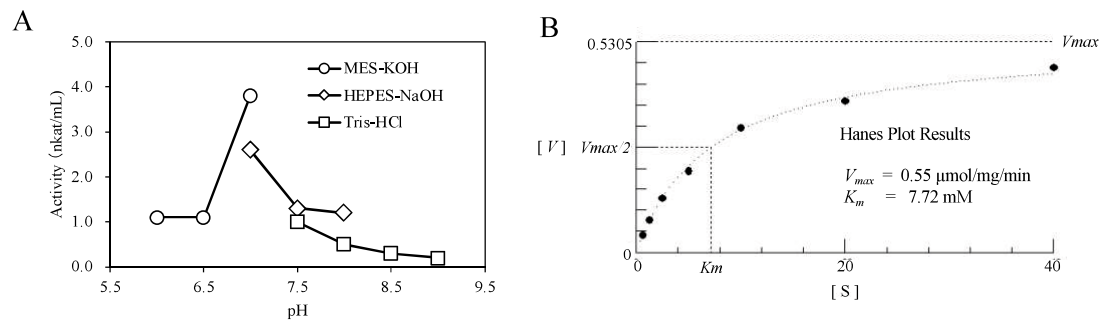


Fig. 14. The pH-activity profiles (A) and [S] vs. [V] plots (B) of recombinant GmMGL1 with L-Met as the substrate.

Comparison of L-Met Metabolism Genes in FY and NH

BLAST searches for *GmMGL1* indicated that the soybean genome encodes the MGL-like genes *Glyma.02g087900* and *Glyma.13g001200* (hereafter referred to as *GmMGL2* and *GmMGL3*, respectively). These genes encode proteins with the amino acid signatures that are conserved among the MGLs described above (Fig. 12). Among the three *GmMGLs*, *GmMGL2* and *GmMGL3* showed higher sequence similarity than the other combinations. The phylogenetic analyses with MGL and MGL-like sequences found in several plant species indicated that *GmMGL1* is located in a clade different from the one that *GmMGL2* and *GmMGL3* belong to (Fig. 15; Table 3).

The RT-qPCR analyses of the FY seeds showed that *GmMGL1* mRNA expression was enhanced at the early stage of seed maturation (from stages 1 to 2) and remained constant thereafter until the mature green stage (stage 5; Fig. 16A). However, *GmMGL1* expression was considerably lower in NH seeds than in FY seeds throughout seed development and differed little between developmental stages. *GmMGL2* and *GmMGL3* expression levels were transiently induced during stage 3, but only in NH seeds, and they were not significantly different between FY and NH cultivars at the other stages. The MGL activity in crude protein extracts prepared from developing seeds (at stage 4) of NH ($5.86 \pm 0.81 \text{ nmol h}^{-1} \text{ g}^{-1}$) was significantly lower than that detected in FY seeds ($12.1 \pm 2.28 \text{ nmol h}^{-1} \text{ g}^{-1}$; $P < 0.05$, Student's *t*-test, $n = 4$). *GmMGL1* expression was significantly lower in the leaves, stems, and roots of NH plants than in the leaves, stems, and roots of FY plantlets at the leaf-expansion stage before flowering (Fig. 16B). Among these, the transcript levels of *GmMGL2* and *GmMGL3* were highest in the leaves and did not differ significantly between the soybean cultivars.

Because the genes of L-Met metabolism are regulated coordinately [35], we examined the effects of *GmMGL1* suppression on the expression of *CGS*, which catalyzes a key regulatory step of the L-Met biosynthetic pathway [36], and of *MMT* and *HMT*, which are directly involved in the formation and decomposition of SMM (Fig. 1) [7]. In SoyBase BLAST searches using *AtCGS* (*At3g01120*), *AtMMT* (*At5g49810*), and *AtHMT1* (*At3g25900*) as queries, two *CGS* homologs (*Glyma.18g261600* and *Glyma.09g235400*; referred to as *GmCGS1* and *GmCGS2*, respectively), two *MMT* homologs (*Glyma.12g163700* and *Glyma.16g000200*; *GmMMT1* and *GmMMT2*, respectively), and three *HMT* homologs (*Glyma.08g261200*, *Glyma.19g158800*, and *Glyma.20g148900*; *GmHMT1*, *GmHMT2*, and *GmHMT3*, respectively) were identified. RT-qPCR analyses of mRNA expression from soybean seeds at different developing stages revealed no

significant differences between FY and NH, except for *GmCGS1/2*, *GmHMT2*, and *GmHMT3* at stage 1 (Fig. 17).

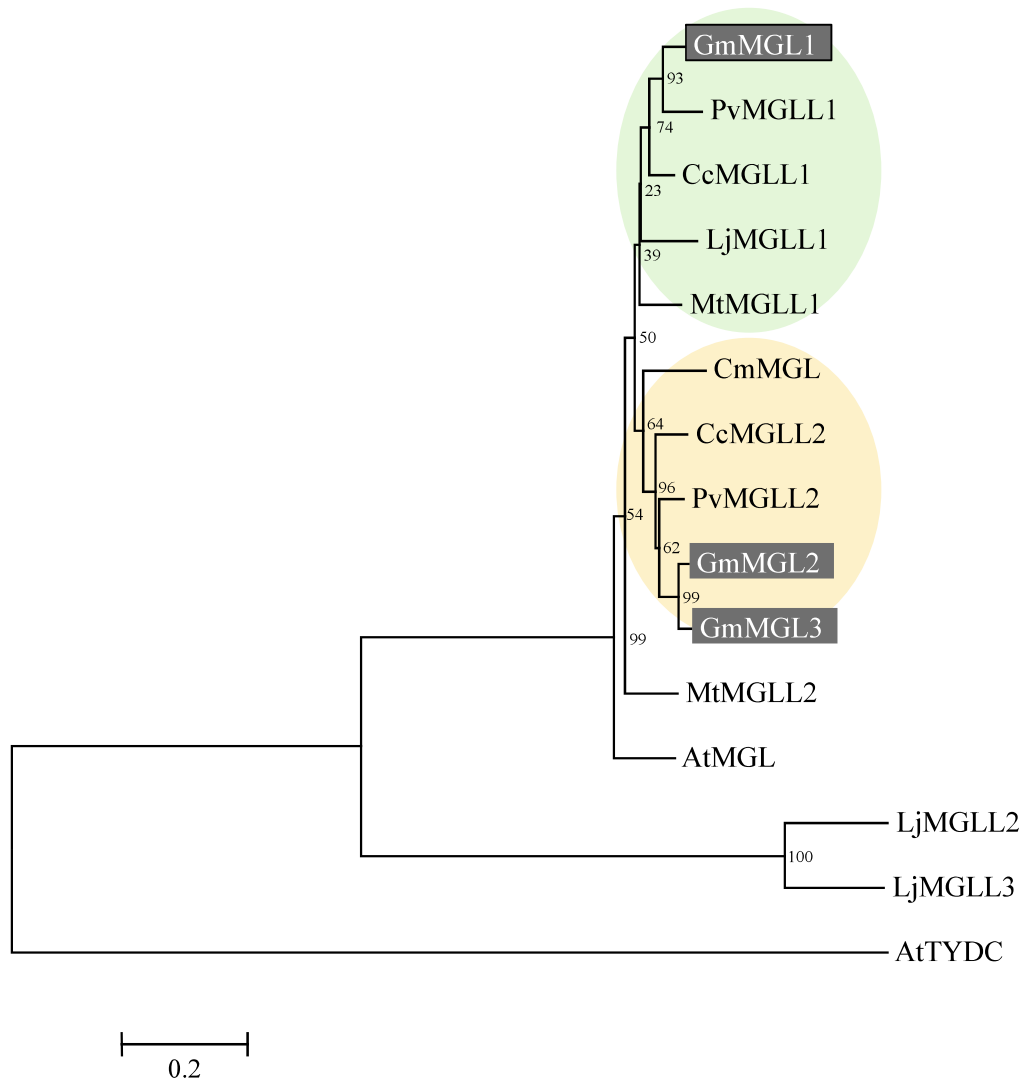


Fig. 15. Phylogenetic analysis of GmMGL1 and its related MGL-like proteins. The amino acid sequences were aligned using MAFFT v7.220, and poorly aligned positions were eliminated using Gblocks (version 0.91b). MEGA6 software was used to construct the phylogenetic tree using a neighbor-joining method with 1000 bootstrap replicates. The proteins used for the analysis are listed in Table 3. *Arabidopsis* tyrosine decarboxylase (*AtTYDC*) was used as an outgroup. GmMGL1 is boxed, and GmMGL2 and GmMGL3 are highlighted.

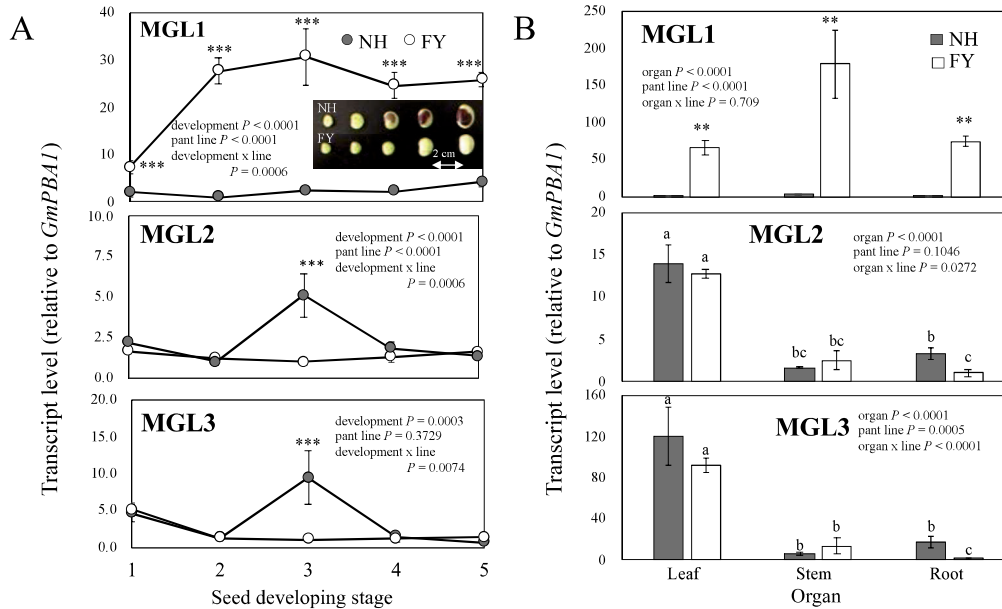


Fig. 16. Expression of *GmMGL1*, *GmMGL2*, and *GmMGL3* in developing seeds (A) and in the leaves, stems, and roots (B) of Fukuyutaka (FY) and Nishiyamahitashi 98-5 (NH) soybean cultivars. Sizes of NH and FY seeds collected for RNA extraction (stages one to five); the *Glycine max* 20S proteasome subunit (*Glyma.06g078500*) was used as an internal control in RT-PCR analyses. Transcript levels relative to the internal control are shown as multiples of the lowest value of 1. Data are presented as means \pm SE ($n = 3$). Significant differences were identified using a two-way analysis of variance (ANOVA) after Box-Cox transformation. *** above the symbols in A indicate significant differences between plant lines in each developing stage ($P < 0.001$, simple main effect test after two-way ANOVA). ** indicate significant differences between plant lines in B (*MGL1*) ($P < 0.05$, simple main effect test after two-way ANOVA). Different lowercase letters around the symbols indicate significant differences between organs in B (*MGL2* and *MGL3*) ($P < 0.05$, Tukey' HSD test after two-way ANOVA).

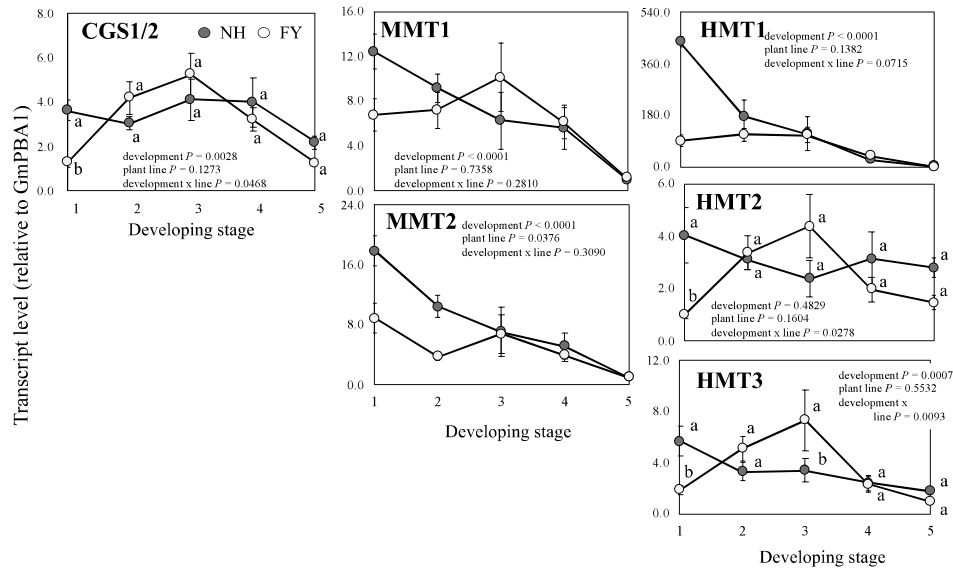


Fig. 17. Expression levels of *GmCGS1/2*, *GmMMT1*, *GmMMT2*, *GmHMT1*, *GmHMT2* and *GmHMT3* in developing Fukuyutaka (FY) and Nishiyamahitashi 98-5 (NH) seeds from stages one to five (refer to Fig. 10). For the RT-PCR analysis, *Glycine max* 20S proteasome subunit (*GmPBA1*; *Glyma06g.078500*) was used as an internal control, and the relative level of each transcript to the internal control is shown with setting the lowest value to 1. The means are shown with SE ($n = 3$). Significant differences were identified using a two-way analysis of variance (ANOVA) after Box-Cox transformation. Different letters around the symbols indicate significant differences between plant lines in each developing stage ($P < 0.05$, simple main effect test after two-way ANOVA).

Administration of L-Met Causes Accumulation of SMM in Developing Seeds

Suppression of *GmMGL1* expression in developing soybean seeds might lead to the accumulation of L-Met, which would otherwise be catabolized to ammonia, methanethiol, and 2KB. One of the alternative fates of free L-Met is the formation of SMM via the activity of MMT (Fig. 1), which is likely to occur in developing soybean seeds because of the substantial expression levels of *GmMMT1* and *GmMMT2* (Fig. 17). To examine whether MMTs are active in developing soybean seeds, we conducted a L-Met-feeding experiment. We fed free L-Met solution onto slices of immature green soybean seeds of the FY and NH cultivars and determined SMM and L-Met contents using liquid chromatography with tandem mass spectrometry (LC-MS/MS; Fig. 18A). Inclusion of 1 or 5 mM L-Met in the solution covering the cut surfaces of the FY seeds yielded incremental increases in the SMM contents, and after 24 h of treatment, the SMM levels increased up to 37.9 and 135 mg g⁻¹ for the 1 and 5 mM L-Met solutions, respectively. The SMM levels of the NH seeds also showed similar incremental increases, but in a more prominent manner, and after 24 h, the SMM levels increased up to 214 and 316 mg g⁻¹ for the 1 and 5 mM L-Met solutions, respectively. The SMM level in the NH seeds treated only with water also significantly increased to 80 mg g⁻¹ after 24 h. No significant difference in the L-Met levels was observed for FY and NH seeds treated with 1 mM L-Met in comparison with the levels in seeds treated with water except those after 24 h with NH seeds; however, following feeding with 5 mM L-Met solution, the L-Met levels increased significantly in both FY and NH, with more prominent increases in NH. The highest L-Met level for FY was 9.71 mg g⁻¹ at 8 h and for NH was 27.2 mg g⁻¹ at 24h.

To confirm substrate-product relationships, we performed feeding experiments using [¹³C] L-Met (C5, 99 atom %) with NH seeds. Subsequent LC-MS/MS analyses of SMM in the extract confirmed that it was predominantly formed from [¹³C] L-Met, as indicated by mass-to-charge ratio (*m/z*) values of 169.1 and 106.1 that were generated from ¹³C₅ labeled SMM (Fig. 18B).

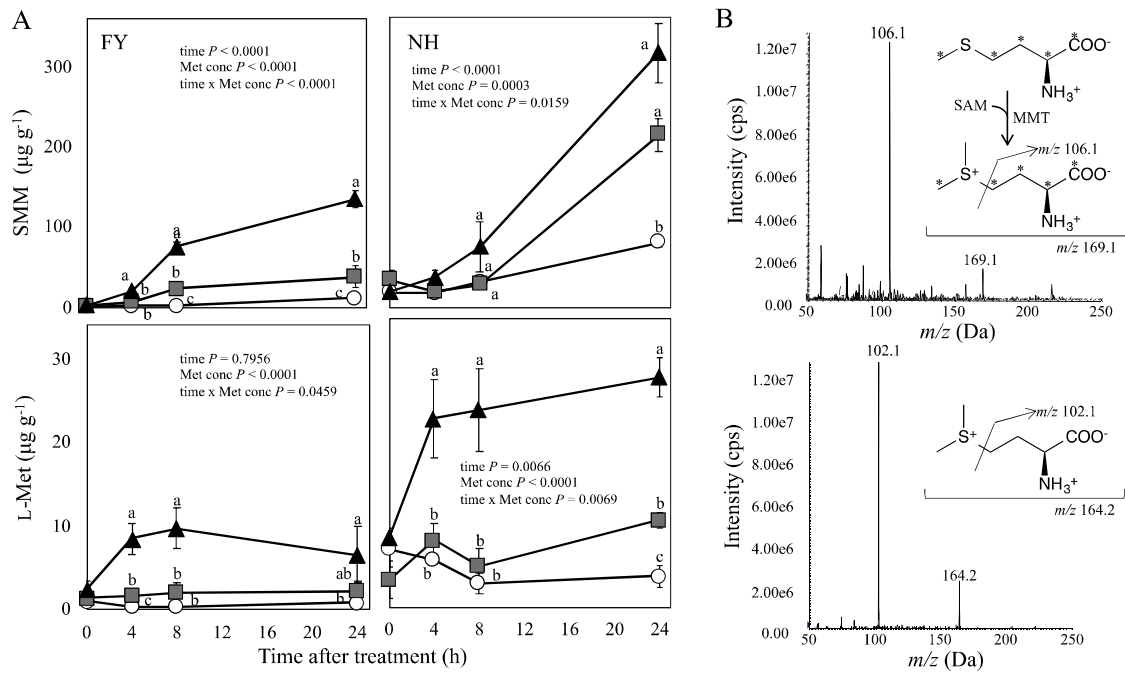
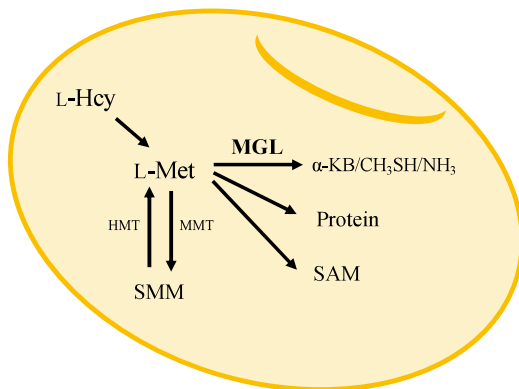


Fig. 18. Absorption and conversion of exogenously supplied Met to SMM in a section of a developing soybean seed; A. SMM and Met contents after treating with 0 (circle and white)-, 1 (square and gray)-, and 5 (triangle and black)-mM Met. Data are shown as means \pm SE ($n = 3$). Significant differences were identified using a two-way analysis of variance (ANOVA) after Box-Cox transformation. Different letters around the symbols indicate significant differences between Met concentrations in each hour ($P < 0.05$, Tukey' HSD tests after simple main effect tests). B. Mass spectra of SMM extracted from the seed sections treated with 5-mM $^{13}\text{C}_5$ -Met for 24 h (upper panel). Reaction of MMT from $^{13}\text{C}_5$ -Met is shown. The positions of ^{13}C in Met and SMM are shown with asterisks. Mass spectra of non-labelled SMM is shown (lower panel). Assignment of molecular and fragment ions are also shown.

1.3 Discussion

Using a molecular genetic approach to locate the allele responsible for hyperaccumulation of SMM, we found that a transposon insertion into the intron of *GmMGL1* is strongly associated with SMM hyperaccumulation in soybean seeds. Expression of the *GmMGL1* gene and, accordingly, MGL activity in seeds were suppressed due to the transposon insertion. Under these conditions, L-Met catabolism would be low in seeds, leading to L-Met accumulation. Because excess L-Met levels have been associated with various adverse effects in plant tissues, we hypothesized that surplus L-Met in soybean seeds with MGL deficiencies was converted to the better-tolerated compound SMM by MMT activity (Fig. 19). In line with this hypothesis, L-Met-feeding experiments showed that surplus L-Met was efficiently converted into SMM in green mature soybean seeds and that the conversion was more prominent with MGL deficiency.

Fukuyutaka
(FY)



Nishiyamahitashi
98-5 (NH)

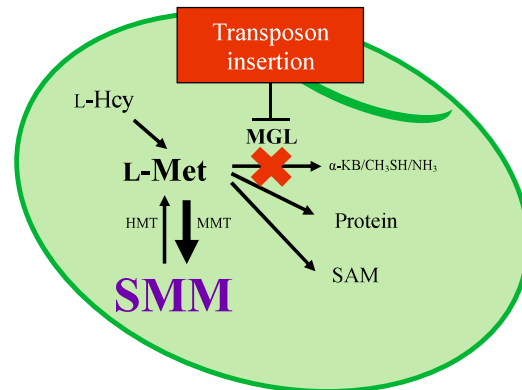


Fig. 19. A proposed mechanism of hyperaccumulation of SMM in soybean seeds with low MGL activity. (A) When the MGL activity is sufficient as in normal soybean seeds, the level of free Met is properly controlled. (B) When MGL activity is suppressed by transposon insertion as in NH soybean seeds, surplus Met left behind is converted into SMM, which seems to account for hyperaccumulation of SMM. Met, methionine; SMM, *S*-methylmethionine; MGL, methionine γ -lyase; MMT, methionine methyltransferase; HMT, homocysteine methyltransferase; SAM, *S*-adenosylmethionine; HomoCys, homocysteine; 2KB, 2-ketobutyric acid.

The Transposon Insertion Suppresses the Expression of *GmMGL1*

The insertion of a transposon into the intron of *GmMGL1* strongly suppressed its mRNA expression, whereas processing of the corresponding precursor mRNA through splicing at the inherent positions was little affected by the intronic insertion. Intronic insertion of transposons generally has minimal impacts on gene expression levels or splicing events [37]. For example, insertion of the retrotransposon *Ty1-copia*, which is approximately 5,000 bp in length, had little impact on transcription with flax (*Linum usitatissimum*) [38]. Hence, the present marked repressive effects of transposon insertion into the intron of *GmMGL1* are unique. Alternatively, in a previous study of soybeans, transposons in or near a gene were related to increased CHG/CHH methylation and, consequently, lower expression levels [39]. Hence, epigenetic regulatory mechanisms likely play roles in the present repression of *GmMGL1*. As such, analyses of DNA methylation should be one of the next priority research areas to reveal more details about the mechanisms of this type of gene suppression.

Suppression of *GmMGL1* Accounts for SMM Hyperaccumulation

In plant tissues, L-Met levels are tightly regulated through biosynthesis and catabolism (Fig. 1). Higher free L-Met contents (in addition to SMM contents) in NH seeds than in FY seeds prompted us to assume that *GmMGL1* participated in controlling free L-Met levels in seeds. If this is the case, in the absence of substantial MGL activity, as found with NH, free L-Met levels should increase, and surplus L-Met could be converted into SMM by the MMT activity in seeds. This scenario showed no fundamental inconsistency with the results obtained in this study about the L-Met metabolism of NH. The function of MGL to adjust free L-Met levels has been demonstrated with *Arabidopsis*, in which knockout of the *AtMGL* gene increased free L-Met contents in leaves, flowers, and seeds [40, 41]. Notably, the *Arabidopsis* knockout mutant contained 4.5-fold higher SMM contents in leaves than its parental wild type; therefore, it is presumed that conversion of surplus L-Met to SMM is common among plants. In support of this hypothesis, SMM accumulation has been reported in multiple transgenic plants with high free L-Met levels [13, 14, 23]. Taken together, it is suggested that *GmMGL1* was involved in controlling free L-Met levels in developing soybean seeds. SMM hyperaccumulation is likely to be a consequence of suppressed *GmMGL1* and a subsequent fail-safe system employing MMT activity to avoid the adverse effect of excess L-Met.

One of the MGL products, 2KB, is partly converted to L-Ile in Arabidopsis, especially under drought stress [28, 41]. However, we found no significant difference in either free or total L-Ile content between NH and FY seeds, suggesting that GmMGL1 accounted little for L-Ile formation in developing seeds. On the contrary, dry NH seeds had higher free L-Thr, L-Phe, L-His, and homoserine levels in addition to increased free L-Met and SMM levels. Therefore, the MGL deficiency is likely to cause pleiotropic effects on the metabolism of other amino acids. Accumulation of free amino acids was often observed in several transgenic plants generated to enhance L-Met levels [16, 18, 37, 42]. Accordingly, it is suggested that the adverse effect of surplus L-Met in NH induced a stress response that led to higher L-Thr, L-Phe, L-His, and homoserine levels.

Limited Significance of Phloem Transport of SMM for SMM Hyperaccumulation

It has been reported for several plant species, including Arabidopsis and wheat (*Triticum aestivum*), that SMM formed in vegetative tissues is transported to seeds through the phloem [6, 20, 43, 44]. Therefore, it was assumed that the phloem transportation of SMM formed in vegetative tissues to seeds could also be accountable for the hyperaccumulation of SMM in NH seeds. The level of SMM in the phloem exudate collected from leaves of NH was higher than that found for FY plants. Therefore, transportation of SMM through the phloem toward the seeds is likely to be at least partly accountable for the hyperaccumulation of SMM in NH seeds. The SMM levels in the pods of both NH and FY showed a tendency to decrease during maturation; thus, the transportation of SMM from the pods to the seeds should also be taken into consideration. However, it was remarkable that the SMM levels found in the phloem exudate of NH plants were 291-fold lower than that in Arabidopsis phloem exudate. Concordant with the fact that amino acid levels in soybean phloem exudate were 8-fold lower than those in Arabidopsis and wheat [6], our observation of low levels of SMM in soybean phloem exudate prompted us to consider that the contribution of phloem transport of SMM toward seeds for SMM hyperaccumulation is not negligible but is limited. Furthermore, the results of the reciprocal crossing of NH and FY indicated that maternal as well as paternal genotypes did not play a substantial role in determining the seed phenotype of SMM hyperaccumulation, which was caused only when the genotype of the seeds was homozygous for *mgll*, and thus, the involvement of vegetative organs in SMM hyperaccumulation in the seeds of NH is likely limited.

The extensively lower levels of SMM and L-Met in the soybean phloem, compared with levels in the Arabidopsis phloem, are noteworthy because the levels of free and total amino acids including L-Met are more than 10-fold higher in soybean seeds than in Arabidopsis seeds [45]. Source-sink transport of amino acids from vegetative organs to seeds, and in situ synthesis of amino acids in seeds, might be accountable in different ways for the accumulation of amino acids in seeds in these two plant species.

Exogenous L-Met Is Converted into SMM

The addition of L-Met at 1 mM onto developing seeds of FY had only a slight effect on L-Met or SMM concentrations, probably because L-Met, supplied exogenously, was appropriately catabolized in part by intrinsic GmMGL1 activity in FY seeds. This L-Met catabolizing system was, however, overwhelmed by treatments with 5 mM L-Met solution, as indicated by transient increases in free L-Met in developing FY seeds, followed by a significant increase in the amount of SMM. The accumulation of L-Met and SMM seemed to be further emphasized for NH. This result indicated that both NH and FY seeds exhibited enough MMT to convert L-Met supplied exogenously into SMM. The exaggerated responses of the accumulation of L-Met and SMM in NH seeds could be explained by the lower activity of GmMGL1 in the seeds and the surplus L-Met left behind in the seed tissues being converted into SMM by MMT. SMM has been considered to be a tentative storage form of L-Met to avoid excessive L-Met concentrations [46]. In agreement, the SMM concentrations in soybean seeds treated with 5 mM L-Met solution were much higher than the L-Met concentrations, suggesting that SMM is a safer storage form of L-Met. In summary, SMM hyperaccumulation was caused exclusively by the suppression of GmMGL1 that regulates free L-Met levels in developing soybean seeds. MMT activity in developing soybean seeds should be sufficient to convert surplus L-Met into SMM, irrespective of MGL activity (Fig. 19). The data presented here indicate that the genetic suppression of MGL in soybean seeds affects L-Met metabolism, favors the hyperaccumulation of SMM, and provides further insights into the regulatory mechanisms of L-Met metabolism. This knowledge should be taken into consideration when attempting to modify L-Met metabolism in soybean seeds.

1.4 Materials and Methods

Plant Materials

Seeds of the soybean cultivars NH, FY, and WI were grown and harvested during 2016 in an experimental field at the Nagano Vegetable and Ornamental Crops Experiment Station, Shiojiri City (E 137°57', N 36°06'; annual mean temperature, 11°C). For the quantification of SMM levels in leaves, pods, and seeds, NH and FY plants were grown and harvested in 2019 in an experimental field at the Yoshida campus of Yamaguchi University, Yamaguchi City (E 131°47', N 34°15'; annual mean temperature, 15°C). To prepare samples at a similar developmental stage, each organ was collected at slightly different dates because FY showed a little early-growth phenotype when compared with NH. For collecting seeds for the RT-qPCR analyses and L-Met-feeding experiments, plants were grown and harvested in 2017 and 2019 in an experimental field at the Yoshida campus of Yamaguchi University. For extraction of RNA from leaves, stems, and roots, plantlets (NH and FY) were germinated with vermiculite and were transplanted to the hydroponic culture system [47] with a 12 h light (at 27°C)/12 h dark (22°C) cycle. NH and FY plants were cultured under these conditions for 40 and 34 d, respectively. Seeds of the cultivars Shinano-Kurakake, Nishiyamahitashi 94-5, Sinanomachi Arasebara Kurakake, Togakushi Morozawa Ganimame, Usuda Zairai, Shinano Midori, Nishiyamahitashi 94-1, Tousanhitashi 94-1, Ogawa Zairai 5, and Chino Zairai 4 were harvested in 2012 and 2015 from the experimental field at the Nagano Vegetable and Ornamental Crops Experiment Station or in 2019 from the experimental field at the Yoshida campus of Yamaguchi University.

Determination of SMM Contents

Seed coats were carefully removed and soybean seeds containing hypocotyls were then powdered using a multibeads shocker (PM2000; Yasui Kikai) equipped with stainless metal cones (MC-0316S; Yasui Kikai) and operated at 2,500 rpm for two 30-s periods with a 10-s interval. Powder samples of 20 mg were then mixed with 1 mL of distilled water containing 50 mg mL⁻¹ L-Met-*S*-methyl d6 sulfonium chloride (d6-SMM; Toronto Research Chemicals) and were then placed in a water bath sonicator (US-2; SND) for 10 min. The resulting suspensions were centrifuged at 15,000 rpm (20,000 × g) for 10 min at 4°C. Subsequently, 100 mL aliquots were added to Strata C18-E (100 mg mL⁻¹; Phenomenex), and SMM was eluted twice with 0.5-mL aliquots of distilled water. Elutes were cleared using an Ekicrodisc 3 (0.45 mm, 3 mm; Pall).

LC-MS/MS analyses were performed using an AB Sciex 3200 Q-TRAP LC-MS/MS system equipped with a Prominence UFLC (Shimadzu) in multiple reaction monitoring (MRM) mode with positive electrospray ionization (ESI). Chromatography was conducted using a Discovery HS F5 column (15 cm × 2.1 mm, 3 μm; Supelco), and HPLC and MS analyses were performed using previously described conditions [25]. To quantify ¹³C-labeled SMM formation from [¹³C] L-Met (Cambridge Isotope Laboratories), MS analyses were performed in the enhanced production mode with *m/z* 169.2 (for labeled SMM) or 164.2 (for nonlabeled SMM) using positive ESI with a capillary voltage of 4,500 V, an arbitrary source temperature, a curtain gas of 10 (arbitrary units), ion source gases 1 and 2 of 16 and 0 (arbitrary units), respectively, a declustering potential of 26 V, and an entrance potential of 2.5 V. The level of free L-Met was also analyzed using the same LC-MS/MS condition but with different MRM transitions. The detailed parameters for LC-MS/MS analysis are shown in Table 4.

To collect phloem exudate, fully expanded leaves of NH and FY plants at their seed-filling stage were detached with the base of the petiole under a solution of 20 mM EDTA (pH 7), immersed into 0.2 mL of the same solution in 0.5 mL microtubes, and placed in humid chambers in the dark at 25°C [48]. After 5 h, the EDTA solution was collected and used for the LC-MS/MS analyses as described above to estimate the concentrations of SMM and free L-Met. As a comparison, fully expanded rosette leaves of *Arabidopsis* (*Arabidopsis thaliana*; ecotype Wassilewskija-0) were used at its seed-filling stage.

Determination of Amino Acid and Protein Contents

Soluble amino acids were extracted from dry seed flour (20 mg) as described by Hanafy et al. (2013). Flour samples were suspended in 240 mL of 3% (w/v) sulfosalicylic acid and were suspended with vigorous shaking for 30 min. After centrifugation at $12,000 \times g$ for 10 min at 25°C , precipitates were extracted two more times as described above. Combined supernatants were then filtered and analyzed using LC-MS/MS with an ESI interface [49] as detailed above. An Intrada amino acid column (100×3 mm internal diameter, $3 \mu\text{m}$; Imtakt) was used with a column temperature of 40°C . Mobile phases were applied at 0.4 mL min^{-1} and comprised solvents A (acetonitrile:formic acid at 100:0.3 [v/v]) and B (0.1 M acetonitrile:ammonium formate at 20:80 [v/v]) at 15% B for 10 min, followed by a linear increase from 15% B to 60% B over 15 min, then from 60% B to 100% B over 5 min, and then 100% B for 10 min. The injection volume was $4 \mu\text{L}$. The MS system was operated in MRM mode using positive ESI with a capillary voltage of 3,000 V, a source temperature at 550°C , a curtain gas of 35 (arbitrary units), ion source gases 1 and 2 of 80 and 60 (arbitrary units), respectively, a declustering potential of 16 V, and an entrance potential of 5 V. MRM transitions of the precursor to product ions used for the quantification and collision energy are summarized in Table 4. Quantification was done using calibration curves constructed using amino acid mixture standard solution (Wako Pure Chemicals) supplemented with homoserine and homocysteine (Wako Pure Chemicals).

Analyses of QTLs for SMM Contents

RILs, including 155 F5 lines, were developed from a single seed descendant of the cross between NH and WI. Total DNA extraction and linkage map construction by simple sequence repeat markers (WSGP version 2) were performed as described previously [50]. SMM contents in each RIL were quantified using bulked F6 seeds that were derived from the F5 individual. Because SMM contents varied widely among RILs, QTL analysis was conducted with the common logarithm value for contents.

QTL analyses were performed using composite interval mapping, as implemented in QTL Cartographer 2.5 software [51]. The genome was scanned at 1 cM intervals. One thousand permutation tests were conducted to determine the threshold value of the limit of detection score.

Mapping of Responsible Genes

F6 and F7 progeny of parent individuals with hetero genotypes in the chromosomal region that corresponded with QTLs were used for fine genetic mapping of responsible genes. Initial QTL analyses indicated a region of around 486 kb ranging from Satt477 and Satt592 on chromosome 10. A population of F7 progeny was then used to delimit the locus using marker genotyping and SMM quantification. Gene mapping was performed using the BARCSOYSSR markers (BSSR) described by Song et al. (2010). The tail sequence CACGACGTTGTA AAACGAC was added to the 59 end of the reverse primer, and oligonucleotides that were complementary to tail sequences were fluorescently labeled with 6- FAM, VIC, NED, and PET (Thermo Fisher Scientific) before addition to PCR solutions. PCRs and PCR fragment length analyses were conducted following Fujii et al. (2018). Only one ORF (i.e., *Glyma.10g172700*) was identified in the region after the second round of fine-mapping.

cDNA Cloning and Expression of Recombinant Proteins

Total RNA was extracted from developing seeds of WI using RNeasy Plant Mini Kits (Qiagen) according to the manufacturer's instructions. DNA was degraded using DNA-free Kits (Ambion, Thermo Fisher Scientific), and cDNA was synthesized using SuperScript VILO cDNA Synthesis Kits (Invitrogen). Subsequently, *Glyma.10g172700* (GmMGL1) cDNA was PCR amplified using primers for 5' and 3' ends of the translation initiation site (Supplemental TableS4). The resulting PCR products were cloned into pGEM T-easy vectors (Promega) for sequencing. PCR products were then subcloned into the *EcoRI-XhoI* site of the pET24a vector (Merck & Co., Kenilworth, NJ, USA), and the resulting plasmid was transfected into *E. coli* Rosetta 2(DE3)pLysS cells (Merck). Cells were subsequently grown in Luria broth supplemented with kanamycin (50 $\mu\text{g mL}^{-1}$) and chloramphenicol (30 $\mu\text{g mL}^{-1}$) at 37°C to an OD₆₀₀ of 0.6 to 0.8. After chilling the cultures on ice for 15 min, isopropyl β -D-1-thio-galactosylpyranoside was added to a concentration of 1 mM, and cells were then cultured at 30°C for 16 h. Cells from 50 mL cultures were recovered by centrifugation at 4,000 \times g for 20 min at 4°C and were resuspended in 5 mL of 100 mM potassium phosphate buffer (pH 7.5) containing 0.01% (w/v) DTT and 1.3 mM PLP. After the addition of 5 μL aliquots of 100 mM phenylmethane sulfonyl fluoride and 50 mg mL⁻¹ lysozyme, suspensions were kept on ice for 15 min, and cells were then disrupted using a tip-type ultrasonic disruptor (UD-211; Tomy Seiko). After centrifugation at 12,000 \times g for 10 min, supernatants were directly applied to a column (2 mL) of Ni-NTA agarose (Nacalai Tesque) that had been equilibrated with 100 mM potassium phosphate buffer (pH 7.5) containing 0.01% (w/v) DTT and 10 μM PLP. The column was then washed with 10 mL of the same buffer containing 10 mM imidazole, and His-tagged recombinant proteins were eluted with 10 mL of the same buffer containing 250 mM imidazole. Active fractions were finally combined and desalted using a PD-10 column (GE Healthcare).

Enzyme Assays

MGL enzyme assays were performed according to previous reports [33, 52]. Given volumes of purified enzyme solution were mixed with 100 mM potassium phosphate buffer (pH 7.5) containing 10 mM PLP and 40 mM L-Met and were incubated at 30°C with gentle shaking. Aliquots of 2 mL were taken every 2 min and were added to 100 mL of 50% (w/v) TCA. After centrifugation at $20,000 \times g$ for 8 min at 25°C, 0.8 mL supernatants were mixed with 1.6 mL aliquots of 1 M sodium acetate buffer (pH 5) and 0.6 mL aliquots of 0.1% (w/v) MBTH. Reaction tubes were then tightly closed and incubated at 50°C for 40 min. The MGL product 2KB was quantified according to A278, which is derived from the MBTH derivative of 2KB. The absorbance at 0 min was subtracted from later measurements, and a calibration curve was generated using authentic 2KB (Sigma-Aldrich). The structure of 2KB was confirmed using GC-MS after converting the acid into a trimethylsilylated product [29]. After incubating the recombinant enzyme with L-Met and PLP overnight in a total volume of 3 mL, reactions were terminated by adding 40 μL of 6 N HCl. Products were then extracted in 2 mL of ethyl acetate, and extracts were washed once with 1 mL of water prior to removing the solvent under a stream of nitrogen gas. After confirming complete dryness, extracts were incubated with 100 μL aliquots of anhydrous pyridine at 25°C for 90 min. Thereafter, 100 μL aliquots of *O*-bis(trimethylsilyl)trifluoroacetamide (Tokyo Chemical Industry) were added and incubated for 90 min. GC-MS was performed using a QP-5050 (Shimadzu) instrument equipped with a 0.25 mm \times 30 m DB-5MS column (film thickness, 0.25 mm; Restek). The column temperature was programmed as follows: 50°C for 1 min, increasing by 5°C min⁻¹ to 120°C, then by 20°C min⁻¹ to 280°C, and then maintenance at 280°C for 1 min. The carrier gas (He) was delivered at a flow rate of 30 kPa. Injector and interface temperatures were 240°C and 300°C, respectively. The mass detector was operated in electron impact mode with an ionization energy of 70 eV. Compounds were assigned by comparing MS profiles and retention times with those of trimethylsilyl derivatized 2KB that was prepared separately.

To determine MGL activity in developing soybean seeds, the seeds of NH and FY at seed developmental stage 4 (compare with the photograph in Fig. 10) were homogenized with 4 volumes of 50 mM sodium phosphate buffer (pH 7.5) containing 5% (w/v) sorbitol, 10 mM DTT, 5 mM sodium metabisulfite, and 2.5 mM PLP. After

centrifugation at $20,000 \times g$ for 20 min at 4°C , the cleared supernatant (0.5 mL) was mixed with 0.25 mL of 0.2 M L-Met in a buffer (50 mM sodium phosphate, pH 7.5, containing 2.5 mM PLP) in a total volume of 4.5 mL and incubated at 30°C with a shaking water bath for 17 h. After the reaction, the reaction mixture was acidified by adding 66.6 μL of 6 N HCl, and then the products were extracted with 4 mL of ethyl acetate. After washing the ethyl acetate extract with 1 mL of saturated NaCl solution, the extract was used for derivatization with *O*-bis(trimethylsilyl)tri-fluoroacetamide as described above. The amount of 2KB was determined using GC-MS analysis and a calibration curve constructed with authentic 2KB. Molecular ion chromatograms with m/z 73 and 115 were used for quantification.

Genomic PCR and RT-qPCR Analysis

Genomic DNA was isolated according to Hanafy et al. (2013). Total RNA was isolated using the Qiagen RNeasy Plant Mini Kit according to the manufacturer's instruction. Total RNA (0.25 μg) was then reverse transcribed with 2.5 mM aliquots of oligo(dT)15 primer (Invitrogen) and ReverTra Ace (derived from Moloney murine leukemia virus reverse transcriptase; Toyobo) according to the manufacturer's instructions. RT-qPCR was performed with an Eco RealTime PCR System (Illumina). Cycle threshold (Ct) values for the genes of interest were normalized to means of the reference gene for the 20S proteasome subunit b (*Glyma.06g078500*) [53]. Expression levels were calculated as relative amounts using $\Delta\Delta\text{Ct}$ values. The lowest $\Delta\Delta\text{Ct}$ value in each experiment was set at 1. Homologs of MGL, CGS, MMT, and HMT were searched using BLASTP analysis on SoyBase (<https://soybase.org/>) with *GmMGL1* (*Glyma.10g17200*), *AtCGS* (*At3g01120*), *AtMMT* (*At5g49810*), and *AtHMT1* (*At3g25900*) as queries, respectively. Primers for genomic PCR and RT-qPCR are shown in Table 5.

L-Met Feeding

Pods harboring the seeds of developmental stage 2 (comparison with the photograph in Fig. 10) were collected and were gently removed with their seed coats. Thin sections of 1 mm thickness were excised at the short axis using a razor blade, and they were immediately placed on a sheet of Parafilm (Bemis Flexible Packaging) in a glass petri dish. The inner surface of the petri dish was covered with a moistened paper towel. Fifty-microliter aliquots of 0, 1, or 5 mM L-Met or [¹³C] L-Met in water were then placed on the surfaces of seed sections at 11 AM, and the petri dish was immediately closed and incubated at 25°C for 0, 4, 8, and 24 h under light/dark conditions of 14 h of light (8 AM–10 PM)/10 h of dark (10 PM–8 AM). To determine L-Met and SMM concentrations, sections were carefully washed with water and were mixed with 1 mL aliquots of distilled water containing 1 mg mL⁻¹ d6-SMM. Sections were then homogenized in a mortar, and homogenates were placed in a water bath sonicator (US-2; SND) for 10 min to facilitate extraction of L-Met and SMM. Suspensions were centrifuged at 15,000 rpm (20,000 × g) for 10 min at 4°C, and 100 mL aliquots were applied to a Strata C18-E cartridge (55 μm, 100 mg mL⁻¹, 70A; Phenomenex). L-Met and SMM were eluted twice with 0.5 mL of distilled water, and eluted solutions were cleared with Ekicrodisc 3 (0.45 μm, 3 mm; Pall) prior to LC-MS/MS analyses as described above.

Table 3. Protein sequences used to construct the phylogenetic tree.

Plant species	Enzymes	Gene name	Accession number
<i>Arabidopsis thaliana</i>	tyrosine decarboxylase	AtTYDC	NP_194597
	methionine γ -lyase	AtMGL	At1g64660
<i>Cajanus cajan</i>	methionine γ -lyase like 1	CcMGLL1	C.cajan_07057
	methionine γ -lyase like 2	CcMGLL2	C.cajan_43190
<i>Cucumis melon</i>	methionine γ -lyase	CmMGL	JX673982
<i>Glycine max</i>	methionine γ -lyase 1	GmMGL1	Glyma.10g172700
	methionine γ -lyase 2	GmMGL2	Glyma.2g087900
	methionine γ -lyase 3	GmMGL3	Glyma.13g001200
<i>Lotus japonicus</i>	methionine γ -lyase like 1	LjMGLL1	chr5.CM0431.10.r2.d
	methionine γ -lyase like 2	LjMGLL2	chr2.CM1835.300.r2.a
	methionine γ -lyase like 3	LjMGLL3	chr1.CM0141.340.r2.m
<i>Medicago truncatula</i>	methionine γ -lyase like 1	MtMGLL1	Medtr1g077890.1
	methionine γ -lyase like 2	MtMGLL2	Medtr3g080850.1
<i>Phaseolus vulgaris</i>	methionine γ -lyase like 1	PvMGLL1	Phvul.001G082000.1
	methionine γ -lyase like 2	PvMGLL2	Phvul.004G090200.1

Table 4. MRM transitions and MS parameters used to detect amino acids.

AA	Retention time (min)	Q1	Q3	DP	CEP	CE	CXP	Dwell (msec)	Remarks
Trp	12.53	205.10	146.00	12.00	15.65	11.00	23.00	7.00	Only for free amino acid
Phe	12.00	166.10	120.10	16.00	14.16	21.00	17.00	7.00	
Leu	13.02	132.10	86.10	8.00	12.86	26.00	13.00	7.00	
Ile	14.05	132.00	69.00	8.00	12.86	8.00	23.00	7.00	
Pro	14.88	116.10	70.00	8.00	12.25	36.00	21.00	7.00	
Met	15.07	150.10	104.00	6.00	13.55	16.00	11.00	7.00	Only for free amino acid
Tyr	15.60	182.10	136.00	10.00	14.77	26.00	17.00	7.00	
Val	15.61	118.10	72.10	10.00	12.32	26.00	15.00	7.00	
Ala	18.15	90.10	44.00	8.00	11.25	16.00	43.00	7.00	
Thr	18.81	120.10	74.00	10.00	12.40	16.00	15.00	7.00	
Cys	18.82	122.00	75.90	8.00	12.47	15.00	29.00	7.00	Only for free amino acid
Glu	19.04	148.10	83.90	10.00	13.47	66.00	21.00	7.00	
Gly	19.20	76.00	30.00	14.00	10.71	6.00	19.00	7.00	
Gln	19.74	147.10	83.90	10.00	13.43	6.00	21.00	7.00	
Ser	19.75	106.10	60.00	8.00	11.86	16.00	15.00	7.00	
Asn	20.03	133.10	73.90	10.00	12.90	31.00	27.00	7.00	
Asp	21.93	134.10	88.00	10.00	12.94	36.00	17.00	7.00	
Lys	32.65	147.10	83.90	10.00	13.43	6.00	21.00	7.00	
His	32.73	156.10	110.00	14.00	13.78	31.00	19.00	7.00	
Arg	34.56	175.10	70.00	8.00	14.51	41.00	27.00	7.00	
Met sulfone	17.20	182.10	56.00	20.00	14.77	18.00	20.00	7.00	
Homoserine	15.33	120.03	56.03	14.00	12.40	16.00	15.00	7.00	
Homocysteine	12.27	136.00	90.00	15.00	13.01	10.00	29.00	7.00	
Cysteic acid	17.09	167.90	80.80	-6.00	-17.87	-60.00	-26.00	1000.00	
SMM	20.45	164.11	102.00	16.00	10.00	13.00	4.00	330.00	
d6-SMM	20.66	170.11	102.00	16.00	14.32	13.00	4.00	330.00	
Met	10.27	150.11	104.10	66.00	10.00	13.00	4.00	330.00	
13C-SMM	20.70	169.11	106.00	16.00	14.28	13.00	4.00	200.00	
14C-Met	10.16	155.11	108.10	66.00	13.74	13.00	4.00	200.00	

Table 5. Primers used in this study.

Purpose	ID	Direction	Sequence (5' -> 3')	Remarks
Gnomic cloning	Glyma.10g172700	F	GCGGATCCGGGGACACTTACGTTTTGGCCACAC	<i>GmMGL1</i>
		R	TGCTCGAGAGCGATCTTGTGTATCCAGAGTCG	
qRT-PCR	Glyma.10g172700	F	GTGCTGATGTTGTCGTTACACA	<i>GmMGL1</i>
		R	AGCATTAGTGACCCTTGTTGC	
	Glyma.02g087900	F	GTGGCGGTGCTGATGTTATTG	<i>GmMGL2</i>
		R	CACCTTCGCATTCATTGTTG	
	Glyma.13g001200	F	CGTTCACAGCATCTCCAAGTT	<i>GmMGL3</i>
		R	CCATCATCGAATTCAGTAGGC	
	Glyma.18g261600/ Glyma.09g235400	F	CTGTGAGAGCATTGTGGATCA	<i>GmCGS1/GmCGS2</i>
		R	GAAGCGAACCAGGTTGCATA	
	Glyma.12g163700	F	TAGGTCCAGGTGCTTAAAAGA	<i>GmMMT1</i>
		R	CTTGCCACAACAGACACAC	
	Glyma.16g000200	F	ATTGCTGGAACGTAGAGAGCA	<i>GmMMT2</i>
		R	CACACGATTCAAGCACATCC	
	Glyma.08g261200	F	ACCTCCCATCTTATGGAAA	<i>GmHMT1</i>
		R	CATCGTGAACACTTAGATGG	
	Glyma.19g158800	F	TGGAATCAACTGACTCCACCA	<i>GmHMT2</i>
		R	GGGAAGCTCCTAACTCACACC	
	Glyma.20g148900	F	GTAAGTCTCCTAGATTATTCATGG	<i>GmHMT3</i>
		R	CTGTGCCCCACTTGATT	
Glyma.06g078500	F	CACCAACACACGATACAAC	<i>20S proteasome subunit</i>	
	R	TCCAACCAACAATAAACC		
Glyma.08g146500	F	ATTGAACCCCTGTTTGCGA	<i>Actin3</i>	
	R	ATCAGGAAGTCATGGCTTT		
Genotyping	Sat_196	F	CGAGATACTAGGATTTTGACTT	
		R	GTTTGCCACAAGAGAGAGG	
	BARCSOYSSR_10_0190	F	GCTTAGACTTGGTTATCATCCATAGC	
		R	CAACCTGCAACCCATCTCTCTA	
	WGSP10_0040 (GM10.SSR2.1?)	F	CATGATGGTTAGAAAAAGTATTGAGA	
		R	TTGATAGACCATGACTGCACATTCT	
	Satt653	F	CAAAATTTGACACAACCTGGAC	
		R	TGGTGTTTTAGGAGTGGATT	
	Satt345	F	CTATGGCATAATTGGCTCTT	
		R	GATTTGTGGTAATCGGCTAA	
	Satt479	F	GGAATTTGGTTAATCTCATCGTG	
		R	GTCCAAATAAGGGAGTAAAAACAA	
	Satt478	F	GCTTCTCTCTCCCGTATG	
		R	TATGAATGCCACACTCCC	
	Satt477	F	TGGTTGGGAAAAGGTTACTA	
		R	CCTTGCAATTCGCTACTACT	
	BARCSOYSSR_10_1261	F	TTATCATTCTCATTCTCTCTCTCTT	
		R	TTGAATTTGGGATGGATATGGA	
	Satt592	F	CAAACTCAAAGGCAAAGTG	
		R	TACATGCATGGCATACTTA	
	Sat_038	F	CCCCATTTAGCTCTCACA	
		R	TCCATGGATGGTACTAGTTCTT	
	Satt243	F	GCATTGCACATTAGGTTTTT	
		R	CTTTGTAAGATCACGCCATT	
	CSSR141	F	CGGAGAGATTCCAGGTGTAC	
		R	ATGCACGCGCACTTGATGAC	
	BSSR10_1156	F	GGTCTTCAAATTTCTCCCG	
		R	CACGACGTTGTAACGACTGGAGAGGGTGTG GAAGTG	
	BSSR10_1174	F	AAATCTGGGGAAATGACCAA	
		R	CACGACGTTGTAACGACTCACCGAACGAAAG ATAAACG	
	BSSR10_1176	F	AAAGTCCAAGTCAAAGTCAACAA	
		R	TATCATGGACGGAGAAAAGC	
	BSSR10_1177	F	TAAATTTAAGGCCGGCAAGC	
		R	CGGATCTAAGAATGCACAAA	
	BSSR10_1179	F	CGCATGTGGAATATGCTGTT	
		R	CCTTCAAATTAAGATGAAAATGTC	
BSSR10_1181	F	TTGCTAACAAATTCACCACTTG		
	R	AAAACATTTGTCCCATTTTT		
BSSR10_1182	F	TTCTGCACAGTCAAACCTGA		
	R	CAATTTGGACTAAAACTAGAATCTT		
BSSR10_1189	F	TGGATCACTGGGACATGAAG		
	R	AATGCAAAATGACGTGCAAA		
BSSR10_1194	F	CATGTGTTGCTCCTCTTGA		
	R	CACGACGTTGTAACGACTTCTCGCATTATC AACAA		
Amplification of Glyma.10g172700	Glyma.10g172700	F	CTCCGTTTTCAATTCATCACA	
		R	GGAGACAGATCGAGTAGCA	
Sequencing Glyma.10g172700	Glyma.10g172700		CCCACCGTAGAGAGTTCTGG	
			GCACGTGCGGAATATCCA CGAGTACGAATACACAAACG	

1.5 References

1. Hesse H, Hoefgen R (2003) Molecular aspects of methionine biosynthesis. *Trends Plant. Sci.* **8**, 259–262
2. Galili G, Amir R, Fernie AR (2016) The regulation of essential amino acid synthesis and accumulation in plants. *Annu. Rev. Plant. Biol.* **67**, 153-178
3. Krishnan HB, Jez JM (2018) The promise and limits for enhancing sulfur- containing amino acid content of soybean seed. *Plant. Sci.* **272**, 14-21
4. Amir R, Cohen H, Hacham Y (2019) Revisiting the attempts to fortify methionine content in plant seeds. *J. Exp. Bot.* **70**, 4105-4114
5. Ranocha P, McNeil SD, Ziemak MJ, Li C, Tarczynski MC, Hanson AD (2001) The *S*-methylmethionine cycle in angiosperms: Ubiquity, antiquity and activity. *Plant. J.* **25**, 575–584
6. Bourgis F, Roje S, Nuccio ML, Fisher DB, Tarczynski MC, Li C, Herschbach C, Rennenberg H, Pimenta MJ, Shen TL, et. al. (1999) *S*-Methylmethionine plays a major role in phloem sulfur transport and is synthesized by a novel type of methyltransferase. *Plant Cell.* **11**, 1485–1498
7. Cohen H, Salmon A, Tietel Z, Hacham Y, Amir R (2017). The relative contribution of genes operating in the *S*-methylmethionine cycle to methionine metabolism in *Arabidopsis* seeds. *Plant. Cell. Rep.* **36**, 731-743
8. Gallardo K, Firnhaber C, Zuber H, Hélicher D, Belghazi M, Henry C, Küster H, Thompson R (2007) A combined proteome and transcriptome analysis of developing *Medicago truncatula* seeds: Evidence for metabolic specialization of maternal and filial tissues. *Mol. Cell. Proteomics.* **6**, 2165–2179
9. Sato D, Nozaki T (2009) Methionine gamma-lyase: The unique reaction mechanism, physiological roles, and therapeutic applications against infectious diseases and cancers. *IUBMB. Life.* **61**, 1019–1028
10. Joshi V, Jander G (2009) *Arabidopsis* methionine γ -lyase is regulated according to isoleucine biosynthesis needs but plays a subordinate role to threonine deaminase. *Plant Physiol.* **151**, 367–378
11. Inaba K, Fujiwara T, Hayashi H, Chino M, Komeda Y, Naito S. (2009) Isolation of an *Arabidopsis thaliana* mutant, *mtol*, that overaccumulates soluble methionine: temporal and spatial patterns of soluble methionine accumulation. *Plant Physiol.* **104**, 881–887
12. Bartlem, D., Lambein, I., Okamoto, T., Itaya, A., Uda, Y., Kijima, F., Tamaki,

- Y., Nambara, E. and Naito, S. (2000) Mutation in the threonine synthase gene results in an over-accumulation of soluble methionine in *Arabidopsis*. *Plant Physiol.* **123**, 101–110
13. Kim J, Lee M, Chalam R, Martin MN, Leustek T, Boerjan W (2002) Constitutive overexpression of cystathionine γ -synthase in *Arabidopsis* leads to accumulation of soluble methionine and *S*-methionine. *Plant Physiol.* **128**, 95–107
 14. Hacham Y, Matiyahu I, Schuster G, Amir R (2008) Overexpression of mutated forms of aspartate kinase and cystathionine γ -synthase in tobacco leaves resulted in the high accumulation of methionine and threonine. *Plant J.* **54**, 260–271
 15. Cohen M, Hacham Y, Panizel I, Rogachev I, Aharoni A, Amir R (2017) Repression of CYSTATHIONINE γ -SYNTHASE in seeds recruits the *S*-methionine cycle. *Plant Physiol.* **174**, 1322–1333
 16. Hanafy MS, Rahman SM, Nakamura Y, Fujiwara T, Naito S, Wakasa K, Ishimoto M (2013) Differential response of methionine metabolism in two grain legumes, soybean and azuki bean, expressing a mutated form of *Arabidopsis* cystathionine γ -synthase. *J. Plant. Physiol.* **170**, 338–345
 17. Song S, Hou W, Godo I, Wu C, Yu Y, Matiyahu I, Hacham Y, Sun S, Han T, Amir R (2013) Soybean seeds expressing feedback-insensitive cystathionine γ -synthase exhibit a higher content of methionine. *J. Exp. Bot.* **64**, 1917–1926
 18. Cohen M, Israeli H, Matiyahu I, Amir R (2014) Seed-specific expression of a feedback-insensitive form of CYSTATHIONINE γ -SYNTHASE in *Arabidopsis* stimulates metabolic and transcriptomic responses associated with desiccation stress. *Plant Physiol.* **166**, 1575–1592
 19. Kumar P, Jander G (2017) Concurrent overexpression of *Arabidopsis thaliana* cystathionine γ -synthase and silencing of endogenous methionine γ -lyase enhance tuber methionine content in *Solanum tuberosum*. *J. Agric. Food Chem.* **65**, 2737–2742.
 20. Lee M, Huang T, Toro-Ramos T, Fraga M, Last RL, Jander G (2008) Reduced activity of *Arabidopsis thaliana* HMT2, a methionine biosynthetic enzyme, increases seed methionine content. *Plant J.* **54**, 310–320
 21. Krishnan HB, Jez JM (2018) Review: The promise and limits for enhancing sulfur-containing amino acid content of soybean seed. *Plant Sci.* **272**, 14–21
 22. Dancs G, Kondrák M, Bánfalvi Z (2008) The effects of enhanced methionine synthesis on amino acid and anthocyanin content of potato tubers. *BMC Plant Biol.* **8**:65, doi:10.1186/1471-2229-8-65
 23. Hacham Y, Matiyahu I, Amir R (2017) Transgenic tobacco plants having a higher

- level of methionine are more sensitive to oxidative stress. *Physiol Plant*. **160**, 242-252
24. Cohen H, Amir R (2017) Dose-dependent effects of higher methionine levels on the transcriptome and metabolome of transgenic Arabidopsis seeds. *Plant Cell Rep*. **36**, 719-730
 25. Morisaki A, Yamada N, Yamanaka S, Matsui K (2014) Dimethyl sulfide as a source of the seaweed-like aroma in cooked soybeans and correlation with its precursor, S-methylmethionine (vitamin U). *J. Agric. Food Chem*. **62**, 8289-8294
 26. Schmutz J, Cannon SB, Schlueter J, Ma J, Mitros T, Nelson W, Hyten DL, Song Q, Thelen JJ, Cheng J, et al (2010) Genome sequence of the palaeopolyploid soybean. *Nature* **463**, 178–183
 27. Liu, B., Kanazawa, A., Matsumura, H., Takahashi, R., Harada, K., & Abe, J. (2008). Genetic redundancy in soybean photoresponses associated with duplication of the phytochrome A gene. *Genetics*. **180**(2), 995-1007
 28. Rébeillé F, Jabrin S, Bligny R, Loizeau K, Gambonnet B, Van Wilder V, Douce R, Ravanei S (2006) Methionine catabolism in Arabidopsis cells is initiated by a γ -cleavage process and leads to S-methylcysteine and isoleucine syntheses. *Proc. Natl. Acad. Sci. U S A* **103**, 15687-15692
 29. Gonda I, Lev S, Bar E, Sikron N, Portnoy V, Davidovich-Rikanati R, Burger J, Schaffer AA, Tadmor Y, Gionannonni JJ, Huang M, Fei Z, Katzir N, Fait A, Lewinsohn E (2013) Catabolism of L-methionine in the formation of sulfur and other volatiles in melon (*Cucumis melo* L.) fruits. *Plant J*. **74**, 458-472
 30. Martel A, Bouthier de la Tour C, Le Goffic F (1987) Pyridoxal 5' phosphate binding site of Escherichia coli beta cystathionase and cystathionine gamma synthase. Comparison of their sequences. *Biochem. Biophys. Res. Commun*. **147**, 565-571
 31. Sato D, Nozaki T (2009) Methionine gamma-lyase: the unique reaction mechanism, physiological roles, and therapeutic applications against infectious diseases and cancers. *IUBMB Life* **61**, 1019-1028
 32. Goyer A, Collakova E, Shachar-Hill Y, Hanson AD (2007) Functional characterization of a methionine γ -lyase in Arabidopsis and its implication in an alternative to the reverse trans-sulfuration pathway. *Plant Cell Physiol*. **48**, 232-242
 33. Esaki N, Soda K (1987) L-Methionine γ -lyase from Pseudomonas putida and Aeromonas. *Methods Enzymol*. **143**, 459-465
 34. Inoue H, Inagaki K, Sugimoto M, Esaki N, Soda K, Tanaka H (1995) Structural analysis of the L-methionine γ -lyase gene from Pseudomonas putida. *J. Biochem*. **117**, 1120–1125

35. Liao D, Pajak A, Karcz SR, Chapman BP, Sharpe AG, Austin RS, Datla R, Dhaubhadel S, Marsolais F (2012) Transcripts of sulphur metabolic genes are coordinately regulated in developing seeds of common bean lacking phaseolin and major lectins. *J. Exp. Bot.* **63**, 6283–6295
36. Hesse H, Hoefgen R (2003) Molecular aspects of methionine biosynthesis. *Trends Plant Sci.* **8**, 259-262
37. Hirsch CD, Springer NM (2017) Transposable element influences on gene expression in plants. *Biochim. Biophys. Acta.* **1860**, 157-165
38. Galindo-González L, Mhiri C, Grandbastien MA, Deyholos MK (2016) Ty1-*copia* elements reveal diverse insertion sites linked to polymorphisms among flax (*Linum usitatissimum* L.) accessions. *BMC Genomics.* **17**, 1002 doi10.1186/s12864-016-3337-3.
39. Kim KD, Baidouri ME, Abernathy B, Iwata-Otsubo A, Chavarro C, Gonzales M, Libault M, Grimwood J, Jackson SA (2015) A comparative epigenomic analysis of polyploidy-derived genes in soybean and common bean. *Plant Physiol.* **168**, 1433-1447
40. Goyer A, Collakova E, Shachar-Hill Y, Hanson AD (2007) Functional characterization of a methionine γ -lyase in Arabidopsis and its implication in an alternative to the reverse trans-sulfuration pathway. *Plant Cell Physiol.* **48**, 232-242
41. Joshi V, Jander G (2009) Arabidopsis methionine γ -lyase is regulated according to isoleucine biosynthesis needs but plays a subordinate role to threonine deaminase. *Plant Physiol.* **151**, 367-378
42. Huang T, Joshi V, Jander (2014) The catabolic enzyme methionine gamma-lyase limits methionine accumulation in potato tubers. *Plant Biotechnol. J.* **12**, 883-893
43. Frank A, Cohen H, Hoffman D, Amir R (2015) Methionine and S-methylmethionine exhibit temporal and spatial accumulation patterns during the Arabidopsis life cycle. *Amino Acids* **47**, 497-510
44. Cohen M, Hacham Y, Panizel I, Rogachev I, Aharoni A, Amir R (2017) Repression of CYSTATHIONINE γ -SYNTHASE in seeds recruits the S-methylmethionine cycle. *Plant Physiol.* **174**, 1322-1333
45. Cohen M, Israeli H, Matityahu I, Amir R (2014) Seed-specific expression of a feedback-insensitive form of CYSTATHIONINE- γ -SYNTHASE in Arabidopsis stimulates metabolic and transcriptomic responses associated with desiccation stress. *Plant Physiol.* **166**, 1575-1592
46. Mudd SH, Datko AH (1990) The S-methylmethionine cycle in *Lemna paucicostata*. *Plant Physiol.* **93**, 623-630

47. Kuroda M, Ikenaga S (2015) Single-tube hydroponics as a novel idea for small scale production of crop seed in a plant incubator. *Biosci. Biotechnol. Biochem.* **79**, 63-67
48. Urquhart AA, Joy KW (1981) Use of phloem exudate technique in the study of amino acid transport in pea plants. *Plant Physiol.* **68**, 750-754
49. Tomita R, Todoroki K, Maruoka H, Yoshida H, Fujioka T, Nakashima M, Yamaguchi M, Nohta H (2016) Amino acid metabolomics using LC-MS/MS: assessment of cancer-cell resistance in a simulated tumor microenvironment. *Anal. Sci.* **32**, 893-900
50. Fujii K, Sayama T, Takagi K, Kosuge K, Okano K, Kaga A, Ishimoto M (2018) Identification and dissection of single seed weight QTLs by analysis of seed yield components in soybean. *Breed Sci.* **68**, 177-187
51. Wang S, Basten CJ, Zeng ZB (2005) Windows QTL Cartographer 2.5. Department of Statistics, North Carolina State University, Raleigh, NC.

1.6 Acknowledgment

I wish to express my sincere thanks to Professor Dr. Kenji Matsui, Department of Biological Chemistry, Faculty of Agriculture, Yamaguchi University for his kind guidance, suggestions and encouragement. I am also grateful to Associate Prof. Dr. Takao Koeduka of Department of Biological Chemistry, Faculty of Agriculture, Yamaguchi University Japan, and Prof. Dr. Kenji Inagaki of Department of Biofunctional Chemistry, Graduate School of Environmental and Life Science, Okayama University, Japan, for their helpful discussions and suggestions. I also thanks to Dr. Yuko Yokota, Dr. Takashi Sayama and Dr. Masao Ishimoto of Institute of Crop Science, National Agriculture and Food Research Organization, Japan, for Quantitative trait locus (QTL) analyses. I also thanks to Prof. Dr. Masayoshi Uefune of Department of Agrobiological Resources, Faculty of Agriculture, Meijo University, Japan, for statistical analysis. I also thanks to Dr. Naohiro Yamada of Nagano Vegetable and Ornamental Crops Experiment Station, Japan, for providing various soybeans.

CHAPTER 2

***Coprinopsis cinerea* Dioxygenase is an Oxygenase
Forming 10(*S*)-Hydroperoxide of Linoleic Acid,
Essential for Mushroom Alcohol, 1-Octen-3-ol,
Synthesis**

2.1 Introduction

The Biosynthetic Pathway for 1-Octen-3-ol Formation in Mushrooms

1-Octen-3-ol is a volatile compound with an earthy and mushroom-like organoleptic property that commonly occurs in nature, such as in mushrooms, molds, and moist air in a laurel forest. It is also found in human breath and sweat. It attracts biting insects, such as mosquitoes [1]. An olfactory receptor specific to 1-octen-3-ol has been isolated from malaria-causing mosquitoes [2]. Despite its familiarity, the details of the biosynthesis of 1-octen-3-ol, as well as its ecological and physiological significance, are not fully understood.

The biosynthetic pathway for 1-octen-3-ol formation in common mushrooms (*Agaricus bisporus*) has been elucidated by Wurzenberger and Grosch [3-5]. Linoleic acid is the substrate, and its stereospecific oxygenation yields the 10(*S*)-hydroperoxide of linoleic acid (10(*S*)HPODE) and subsequent cleavage yields (*R*)-(-)-1-octen-3-ol and 10-oxo-(*E*)-9-decenoic acid (Fig. 1). The involvement of the 10(*S*)-isomer as an intermediate to form 1-octen-3-ol from linoleic acid was also confirmed in *Lentinula edodes* (Shiitake mushroom) and *Tricholoma matsutake* (Matsutake mushroom) [6, 7]. However, despite the efforts of many researchers, the enzymes involved in this biosynthetic pathway have not been identified for 40 years.

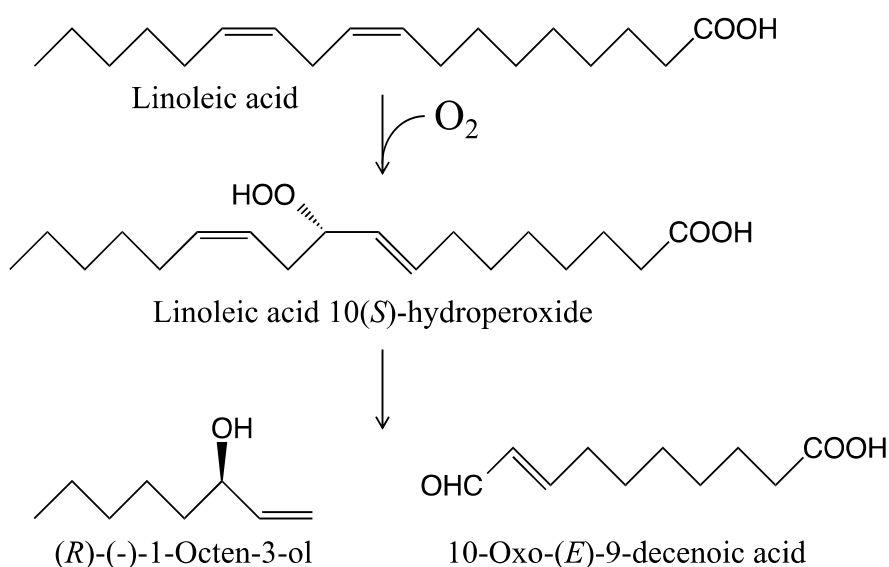


Fig. 1. Pathway for the biosynthesis of 1-octen-3-ol from linoleic acid in Basidiomycota.

The Study of Oxylipin Biosynthetic Enzyme in Ascomycota

Filamentous Ascomycota produce an array of oxylipin metabolites called precocious sexual inducer (psi) factors, which function as hormone-like signals. Psi-producing oxygenases (Ppos) are responsible for the biosynthesis of psi factors [8-11]. Each Ppo is a fusion protein consisting of a cyclooxygenase (COX)-like domain at its N-terminus and cytochrome P450-like domain at the C-terminus. The COX domain catalyzes a dioxygenase (DOX) reaction with unsaturated fatty acids, such as linoleic acid and oleic acid, and the P450-like domain catalyzes a rearrangement reaction with the fatty acid hydroperoxide formed by the COX domain [10, 11]. The filamentous Ascomycota have several subtypes of Ppos, such as PpoA, B, C, or D, which show diversity in the position of oxygenation on fatty acid substrates, catalyzed by the COX domain, and the mode of the rearrangement of hydroperoxides thus formed, which is catalyzed by the P450 domain [10, 11]. For example, PpoA, also called linoleate diol synthase, converts linoleic acid to its 8-hydroperoxide, which subsequently isomerizes to form 5,8- or 7,8-dihydroxy linoleic acid [12]. PpoC from *Aspergilli* also consists of an N-terminal COX domain and C-terminal P450-like domain. The COX domain accounts for the formation of the 10-hydroperoxide of linoleic acid, but the P450-like domain does not rearrange hydroperoxide; thus, PpoC almost exclusively forms the 10-hydroperoxide of linoleic acid [13]. Because of the same position of the hydroperoxide group in linoleic acid, PpoC-like enzymes are expected to be involved in the production of 1-octen-3-ol in filamentous Ascomycota. Disruption of *ppoC-like* genes in *Podospora anserina* and *Aspergillus luchuensis* diminishes their ability to produce 1-octen-3-ol [14, 15]. However, it has not been confirmed whether the *ppoC-like* genes of *P. anserina* and *A. luchuensis* are directly involved in the formation of 1-octen-3-ol because the catalytic properties of these gene products have not been studied. Furthermore, the configuration of the PpoC reaction products from filamentous ascomycetes analyzed to date was 10(*R*)-hydroperoxide [7], which was not cleaved to form 1-octen-3-ol by the crude extract prepared from common mushrooms [5].

Aim of This Work

To date, four genes with substantial similarities with ascomycete ppos have been reported in Basidiomycota, such as *Ustilago maydis* and *Rhizoctonia solani* [16, 17] however, the properties and functions of the enzymes encoded by these basidiomycete genes have never been studied. In this study, we identified two genes, *Ccdox1* and *Ccdox2*, in the genome of the model basidiomycete *Coprinopsis cinerea*, which shares homology with ppos from filamentous ascomycetes. *C. cinerea*, commonly known as the gray shag, is a model multicellular basidiomycete that forms 1-octen-3-ol of various strains and completes its entire life cycle through a sexual cycle within two weeks in the laboratory [18] (Fig. 2). A rich genetic resource, with genome sequences, morphological and developmental mutants, and DNA markers, is available for the mushroom. *C. cinerea* is relatively easy to genetically transform, and a procedure for targeted gene disruption has been established [19]. We characterized the enzymatic properties of recombinant CcDOX1 and CcDOX2 expressed in insect cells. *Ccdox1* gene was disrupted through homologous recombination to confirm its involvement in 1-octen-3-ol formation. The ecophysiological role of 1-octen-3-ol may confer the benefit of sporophyte dispersal by attracting mosquitoes and flies. 1-Octen-3-ol has also been reported to have behavioral suppression and repellent effects on several arthropods and nematodes [20], indicating its potential involvement in the defense against fungivores. However, there is no clear evidence confirming the contribution of 1-octen-3-ol to Basidiomycota. In this study, a *C. cinerea* strain deficient in the ability to form 1-octen-3-ol was used to examine the ecological and/or physiological significance of 1-octen-3-ol.

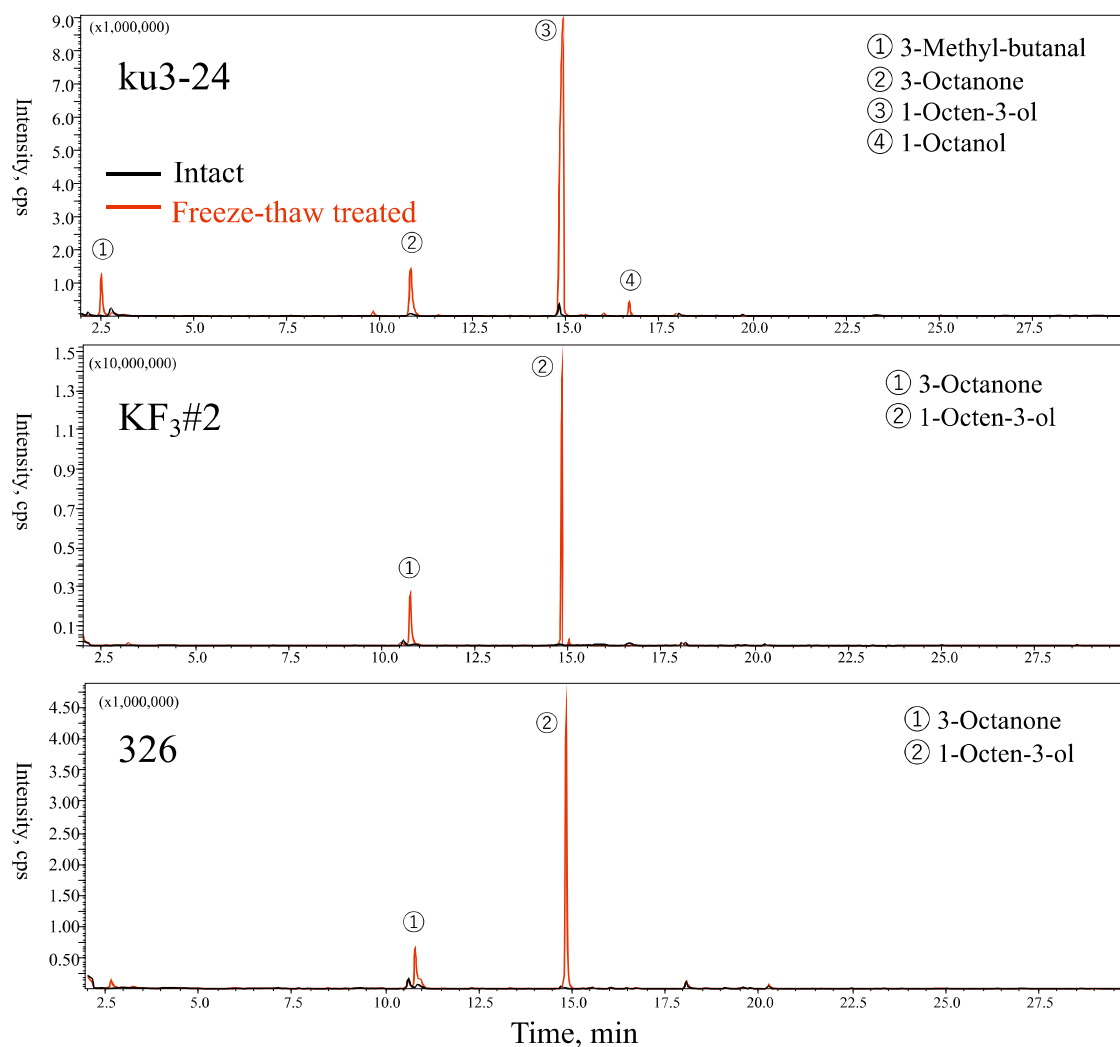


Fig. 2. Formation of 1-octen-3-ol by the mycelia of *Coprinopsis cinerea*.

Representative chromatograms of the volatiles formed from intact and freeze-thaw-treated mycelia (strain ku3-24, KF3#2 and 326). The volatiles in the headspace of a vial containing intact and freeze-thaw treated mycelia were collected with an SPME fiber.

2.2 Results

1-Octen-3-ol Formation in *C. cinerea*

1-Octen-3-ol was barely detected in the intact mycelia of *C. cinerea* (strain ku3-24) grown on yeast extract-malt extract-glucose (YMG) agar plates, but the formation of considerable amounts of 1-octen-3-ol along with 3-octanone, 1-octanol, and 3-methylbutanal was observed within 30 min of damaging the mycelia with freeze-thaw treatment (Fig. 3A). The rapid formation of 1-octen-3-ol was effectively suppressed in the absence of molecular oxygen (Fig. 3B), indicating de novo biosynthesis of 1-octen-3-ol from linoleic acid. Rapid formation of 1-octen-3-ol was also observed when the mycelia were disrupted with a bead crusher, and the formation was suppressed by the addition of Ca²⁺ chelating reagents, such as BAPTA or EGTA (Fig. 3C). Acetylsalicylic acid, a typical cyclooxygenase inhibitor, also suppressed 1-octen-3-ol formation; however, only minimal suppression was observed with the cyclooxygenase inhibitors ibuprofen and mefenamic acid (Fig. 3D).

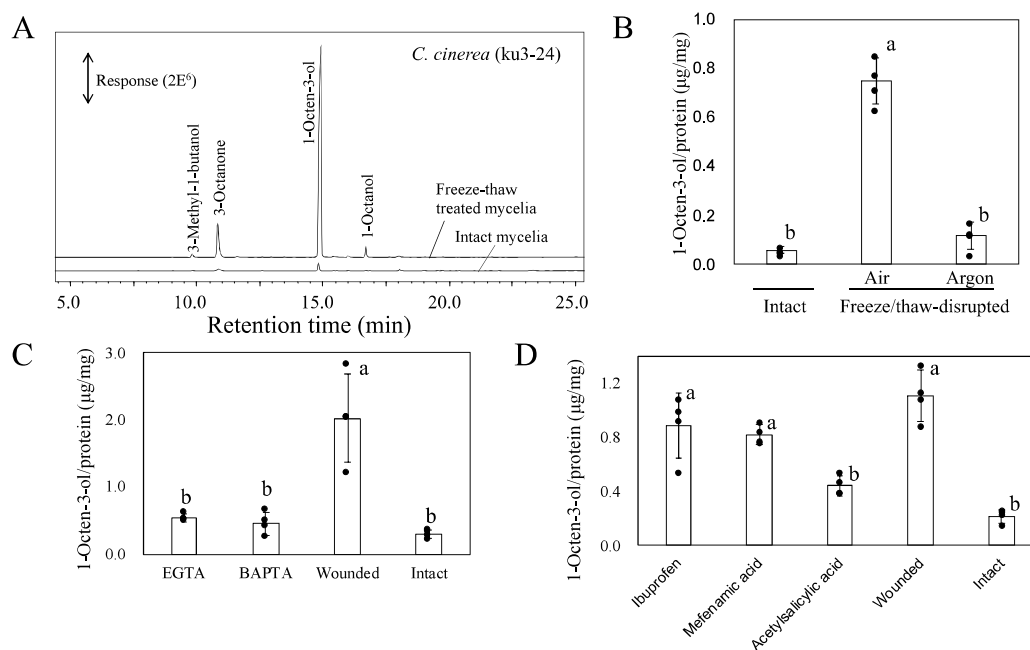


Fig. 3. Formation of 1-octen-3-ol by the mycelia of *Coprinopsis cinerea* (strain ku3-24).

Representative chromatograms of the volatiles formed from intact and freeze-thaw treated mycelia. The volatiles in the headspace of a vial containing intact and freeze-thaw treated mycelia were collected with an SPME fiber (A). Effect of anaerobic condition (B), Ca^{2+} -chelating reagents (EGTA and BAPTA, at 1 mM) (C), and cyclooxygenase inhibitors (at 5 μM) (D) on 1-octen-3-ol formation accelerated by disrupting the mycelia. For these analyses, 1-octen-3-ol was extracted with MTBE for quantification with GC-MS analyses. The amount of 1-octen-3-ol is presented as mean \pm SD (error bar, $n = 3$). The different letters indicate significant differences, as identified using one way ANOVA and least squares method; $P < 0.05$. MTBE, methyl *tert*-butyl ether; SPME, solid-phase microextraction.

***C. cinerea* Dioxygenases**

Because Ppo and lipoxygenase (LOX) have been reported in fungi as enzymes catalyzing the dioxygenation of fatty acids to yield the hydroperoxide derivative [10], we assumed that an enzyme similar to Ppo or LOX participated in the first fatty acid oxygenation step in the biosynthetic pathway to form 1-octen-3-ol. When manganese LOX in the filamentous ascomycete *Gaeumannomyces graminis var. avenae* (oat-take-all root rot fungus) (GenBank, AAK81882.2) [21] was used as a query for BLASTP search with the *C. cinerea* genome database (*Coprinopsis cinerea* AmutBmut pab1-1 v1.0 in MycoCosm) [22], no protein with a substantial similarity was detected. When the same BLASTP search was performed with *A. nidulans* PpoC protein (AAT36614) as the query, two proteins with protein IDs 423716 and 398037 (GenBank: EAU90460.2 and EAU86789.2, respectively) were found, with E-values smaller than $1.0e^{-100}$. They were tentatively named CcDOX1 and CcDOX2. CcDOX1 and CcDOX2 are 1066 and 1118 amino acids long, respectively, and share 38% identity and 54% homology. TargetP-2.0 analyses (<http://www.cbs.dtu.dk/services/TargetP/>) showed that both proteins contained neither a signal peptide nor a mitochondrial transit peptide. InterProScan (<https://www.ebi.ac.uk/interpro/search/sequence/>) with CcDOX1 indicated that it consists of an N-terminal domain belonging to the animal heme peroxidase family (IPR037120) and a C-terminal domain that was classified as a sequence homologous to the cytochrome P450 superfamily (IPR036396), although the sequence was not classified as a member of any protein family specified in InterPro (Fig. 4A). This was mostly the case with CcDOX2, but a short segment of its C-terminal domain was classified as a member of the cytochrome P450 family (IPR001128) (Fig. 4A). The catalytic Tyr (Tyr-395 and Tyr-407 in CcDOX1 and CcDOX2, respectively) and distal and proximal His (His-217/His-398 and His-227/His-410 in CcDOX1 and CcDOX2, respectively) essential for binding heme are highly conserved as found with animal COXs [23] (Fig. 5). They are conserved at the apparently suitable positions in the protein sequences in the N-terminal domains of CcDOX1/2. The Arg residue critical for binding fatty acid substrates (Arg-106 in mouse COX2) was not found, and Ser, which is the target of non-steroidal anti-inflammatory drugs (Ser-516 in mouse COX2) [23], was replaced with Thr in CcDOX1/2 (Fig. 5).

The signature of the C-terminal domain of P450 is not distinct. The ExxR motif [24], which is one of the most conserved residues in the K-helix of Cyt P450 enzymes, is conserved in CcDOX1/2; however, the heme signature motif (FxxGx(H/R)xCxG motif) [24] is quite different in CcDOX1/2. For example, the His residue, which has been shown

to be essential for hydroperoxide isomerase activity in *A. nidulans* PpoA (His1004) [24], and the Cys residue, crucial for P450 activity as the fifth heme iron ligand through the heme-thiolate bond [25], are replaced by Phe/Thr and Tyr/Leu in CcDOX1/2, respectively (Fig. 6). Substitution of these amino acid residues, which are essential for P450 catalysis, is also evident in *A. nidulans* PpoC, which has no ability to rearrange the fatty acid hydroperoxide depending on P450 catalysis [13]. Hereafter, the C-terminal domains of CcDOX1/2 is referred to as P450-related domains.

The CcDOX1 sequence was used as a query for BLASTP analyses in MycoCosm [22] against the protein databases of the genome sequences of representative species belonging to diverse classes in Basidiomycota, namely, *A. bisporus* (Agaricales), *Pleurotus ostreatus* (Agaricales), *Schizophyllum commune* (Agaricales), *Rhizoctonia solani* (Cantharellales) [17], *Serpula lacrymans* (Boletales), *Fomitopsis pinicola* (Polyporales), *Rickenella mellea* (Rickenella), and *Ustilago maydis* (Ustilaginomycotina) [16]. Proteins with a significant similarity ($< 1.0e^{-5}$) were chosen and a phylogenetic tree was constructed along with the protein sequences of representative DOX-P450 fusion proteins (Ppos) from Ascomycota (Fig. 4B) [26]. The proteins were divided into four major clades (clade I to IV), three of which (clade I, II, and III) consisted of proteins in Ascomycota, and the other one (clade IV) consisted of those in Basidiomycota. The proteins found in Basidiomycota were further divided into three major clades (subclades a, b, and c), where CcDOX1 and CcDOX2 were located in subclades a and b, respectively. The proteins in subclades a and b had the N-terminal DOX domain and the C-terminal P450-related domain. The heme signature motifs (FxxGx(H/R)xCxG) of almost all of the proteins in subclades a and b were not conserved (Fig. 7). The C-terminal domains of those in subclade c consisted of proteins that harbored an apparently complete heme signature motif. Ssp1 protein is highly expressed in the teliospores of *Ustilago maydis* (Ustilaginomycotina) (AAL38020.1) [16] and did not belong to any subclade.

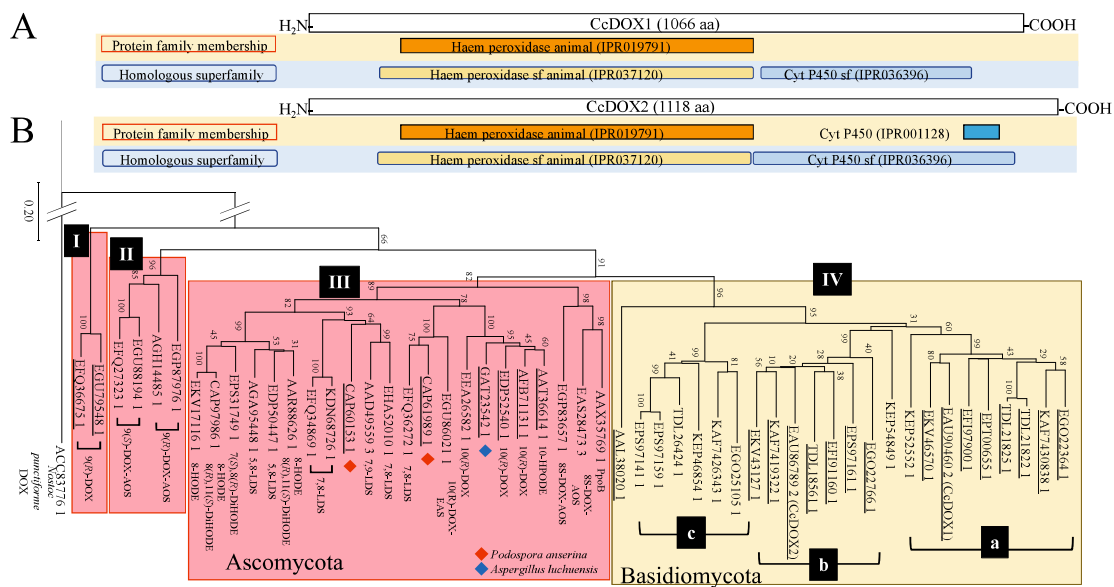


Fig. 4. Characterization of CcDOX1 and CcDOX2 sequences.

Schematic representation of their domain structures identified with InterProScan. The two categories, protein family category and homologous superfamily, are shown (A). Phylogenetic analysis of CcDOX1 and CcDOX2 with the DOX-related proteins from different species belonging to Ascomycota and Basidiomycota. Phylogenetic analysis was performed with MEGA X using the maximum likelihood method. The details of the sequences used here are shown in Table 2. CcDOX1 and CcDOX2 are highlighted with an orange background. The proteins encoded by *ppoC-like* genes that were proposed to be involved in 1-octen-3-ol formation in *Podospora anserina* (red diamonds) and *Aspergillus luchuensis* (blue diamond) are also highlighted. The proteins lacking either or both the His and the Cys in the heme signature motif (FxxGx(H/R)xCxG motif) are underlined. The cyanobacterial (*Nostoc punctiforme*) DOX is used as the outgroup. Each clade is named as I, II, III, and IV. The clade IV is further divided into three sub-clades, a, b, and c (B).

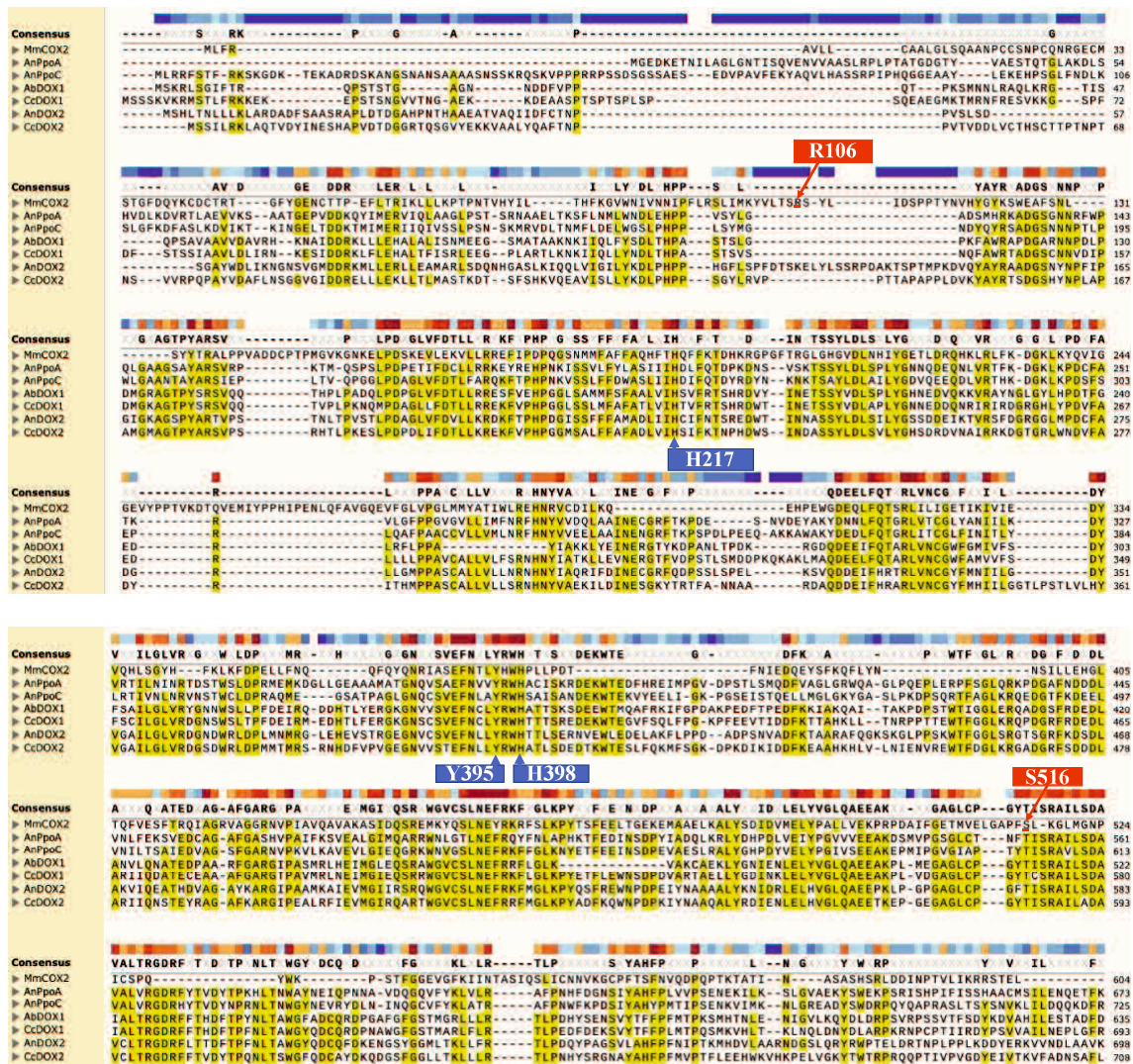


Fig. 5. Alignment of the N-terminal DOX domains of *A. nidulans* AnPpoA (GenBank; AAR88626.1), AnPpoC (AAT36614.1), *C. cinerea* CcDOX1 (EAU90460.2), CcDOX2 (EAU86789.2), *Agaricus bisporus* AbDOX1 (EKV46570.1), AbDOX2 (EKV43127.1), and mouse (*Mus musculus*) MmCOX2 (Q05769.1). The amino acid residues described in the text are indicated by colored arrows with numbering based on the CcDOX1 (blue background) and MmCOX2 (red background) sequences, respectively.

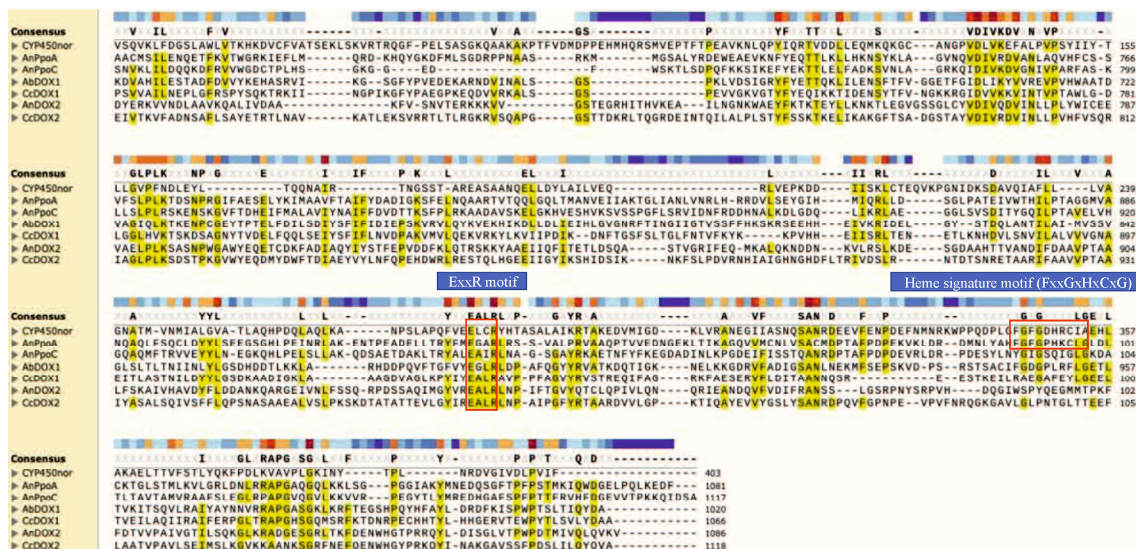


Fig. 6. Alignment of the C-terminal cytochrome P450 domains of AnPpoA, AnPpoC, CcDOX1, CcDOX2, AbDOX1, AbDOX2, and *Fusarium oxysporum* CYP450nor (P23295.2). The ExxR motif widely conserved in P450 enzymes and the heme signature motif (FxxGxHxCxG) essential for P450 activities are highlighted.

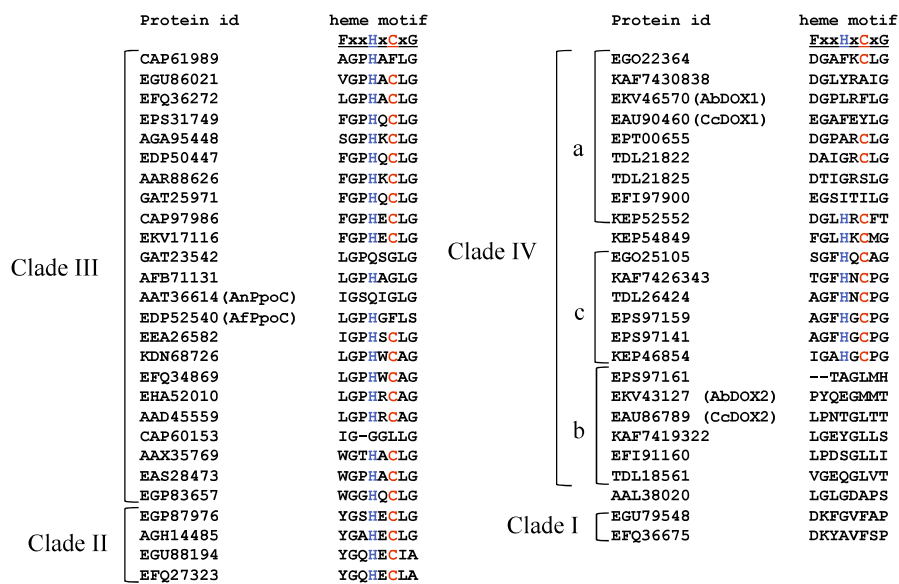


Fig. 7. Alignment of the heme signature motif (FxxGxHxCxG) from the protein sequences used for the construction of the phylogenetic tree shown in Fig. 4B.

Enzymatic Properties of CcDOX1 and CcDOX2

It has been reported that recombinant *A. nidulans* PpoC (AnPpoC) is unstable when the enzyme is expressed in *E. coli* [13]. It has also been reported that recombinant *Gaeumannomyces graminis* linoleate diol synthase (GgLDS) expressed with *Pichia pastoris* showed a product specificity different from that observed for the enzyme prepared from the mycelia of *G. graminis* [27], while recombinant GgLDS expressed with insect cells (Sf9) showed the same product specificity [28]. Accordingly, in this study, we chose insect cells as the host for expression of recombinant CcDOXs. Recombinant proteins encoded by *Ccdox1* and 2 were transiently expressed in BmN4 cells derived from the silkworm *Bombyx mori* with or without enhanced green fluorescence protein (EGFP) fused at their C-terminals. To evaluate the enzymatic activity of the recombinant proteins, the cell lysate expressing the respective proteins was reacted with linoleic acid, and the products were analyzed in the negative-enhanced mass spectrum mode of LC-MS/MS. Chromatograms were drawn by extracting the molecular ions or fragment ions associated with the oxygenated products of linoleic acid, such as hydroperoxides, hydroxides, diols, or epoxyalcohols, which were expected based on the reaction of the Ascomycota Ppo enzymes [10]. Accordingly, the formation of the hydroperoxide derivative of linoleic acid (m/z 293, $[C_{18}H_{32}O_4-H_3O^+]$) and the hydroxide of linoleic acid (m/z 295, $[C_{18}H_{32}O_3-H^+]$) was evident in the crude lysate prepared from the insect cells expressing all four recombinant CcDOXs (CcDOX1 or CcDOX2, with/without EGFP) (Fig. 8). No sign suggestive of compounds other than hydroperoxide and hydroxide of linoleic acid was detected. Peaks 3 and 6 apparent with m/z 295 were tentatively assigned as 10- and 8-hydroperoxide of oleic acid ($[C_{18}H_{34}O_4-H_3O^+]$), respectively (Fig. 9). They were not detected when purified CcDOX1/2 was reacted with linoleic acid. They were most likely formed from oleic acid endogenous to insect cells. Interestingly, the hydroperoxides of oleic acid were not found in the insect cells before disruption. This suggests that either the recombinant CcDOXs in the insect cells were in latent states and were activated upon cell disruption, or that the hydrolysis of membrane lipids facilitated by cell disruption supplied free oleic acid as a substrate for the recombinant CcDOXs. Based on the chromatograms, fusion of the EGFP sequence to the C-terminus of either CcDOX1 or CcDOX2 had little effect on the activity and product specificity of the reaction. The hydroxides were likely formed by unknown components derived from the cell lysates, because the reduction was not observed when purified CcDOX1/2 was used for product analysis.

Recombinant CcDOX1 and CcDOX2 proteins were purified by immunoprecipitation with an anti-GFP antibody (Fig. 11). Linoleic acid was added to the purified recombinant CcDOX1 and CcDOX2, and the products were extracted, reduced with triphenylphosphine, and analyzed by LC-MS/MS in the negative enhanced product ion mode (Fig. 10). With this analysis, a peak tentatively assigned as 10- or 8-hydroxides of linoleic acid based on the fragment ion diagnostic to the position of the hydroxide group [7] was detected as the product formed by CcDOX1 or CcDOX2, respectively.

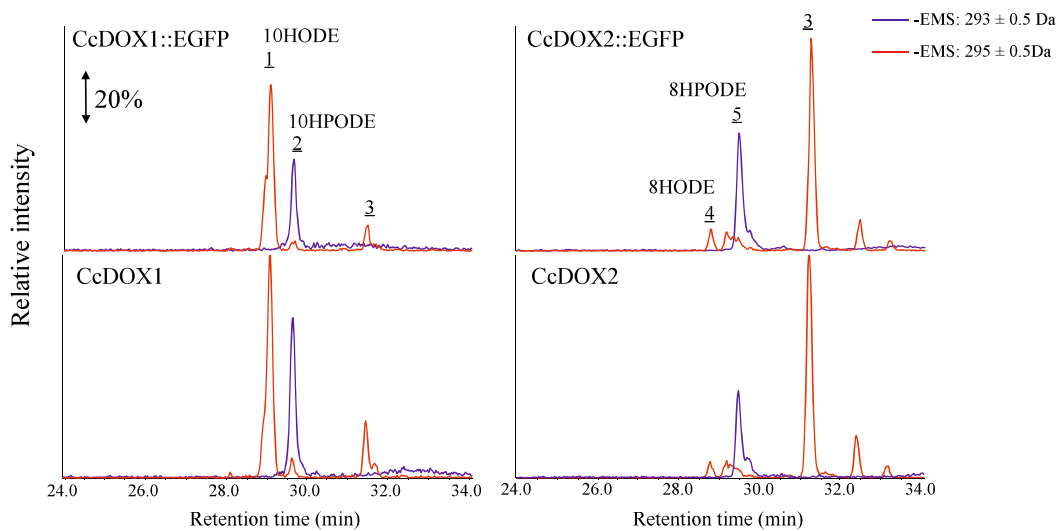


Fig. 8. Products formed by insect cell-expressed recombinant CcDOX1 and CcDOX2 with/without EGFP. The lysate of insect cells expressing CcDOX1, CcDOX1 fused with EGFP (CcDOX1::EGFP), CcDOX2, and CcDOX2 fused with EGFP (CcDOX2::EGFP) were reacted with linoleic acid, and the products were analyzed in the negative enhanced mass spectrum mode of LC-MS/MS. Chromatograms of extracted ions of m/z 293.0 ± 0.5 corresponding to linoleic acid hydroperoxide $[M-H_3O^+]$ and m/z 295.0 ± 0.5 corresponding to linoleic acid hydroxide $[M-H^+]$ are shown in blue and red, respectively. Peak 1 and 2 were tentatively assigned as 10HODE and 10HPODE, respectively. Peak 4 and 5 were as 8HODE and 8HPODE. The conversion of hydroperoxide into hydroxide was likely catalyzed by unknown enzyme in the insect cells. Peak 3 is unknown compound.

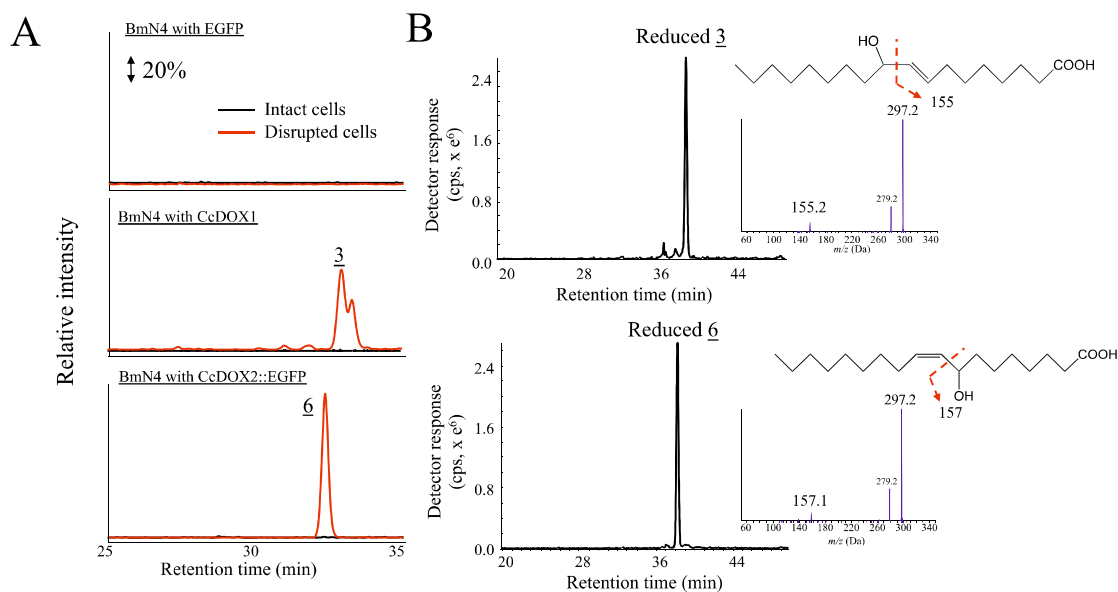


Fig. 9. Products formed by the insect cells (BmN4) expressing EGFP, CcDOX1::EGFP, or CcDOX2::EGFP. The intact cells (black line) or the cells after disruption with a sonicator (red line) were extracted with ethanol for LC-MS/MS analysis in the negative enhanced mass spectrum. Chromatograms of extracted ions of m/z 295.0 ± 0.5 corresponding to oleic acid hydroxide $[C_{18}H_{34}O_4-H_3O^+]$ are shown (A). The products formed in the disrupted insect cells containing recombinant CcDOX1 (upper) and CcDOX2 (lower) were reduced with triphenylphosphine, and served for LC-MS/MS analysis in the enhanced product ion mode with m/z 297.3 $[C_{18}H_{34}O_3-H^+]$ as the parent ion. Based on the fragment profiles, reduced 3 and reduced 6 were tentatively assigned as 10- and 8-hydroxide of oleic acid, respectively (B).

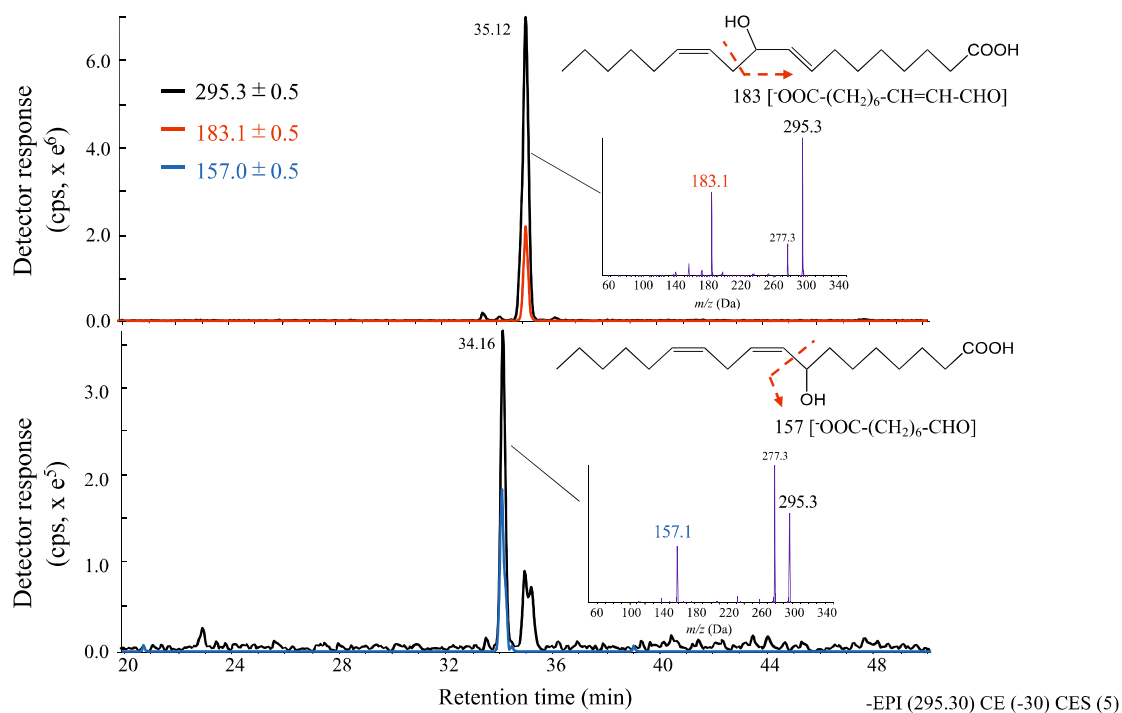


Fig. 10. Chromatograms with the products formed by immuno-purified recombinant CcDOX1::EGFP (upper) and recombinant CcDOX2::EGFP (lower) from linoleic acid obtained with LC-MS/MS in the negative enhanced product ion mode. The products were reduced with triphenylphosphine before analysis. The negative ion of m/z 295.30 corresponding to the hydroxides of linoleic acid $[M-H^+]$ was chosen as the parent ion. The black line is shown with total ion derived from the parent ion, and the red and blue lines are drawn with m/z 183.1 and m/z 157.1, corresponding the fragment ions diagnostic to 10- and 8-hydroxides of linoleic acid. Mass spectrum for each main peak are shown in the insets with expected fragmentation pattern.

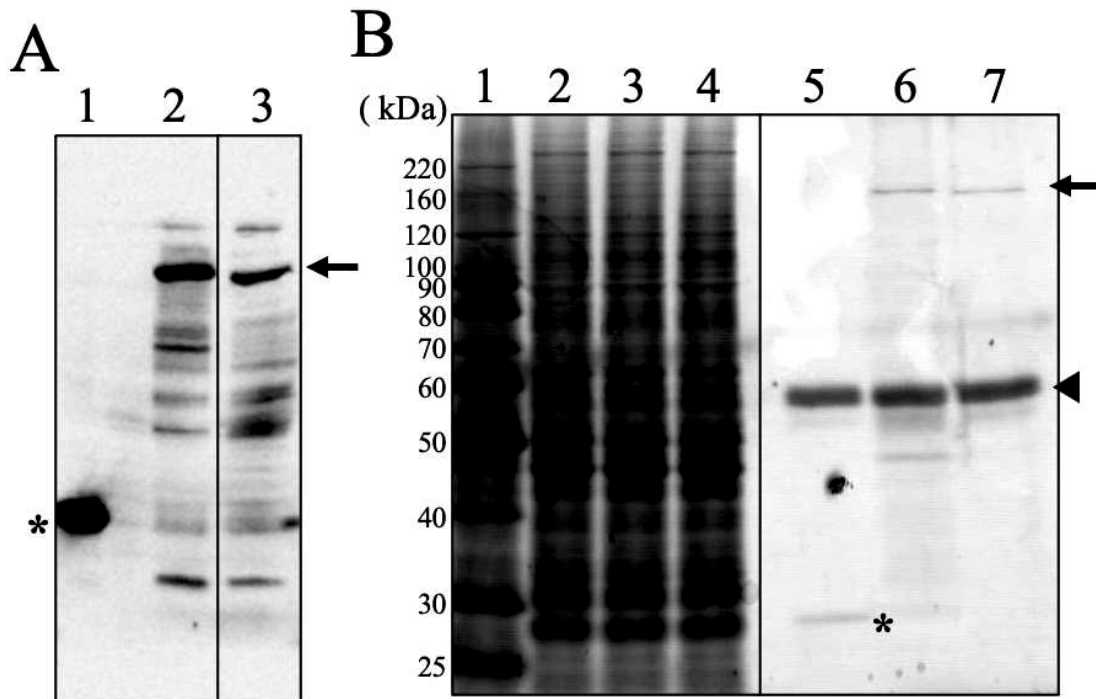


Fig. 11. Expression of recombinant CcDOX1 and CcDOX2 in BmN4 cells. (A) Immunoblot analysis with crude extract expressing EGFP (shown with an asterisk in lane 1, ca. 27 kDa), CcDOX1::EGFP fusion protein (lane 2), and CcDOX2::EGFP fusion protein (lane 3). The arrow indicates the protein bands corresponding to the fusion proteins. (B) Silver-staining of the crude extract expressing EGFP (lane 2), CcDOX1::EGFP fusion protein (lane 3), CcDOX2::EGFP fusion protein (lane 4), immunoprecipitated fraction of the lysate expressing EGFP only (lane 5), immune-purified CcDOX1::EGFP fusion protein (lane 6), and immune-purified CcDOX2::EGFP fusion protein (lane 7). The positions of the fusion protein (147 kDa) and the heavy chain of rabbit immunoglobulin (ca. 50 kDa) used for purification are shown with an arrow and a triangle, respectively. The asterisk in the lane 5 indicates the protein bands corresponding to EGFP. Lane 1: molecular weight marker.

Expression of *Ccdoxs*

To examine the expression of *Ccdox* genes, *C. cinerea* was grown in liquid YMG medium in a static culture. The mycelia grew rapidly under the growth conditions used, and the growth reached a plateau at 4 days after inoculation (Fig. 12A). The amount of 1-octen-3-ol produced by freeze-thaw treatment gradually increased from day 4, it reached a peak on day 12, and then decreased thereafter (Fig. 12B). The transcript level of *Ccdox1* mostly followed the amount of 1-octen-3-ol but remained high even on day 16 (Fig. 12C). The developmental time course of *Ccdox2* expression was distinct from those of *Ccdox1* and of the 1-octen-3-ol formation ability. The expression level of *Ccdox2* reached a peak at 8 days after transplanting. Thereafter, levels decreased to almost undetectable levels on day 16.

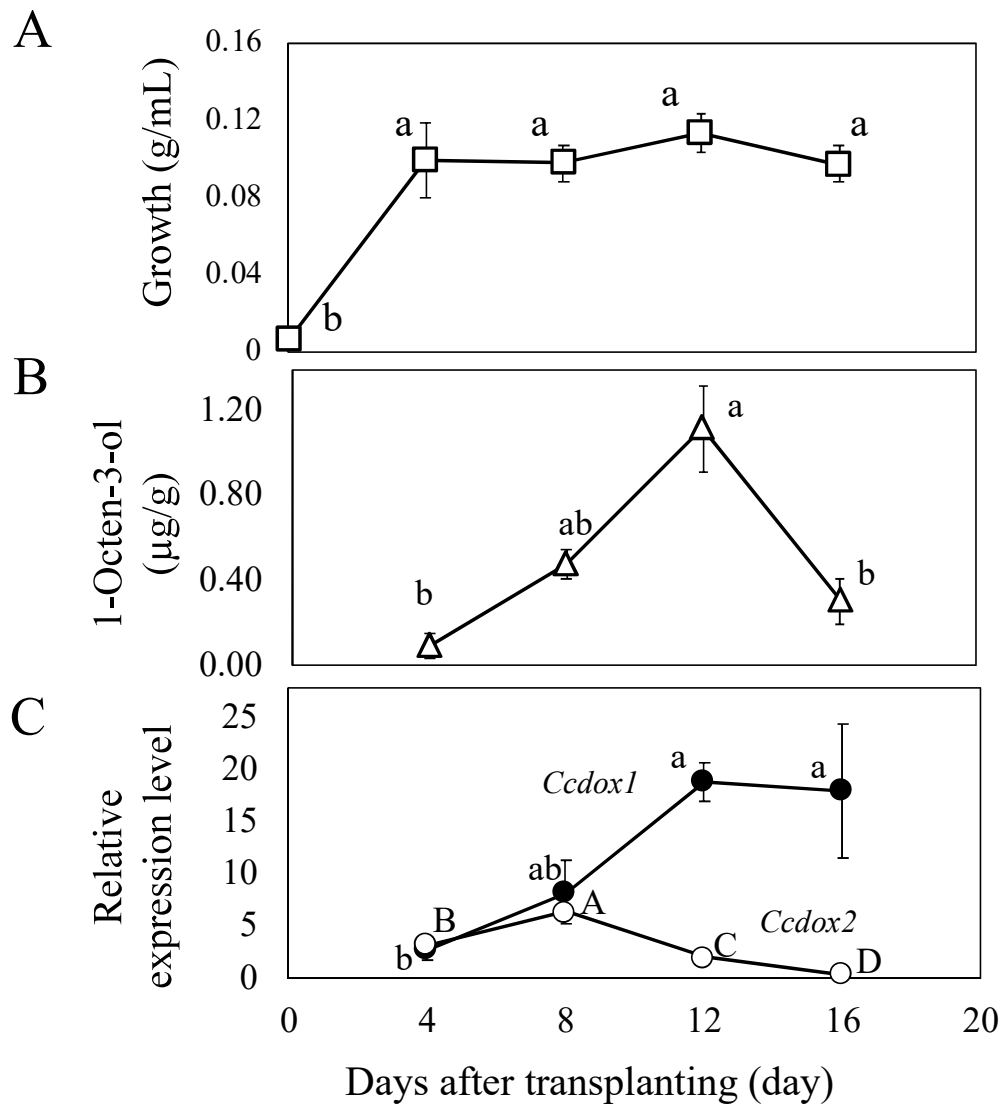


Fig. 12. Changes in 1-octen-3-ol forming ability and *Ccdox* gene expression with growth. Developmental time course of growth (A), the amount of 1-octen-3-ol after freeze-thaw treatment (B), and expression level of *Ccdox1* and *Ccdox2* genes (C) in *C. cinerea* mycelia grown under a static liquid YMG media are shown. *C. cinerea* mycelia were inoculated into YMG liquid media and grown for 16 days. 1-Octen-3-ol was extracted with MTBE for GC-MS analysis. The relative expression levels of *Ccdox1* and *Ccdox2* were determined by RT-qPCR by using β -tubulin as a reference gene. The means \pm SD (error bar, $n = 3$) are shown. The different letters indicate significant differences, as identified using one way ANOVA with Fisher's least significant difference; $P < 0.05$. MTBE, methyl *tert*-butyl ether; RT-qPCR, reverse transcription–quantitative PCR; YMG, yeast extract-malt extract-glucose.

Properties of Recombinant CcDOX1

As the expression profile of *Ccdox1* gene and the result that the main product of the recombinant CcDOX1 from linoleic acid was tentatively assigned as 10HPODE, which was reported to be the intermediate in the biosynthetic pathway to form 1-octen-3-ol in basidiomycetes, CcDOX1 was chosen for further extensive analysis. We used tandem mass spectrometry analysis in the presence of sodium ions, and each isomer of the fatty acid hydroperoxide was identified and quantified using the corresponding authentic specimen [29, 30]. The main product formed from linoleic acid by immunopurified recombinant CcDOX1-EGFP was confirmed to be 10HPODE (Fig. 13A). Other isomers, such as 9, 12, and 13HPODE (Table 1), were barely detected. The positional specificity in terms of the oxygen insertion was strict, and 10-hydroperoxides were the major product, even with oleic acid or α -linolenic acid. Using chiral phase chromatography [31], the two enantiomers of 10HPODE prepared by photo-oxidation of linoleic acid were separated (Fig. 9B). The product formed by recombinant CcDOX1 from linoleic acid showed only one peak with the same retention time as that of 10(*S*)HPODE prepared with recombinant *Nostoc punctiforme* dioxygenase (NpDOX) (Fig. 13B) [32]. Based on the amino acid sequence of CcDOX1 and the 3D structure of CcDOX1 predicted by AlphaFold2 [33], the binding point between the N-terminal DOX domain and the C-terminal P450 domain of CcDOX1 was inferred to be Asn670 and Pro671 (Fig. 14). When only the N-terminal DOX domain (Met1 to Asn670) of CcDOX1, excluding the C-terminal P450-related domain, was fused to EGFP and expressed in insect cells, no activity for the formation of 10HPODE from linoleic acid was detected (Fig. 15). In addition, while normal CcDOX1 was localized in the cytoplasm in insect cells, CcDOX1 with only the DOX domain was also found to be localized in the nucleus (Fig. 16). When the enzyme activity was evaluated based on oxygen consumption, CcDOX1 showed the highest activity with linoleic acid, with a lower but still substantial activity with oleic acid and α -linolenic acid (46.6 ± 6.2 and $50.8 \pm 6.5\%$, respectively, when compared to linoleic acid; Fig. 17). The [S]-v plot obtained with linoleic acid was fitted to the Hill equation with the Hill coefficient (n) of 1.9 ± 0.27 and K_A value of $78 \pm 9.74 \mu\text{M}$ (Fig. 18).

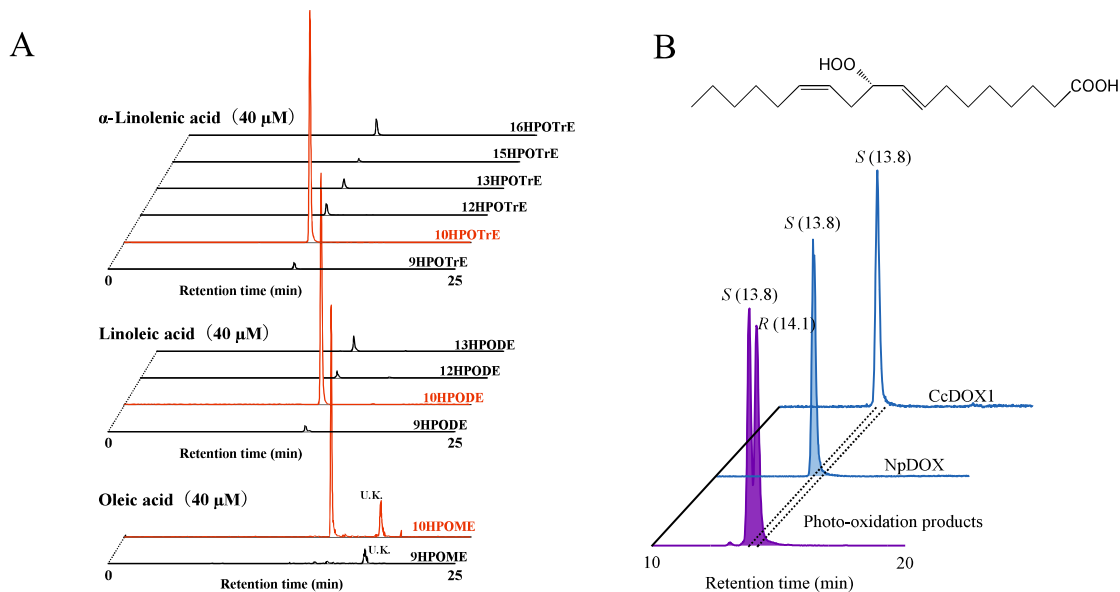
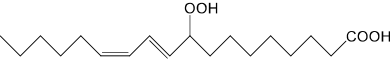
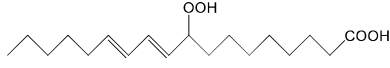
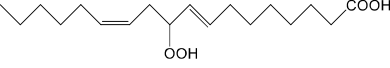
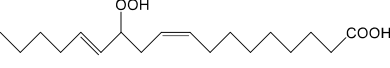
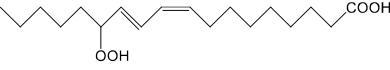


Fig. 13. LC-MS/MS analysis of the reaction products of recombinant CcDOX1. Positive ionization of the hydroperoxides as their Na^+ -adducts were performed. A, the products from α -linolenic acid (top), linoleic acid (center), and oleic acid (bottom) were monitored with MRM transition specific to the hydroperoxides shown on each chromatogram. The detailed parameters for the MRM analysis are shown in Table 3. B, chiral phase separation of 10-hydroperoxide of linoleic acid. 10-Hydroperoxides formed by photo-oxidation reaction (front), by *Nostoc punctiforme* dioxygenase (NpDOX) (center), and by recombinant CcDOX1 (back) were analyzed. The structure of (8*E*,12*Z*)-10(*S*)-hydroperoxyoctadeca-8,12-dienoic acid (10(*S*)HPODE) is shown at the top. HPODE, hydroperoxide of linoleic acid; HPOME, hydroperoxide of oleic acid; HPOTrE, hydroperoxide of α -linolenic acid; U.K., unknown; MRM, multiple reaction monitoring.

Table 1. Product composition formed by recombinant CcDOX1-EGFP from linoleic acid.

Structure	IUPAC Name	Relative abundance (%)
	(10 <i>E</i> ,12 <i>Z</i>)-9-Hydroperoxyoctadeca-10,12-dienoic acid	15.1
	(10 <i>E</i> ,12 <i>E</i>)-9-Hydroperoxyoctadeca-10,12-dienoic acid	1.80
	(8 <i>E</i> ,12 <i>Z</i>)-10-Hydroperoxyoctadeca-8,12-dienoic acid	61.2
	(9 <i>Z</i> ,13 <i>E</i>)-12-Hydroperoxyoctadeca-9,13-dienoic acid	4.73
	(9 <i>Z</i> ,12 <i>E</i>)-13-Hydroperoxyoctadeca-9,12-dienoic acid	15.2
	(9 <i>E</i> ,12 <i>E</i>)-13-Hydroperoxyoctadeca-9,12-dienoic acid	1.95

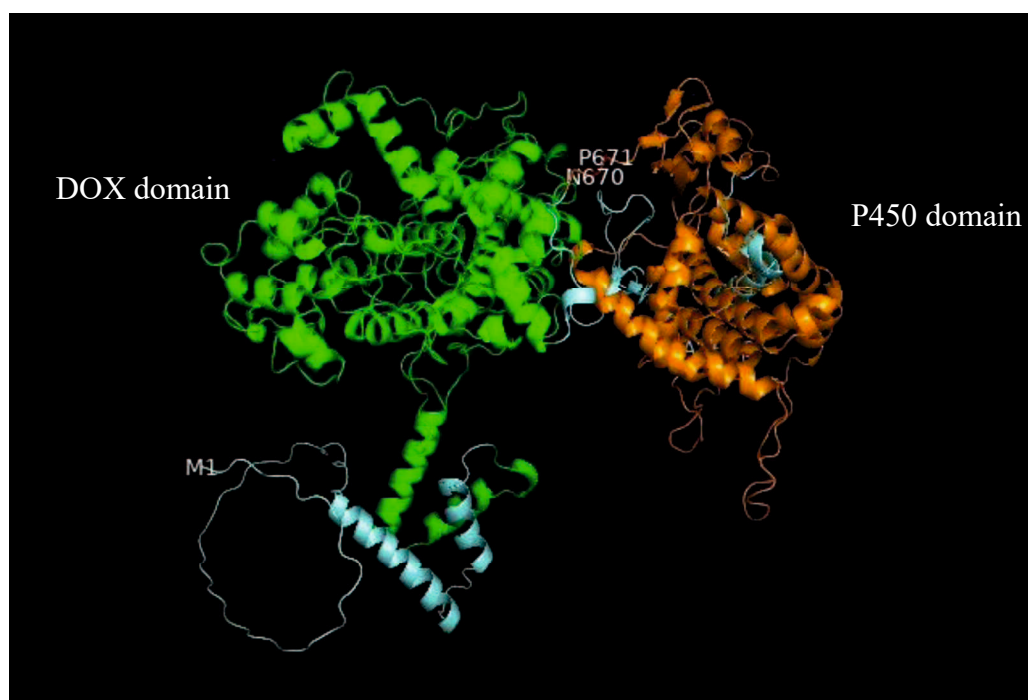


Fig. 14. Structural of the CcDOX1 protein predicted with AlphaFold2. The DOX domains are shown in green and the P450 domains in orange. The junction between the N-terminal DOX domains and the C-terminal P450 domains of CcDOX1 is assigned as between Asn670 and Pro671.

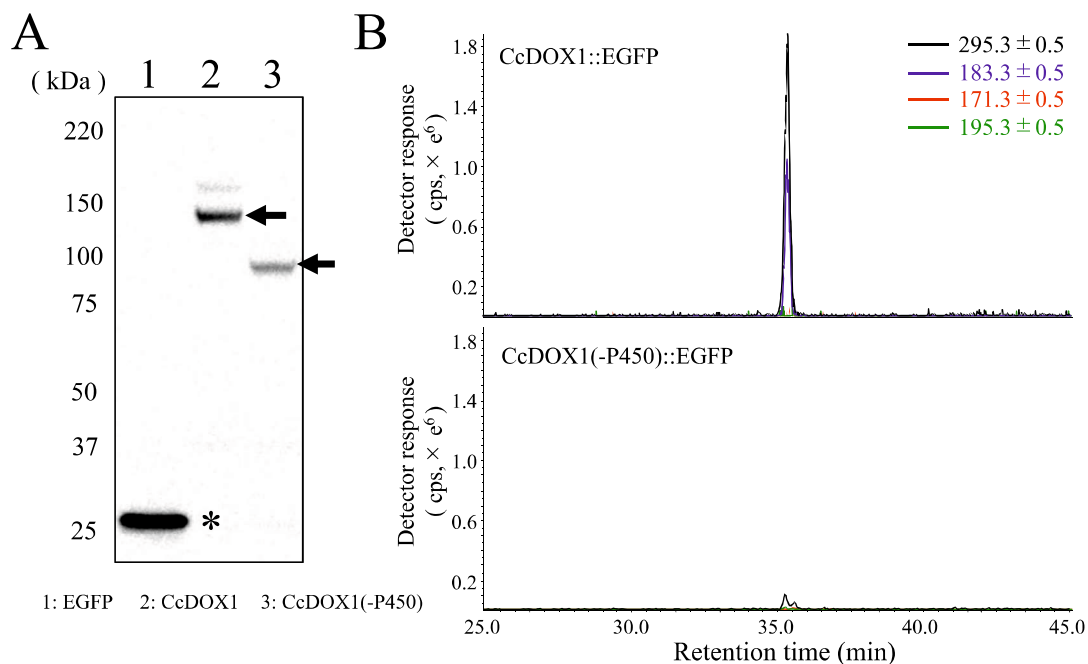


Fig. 15. Deletion of the C-terminal P450-related domain from CcDOX1 resulted in loss of activity. (A) Immunoblot analysis with the immune-purified EGFP (shown with an asterisk in lane 1, ca. 27 kDa), CcDOX1::EGFP fusion protein (lane 2), and CcDOX1 without P450-related domain::EGFP fusion protein (lane 3). The arrow indicates the protein bands corresponding to the fusion proteins. (B) Chromatograms with the products formed by immuno-purified recombinant CcDOX1::EGFP (upper) and immuno-purified recombinant CcDOX1 without P450-related domain (CcDOX1(-P450)::EGFP (lower) from linoleic acid. The chromatograms were obtained with LC-MS/MS in the negative enhanced product ion mode. The products were reduced with triphenylphosphine before analysis. The negative ion of m/z 295.30 corresponding to the hydroxides of linoleic acid $[M-H]^-$ was chosen as the parent ion. The black line is shown with the parent ion, and the blue, red, and green lines are drawn with m/z 183.1, m/z 171.1, and m/z 195.1, corresponding the fragment ions diagnostic to 10-, 9-, and 13-hydroxides of linoleic acid.

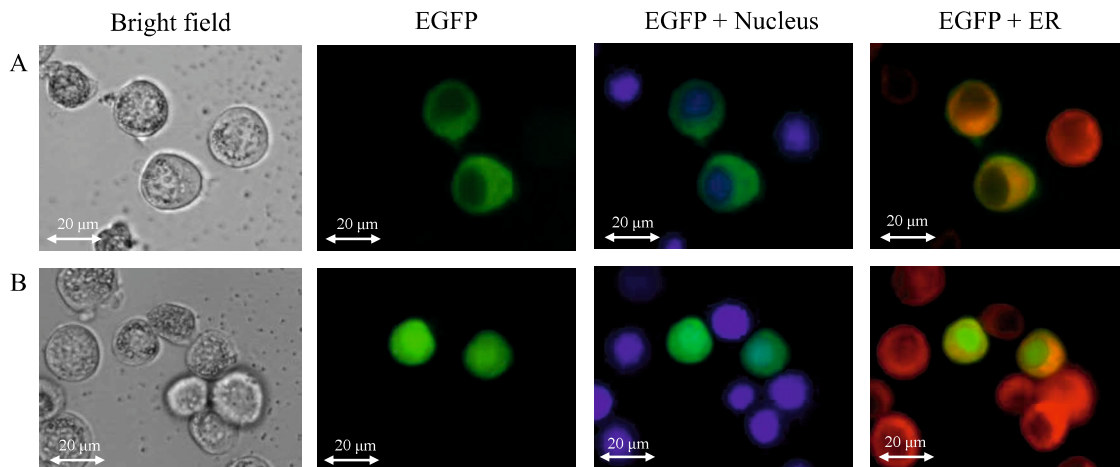
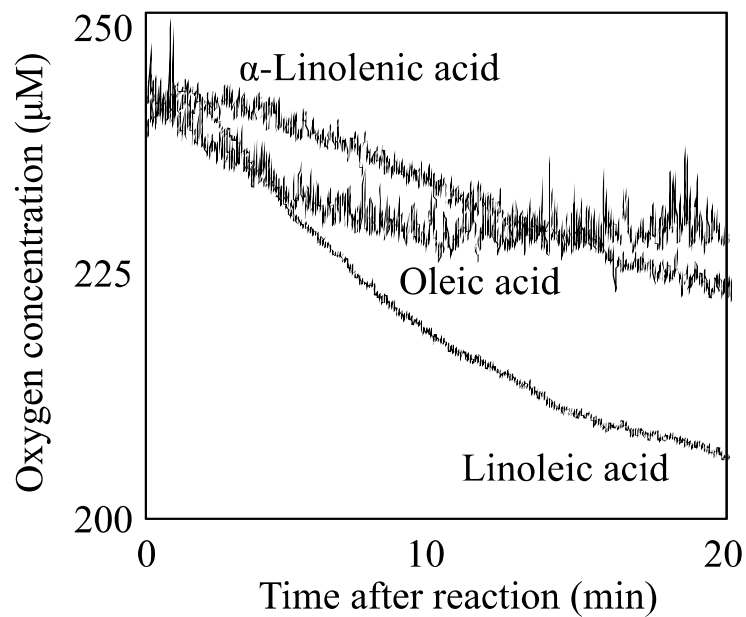


Fig. 16. Subcellular localization of the CcDOX1 protein in insect cells.

Fluorescence signals from the insect cells expressing the CcDOX1-GFP construct were observed under fluorescent dissection microscope (A). Fluorescence signals from the insect cells expressing the CcDOX1₁₋₆₇₀-GFP construct, which encoded only the N-terminal DOX domain of CcDOX1 (B).



Linoleic acid	Oleic acid	α -Linolenic acid
100%	$46.6 \pm 6.2\%$	$50.8 \pm 6.5\%$

Fig. 17. The enzyme activity of CcDOX1 monitored by oxygen consumption.

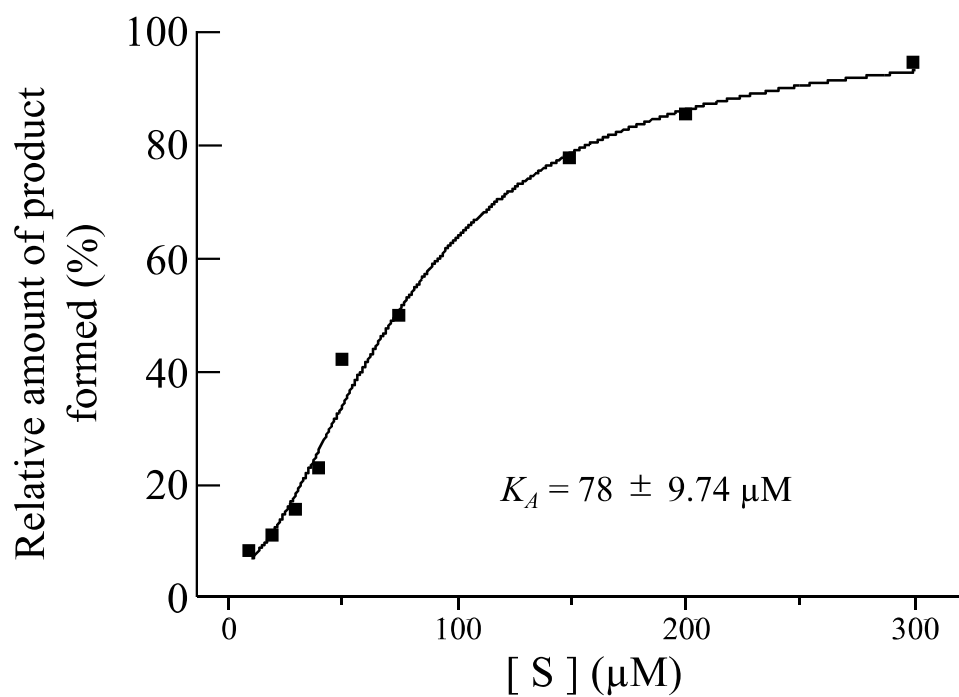


Fig. 18. Hill plot of recombinant CcDOX1 with linoleic acid. The relative peak area obtained with LC-MS/MS with negative enhanced MS mode was plotted (100%, when compared to area of Vmax).

Disruption of *Ccdox1*

The function of *Ccdox1* was disrupted via homologous recombination [34] in the *C. cinerea* ku3-24 strain. Two knockout lines of the *Ccdox1* gene were obtained (Fig. 19). Solid-phase microextraction (SPME)-GC/MS analysis after mycelial freeze-thaw treatment showed that the ability to form 1-octen-3-ol was highly suppressed in both knockout lines (Fig. 19). Line #1 was used for further experiments. When wild-type *C. cinerea* (ku3-24) was cultured in YMG agar medium, 1-octen-3-ol accumulated slightly in the intact mycelia on day 5 of culture and then increased by day 13 (Fig. 20). With mycelia from both of these culture days, 1-octen-3-ol increased markedly after freeze-thaw treatment (Fig. 20). In the $\Delta Ccdox1$ strain, both the rapid formation of 1-octen-3-ol after freeze-thaw treatment of mycelia and the constant formation in intact mycelia were highly suppressed (Fig. 11, inset). The growth of $\Delta Ccdox1$ mycelia was slightly better than that of the parent line (ku3-24) (Fig. 21). Both strains set fruiting bodies with no apparent differences in morphology and timing (Fig. 21).

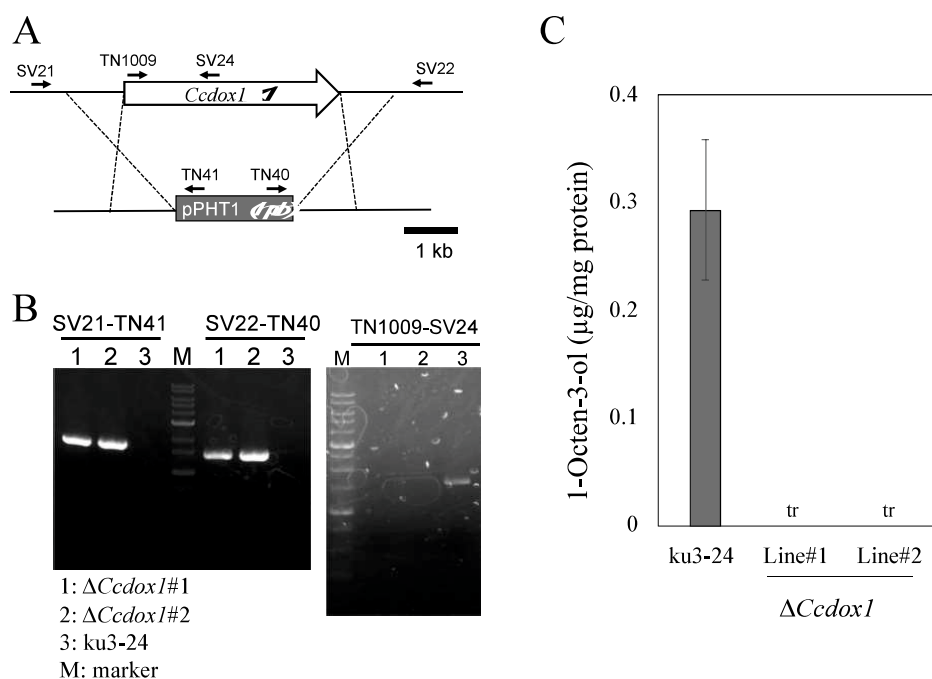


Fig. 19. Disruption of *Ccdox1* gene. Schematic diagram of gene disruption through homologous recombination. Primers used for the PCR reactions are shown (A). PCR analysis to confirm the deletion of *Ccdox1* using genomic DNA as template. The primer sets used in this study are shown in Table 4 (B). Amount of 1-octen-3-ol formed by the ku3-24 and two $\Delta Ccdox1$ strains (C).

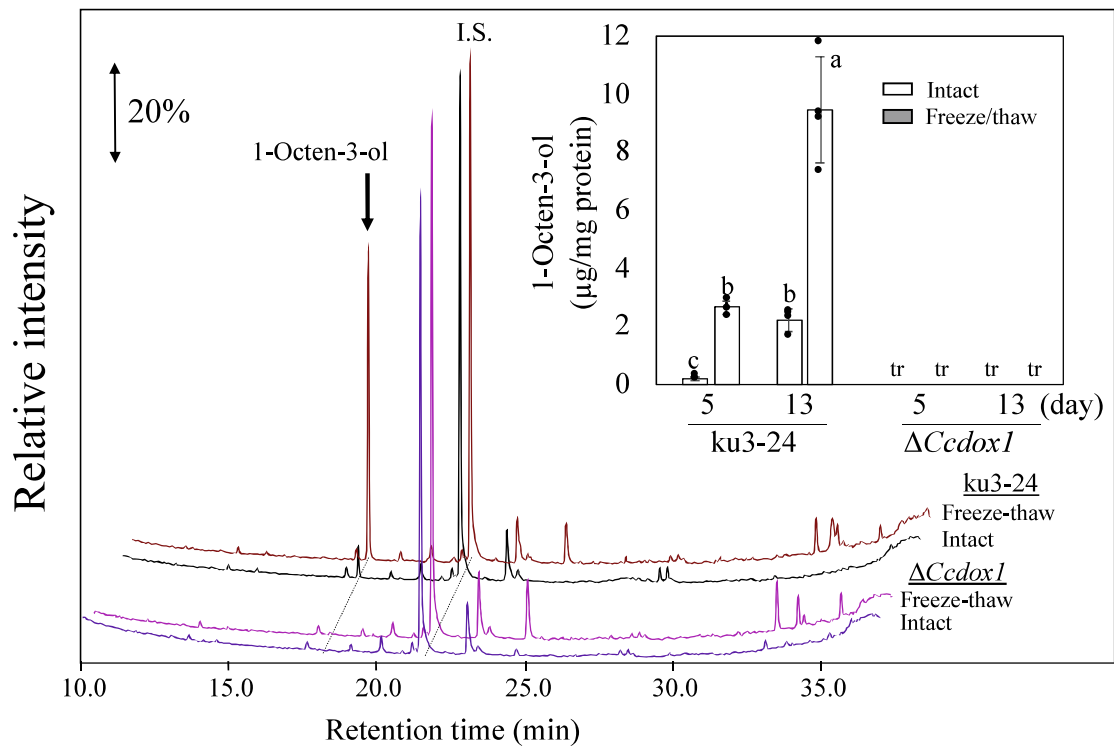


Fig. 20. Suppression of 1-octen-3-ol formation in the $\Delta Ccdox1$ strain.

Representative chromatograms obtained with intact (blue chromatogram) and freeze-thaw treated (magenta) mycelia of the $\Delta Ccdox1$ strain, and intact (black) and freeze-thaw treated (brown) mycelia of the parent WT strain (*ku3-24*). The strains were grown on YMG plate for 5 days. SPME-GC-MS techniques were employed to analyze volatiles. Inset, amount of 1-octen-3-ol formed with *ku3-24* strain and $\Delta Ccdox1$ strain in intact (white bars) and freeze-thaw treated (gray bars) mycelia. The amount of 1-octen-3-ol is presented as mean \pm SD (error bar, $n = 3$). The different letters indicate significant differences, as identified using one way ANOVA with Tukey method; $P < 0.05$. tr: trace. SPME, solid-phase microextraction; YMG, yeast extract-malt extract-glucose.

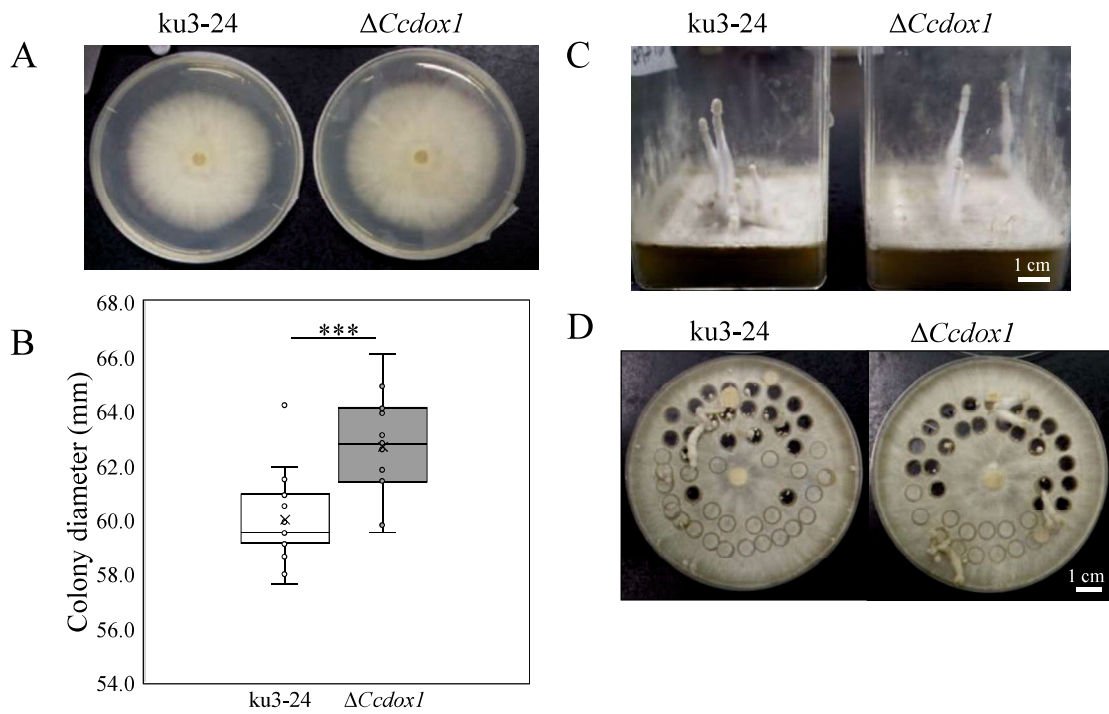


Fig. 21. Growth phenotypes of the wildtype and $\Delta Ccdox1$ mycelia grown on YMG medium. Colonies formed on the 5 days after the onset of culture on YMG medium (A). Diameters of mycelial colonies measured on the 5 days are presented in the respective boxplots (B). Statistically significant differences between *ku3-24* and $\Delta Ccdox1$ were determined by Student's *t*-test. *** $P < 0.001$; $n = 15$. Fruiting bodies formed on the 32 days after the onset of culture on YMG medium (C). Fruiting bodies formed on the 11th day after cutting the mycelia grown for 9 days (D).

10(*S*)-Hydroperoxide is Cleaved into 1-Octen-3-ol, Independent of CcDOX1

Although CcDOX1 lacks the Cys residue essential for functional cytochrome P450 activity, the possibility that CcDOX1 catalyzes the rearrangement reaction on 10(*S*)HPODE to form 1-octen-3-ol cannot be fully ruled out. This is because a few fatty acid oxygenases catalyze similar rearrangement reactions, even without any other domain that might account for the rearrangement reaction [35-38]. When immunopurified recombinant CcDOX1 was placed with 10(*S*)HPODE, no formation of 1-octen-3-ol was observed under the reaction conditions; while 10(*S*)HPODE was converted into 1-octen-3-ol with the microsomal membrane fraction prepared from mycelia of wild-type *C. cinerea* (Fig. 22). When the reaction with 10(*S*)HPODE was carried out with the microsomal membrane fraction prepared from either the wild-type strain or the $\Delta Ccdox1$ strain, no significant difference was observed in their ability to form 1-octen-3-ol from 10(*S*)HPODE (Fig. 23).

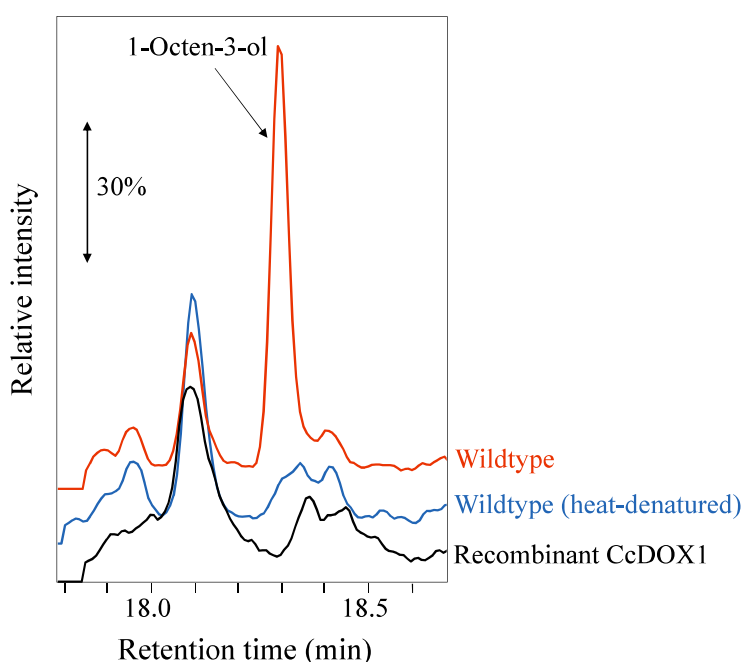


Fig. 22. The formation of 1-octen-3-ol from 10(*S*)HPODE with microsome fraction prepared with the mycelia of *C. cinerea* (red trace) and with immune-purified CcDOX1 expressed in insect cells (black). As it was anticipated that 10(*S*)HPODE spontaneously degraded to yield 1-octen-3-ol, the microsomal fraction was heat-denatured and used as the enzyme source (blue). The molecular ion chromatogram with the fragment ion of m/z 72 that is specific to 1-octen-3-ol is shown.

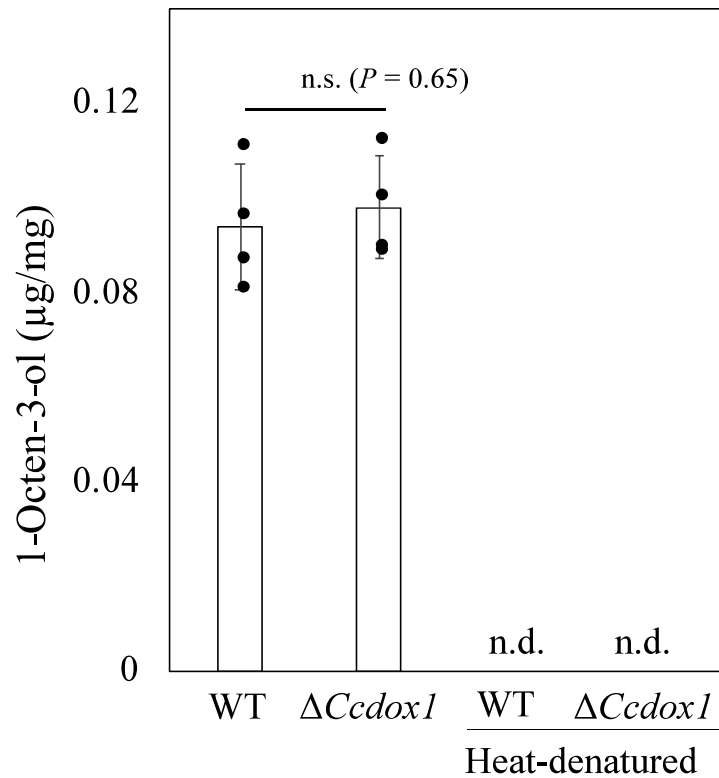


Fig. 23. 1-Octen-3-ol formation from 10(*S*)-hydroperoxide of linoleic acid with the microsome fraction prepared from the mycelia of the WT (ku3-24) strain and $\Delta Ccdox1$ strain. Reaction with heat-denatured microsome fraction formed barely any 1-octen-3-ol. Mean \pm SD ($n = 3$) is shown. Student's *t* test indicated that there was no significant difference in the amount of 1-octen-3-ol formed by WT and $\Delta Ccdox1$ ($P = 0.65$).

Effect of $\Delta Ccdox1$ on the Behavior of Organisms Associating with the Fungus

Drosophila melanogaster larvae show chemotaxis toward mushroom odor, especially toward 1-octen-3-ol [39]. We examined the olfactory preferences of *D. melanogaster* larvae toward the mycelia of *C. cinerea* ku3-24 and $\Delta Ccdox1$ strains (Fig. 24). The larvae showed a significant preference for ku3-24 mycelia when compared to $\Delta Ccdox1$.

Neoempheria dilatata belongs to a genus of fungus gnats in the family Mycetophilidae and they can cause serious damage to shiitake mushroom cultivation in Japan (40). When the *N. dilatata* larvae were placed on the surface of the mycelia of ku3-24 or $\Delta Ccdox1$, they fed on the mycelia of both strains in almost the same manner (Fig. 25). They then pupated and emerged without any distinct differences. *Aphelenchus avenae*, *Aphelenchoides besseyi*, and *Ditylenchus destructor* are fungivorous nematodes [41, 42]. We examined the population growth rates of these nematodes in the wild-type and $\Delta Ccdox1$ strains. *A. avenae* and *A. besseyi* showed no distinct differences in growth between the two *C. cinerea* genotypes (Fig. 26). However, the population growth rate of *D. destructor* was slightly, but significantly, lower with $\Delta Ccdox1$ than with ku3-24.

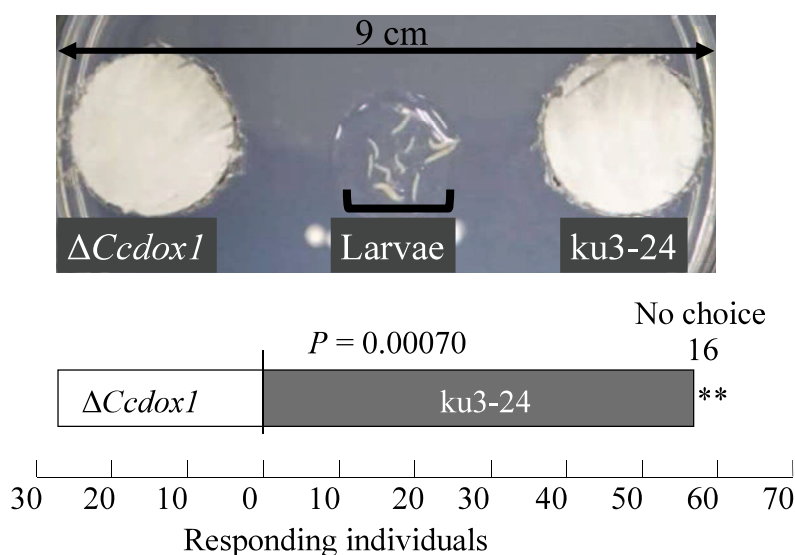


Fig. 24. Choice responses of *D. melanogaster* larvae to the mycelia of *C. cinerea* ku3-24 (wild type) and $\Delta Ccdox1$. The arena used for the assay is shown on top. An assay with 10 individuals was repeated ten times (total 100 individual). $**P < 0.01$ (binominal test). The experiment was repeated with the same results.

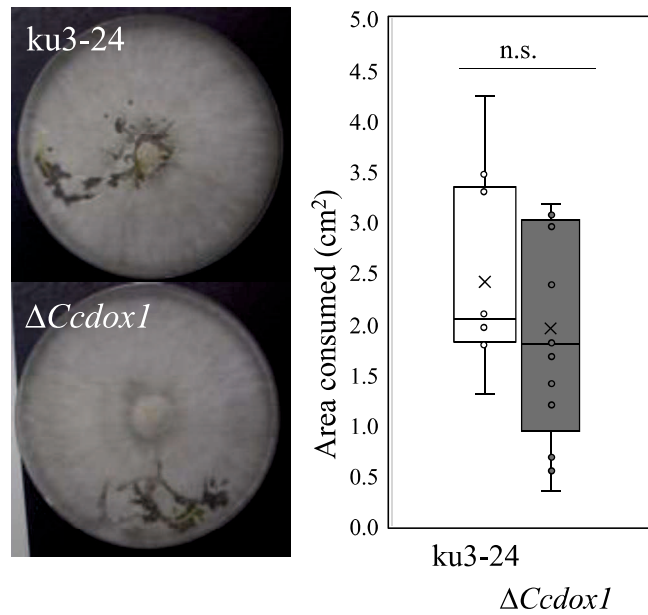


Fig. 25. Feeding behavior (left) of *Neoempheria dilatata* on $\Delta Ccdox1$ and its parent strain (ku3-24) on YMG medium. The area consumed by the larvae (right) after 24 h was measured with ImageJ. There was no statistically significant difference between the two genotypes ($n = 10$, Student's t test).

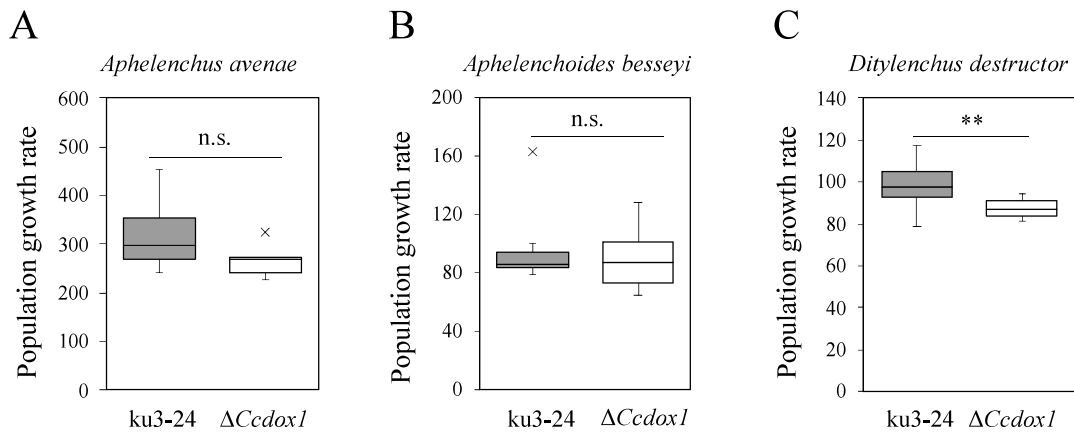


Fig. 26. Nematode propagation on *Coprinopsis cinerea* $\Delta Ccdox1$ and its parent strain ku3-24.

(A) *Aphelenchus avenae*, (B) *Aphelenchoides besseyi*, and (C) *Ditylenchus destructor*. Data from 5 (*A. avenae*) and 10 (*A. besseyi* and *D. destructor*) independent experiments are presented in the respective boxplots. Statistically significant differences between ku3-24 and $\Delta Ccdox1$ were determined by Student's t -test. $**P < 0.01$.

2.3 Discussion

The biosynthetic pathway to form 1-octen-3-ol from linoleic acid through 10(*S*)HPODE was proposed in 1982 in the common mushroom (*A. bisporus*) [3-5] however, the enzymes involved in this biosynthesis have never been unequivocally identified. Assuming an enzyme similar to Ppo or LOX as a possible enzyme that could oxygenate linoleic acid to form its hydroperoxide derivatives, a search of the genome of the model basidiomycete *C. cinerea* yielded two candidate genes, *Ccdox1* and *Ccdox2*, which showed substantial homology with filamentous ascomycete *ppos*. No proteins with substantial similarity to LOX were detected. Through further studies on these two candidate proteins, we have provided several pieces of evidence that suggests CcDOX1 in the basidiomycete *C. cinerea* is essential for the first step in 1-octen-3-ol biosynthesis, converting linoleic acid into 10(*S*)HPODE.

The first piece of evidence was obtained using the recombinant CcDOX1 protein. Recombinant CcDOX1 is a fatty acid dioxygenase that prefers linoleic acid as the substrate to either oleic acid or α -linolenic acid and it predominantly forms 10(*S*)HPODE with high stereospecificity. The recombinant CcDOX2 was also a fatty acid dioxygenase but it barely formed 10HPODE from linoleic acid; thus, the direct involvement of CcDOX2 in 1-octen-3-ol formation in *C. cinerea* was excluded. The main product of recombinant CcDOX2 from linoleic acid was tentatively assigned as 8HODE that was likely derived from 8HPODE. 8HODE is known as an allelochemical formed by a soil-dwelling basidiomycete fungus, *Laetisaria arvalis* [43]. The expression of *Ccdox1* and *Ccdox2* genes during the growth of *C. cinerea* and the comparison of the changes in the ability to form 1-octen-3-ol during growth also supported the involvement of CcDOX1 in the biosynthesis of 1-octen-3-ol. Importantly, the *S*-stereochemistry of 10HPODE formed by CcDOX1 is consistent with that of 10HPODE reported to date as an intermediate for 1-octen-3-ol formation in *A. bisporus* (common mushroom), *L. edodes* (shiitake mushroom), and *T. matsutake* (Matsutake mushroom) [5-7]. The second piece of evidence was obtained by disrupting the *Ccdox1* gene in *C. cinerea*. Disruption of *Ccdox1* function resulted in almost complete suppression of the ability of *C. cinerea* mycelia to form 1-octen-3-ol. The addition of 10(*S*)HPODE into a crude enzyme solution prepared from mycelia of either the wild type or Δ Ccdox1 strains resulted in efficient conversion of the hydroperoxide derivative into 1-octen-3-ol at a similar level of efficiency. This indicates that 10(*S*)HPODE is an intermediate in the biosynthesis of 1-

octen-3-ol from linoleic acid in *C. cinerea* and that the *Ccdox1* gene is required only for the conversion of linoleic acid to 10(*S*)HPODE, but not for the rearrangement reaction of 10(*S*)HPODE to form 1-octen-3-ol. The latter cleavage reaction is likely to be carried out by another enzyme, independent of the function of the *Ccdox1* gene. The involvement of Ppo or Ppo-like enzymes, especially PpoCs, in 1-octen-3-ol formation in fungi has been predicted because the main product of *Aspergillus* PpoC from linoleic acid is 10HPODE [13]. Moreover, the disruption of the *ppoC-like* gene in *P. anserina* and *A. luchuensis* suppresses 1-octen-3-ol production [14, 15]. However, the PpoC enzymes examined so far, that is, those from *A. fumigatus* and *A. nidulans*, produced 10(*R*)HPODE that was not used for 1-octen-3-ol formation, at least with Basidiomycota [5-7]. Since the stereochemistry of 1-octen-3-ol examined so far in Ascomycota and Basidiomycota is mostly the (*R*)-isomer [5, 44], species belonging to different phyla of the same kingdom, that is, Basidiomycota and Ascomycota, may form (*R*)-1-octen-3-ol from 10HPODE with a different stereochemistry. This raises an interesting perspective on the evolution of the biosynthetic pathway of 1-octen-3-ol. However, since the gene disruption experiments of the *ppoC-like* gene were performed only in *P. anserina* and *A. luchuensis*, and the characterization of the PpoC enzymes was performed in other filamentous ascomycetes, *A. nidulans* and *A. fumigatus*, it remains unclear whether 10(*R*)HPODE is responsible for 1-octen-3-ol in ascomycetes. Genetic and biochemical studies on the same gene in the same species are necessary to obtain direct evidence to verify this possibility. In addition, it is necessary to study the orthologs of *Ccdox1* in Basidiomycota to obtain a comprehensive overview of the 1-octen-3-ol formation pathways in Basidiomycota.

Most filamentous ascomycetes contain a subset of Ppo enzymes, including PpoA, PpoB, PpoC, and PpoD. Ppos in filamentous ascomycetes have been extensively studied [11]. PpoA, for example, is a DOX-P450 fusion protein involved in the biosynthesis of factors that determine the timing and balance between sexual and asexual spore development in *A. nidulans* [45]. However, Ppo homologs in Basidiomycota have not been studied extensively. Among Basidiomycota, one gene from *U. maydis* (Ustilaginomycotina) and three genes from *R. solani* (Cantharellales) showing homology to ascomycete ppos have been reported [16, 17], but the properties and functions of the enzymes encoded by these genes have never been studied. CcDOX1 and CcDOX2 found in this study as the proteins homologous to ascomycete Ppos also contain an N-terminal DOX domain and a C-terminal P450-related domain; however, their C-terminal P450-related domains lacked sufficient features to be recognized as members of the P450 protein family, despite substantial homology with the C-terminal P450 domain of ascomycete Ppo proteins. Remarkably, CcDOX1/2 do not have the Cys residue that is

crucial for the activities of almost all P450 enzymes as the fifth heme iron ligand through a heme-thiolate bond [25]. The His residue, located on the two residues upstream of the Cys residue, is essential for hydroperoxide isomerase activity in *A. nidulans* PpoA (His1004) [24]. This is also absent in CcDOX1/2. Accordingly, it is highly plausible that the C-terminal Cyt P450-related domains of CcDOX1/2 do not function as P450 enzymes, as confirmed by the PpoC enzymes in Ascomycota [13]. In fact, the predominant products formed from linoleic acid by recombinant CcDOX1 and CcDOX2 were 10(*S*)HPODE and 8HPODE, respectively, and there was no sign of rearrangement of the hydroperoxides that would have occurred in the presence of active P450. Interestingly, the C-terminal P450-related domains of CcDOX1/2 still retain substantial sequence signatures as P450 proteins, even though the domains do not function as P450 enzymes. The expression of only the N-terminal DOX domain of CcDOX1 in insect cells showed no oxygenation activity for linoleic acid (Fig. 15). This is unexpected but suggests that the P450-related domain plays a role in the correct folding of the N-terminal DOX domain and/or in the stabilization of structure. With the pioneering works done with AnPpoA and AnPpoC [24, 46], it was reported that AnPpoA and AnPpoC form a tetramer, and the status of heme in these hemoproteins was examined with spectral analyses. The fact that the [S]-v plot of CcDOX1 with linoleic acid did not follow the Michaelis-Menten equation but followed the Hill equation with $n = 1.9$, and the subcellular localization of only the N-terminal DOX domain of CcDOX1 changed may be associated with cooperativity based on the subunit structure of CcDOX1. The low amounts of recombinant proteins obtained after immunopurification did not allow us to investigate their structures. Detailed kinetical and structural analyses of CcDOXs are important topics for future research that should be done after developing an efficient and prolific expression system.

The phylogenetic tree we have created showed that the DOX-P450 proteins from Ascomycota and Basidiomycota were clearly separated into two corresponding clades (Fig. 3B), suggesting that the DOX-P450 genes belonging to each clade diversified independently in each phylum after the divergence of Ascomycota and Basidiomycota [22]. When the genome sequences of representative fungal species belonging to different classes of all the subdivisions listed in MycoCosm, namely, Cryptomycota, Microsporidia, Chytridiomycota, Blastociadiomycota, Zoopagomycota, Mucoromycota, Ascomycota, and Basidiomycota [22], were searched using the CcDOX1 sequence as the query, genes containing both the N-terminal DOX and C-terminal P450-related domains were found only in Ascomycota and Basidiomycota (Table 5). The genes found in the genome sequences of *Saitoella complicata* (Taphrinomycotina), *Rhizophagus clarus* (Glomeromycotina), *Entomortierella belijakovae* (Mortierellomycotina), *Basidiobolus*

meristosporus (Entomophthoromycotina), and *Rhizoclosmatium globosum* (Chytridiomycetes) showed significant sequence homology with the DOX domain of CcDOX1 but lacked the P450-related domain. This indicates that fungi acquired DOX-like genes at the early stage of divergence after the establishment of the kingdom of fungi. Thereafter, the gene fused with the P450-related gene to form an ancestral DOX-P450 fusion gene when the Dikarya diverged. The phylogenetic tree (Fig. 3B) and multiple sequence alignment (Fig. 6) show that there are a certain number of proteins that have apparently lost P450 enzyme activity due to the substitution of Cys and/or His in the P450-related domain with other amino acid residues in the ascomycete and basidiomycete clades. It is likely that such amino acid substitutions, which are essential for P450 enzyme activity, occurred independently in these phyla.

This study confirmed that CcDOX1 is essential for 1-octen-3-ol formation from linoleic acid, as a dioxygenase, to form 10(*S*)HPODE. The second step of the biosynthetic pathway, namely, the cleavage of 10(*S*)HPODE to form 1-octen-3-ol, is independent of CcDOX1. In the cyanobacteria *Nostoc punctiforme*, a catalase-like heme protein catalyzes the cleavage reaction to form 1-octen-3-ol from 10(*S*)HPODE [32]. Plant hydroperoxide lyase, a non-canonical cytochrome P450 enzyme classified as CYP74B, cleaves 13-hydroperoxide of linolenic acid to form (*Z*)-3-hexenal and 12-oxo-9(*Z*)-dodecenoic acid [47]. We found no gene that showed a substantial similarity to the cyanobacterial catalase-like gene or that was similar to plant hydroperoxide lyases (CYP74B) in the genome of *C. cinerea*. It is still unknown which enzyme accounts for the cleavage reaction. We are currently attempting to purify the 'hydroperoxide lyase'-type enzyme responsible for 1-octen-3-ol formation in *C. cinerea* using classic chromatography techniques. Identification of the gene essential for 1-octen-3-ol synthesis facilitated the examination of the eco-physiological significance of 1-octen-3-ol formation in mushrooms using the $\Delta Ccdox1$ strain. The current knowledge regarding the function of 1-octen-3-ol in various organisms that are potentially associated with fungi [20] suggests a role for 1-octen-3-ol in fungal defense. However, the fungivores used in the present study, the fungus gnat *N. dilatata* and the fungivorous nematode *A. avenae*, fed on the wild-type and 1-octen-3-ol deficient strain in the same manner. Rather, significant chemotaxis toward the wild-type strain, rather than the 1-octen-3-ol deficient strain was observed in *D. melanogaster* larvae, an opportunistic fungivore. This may be because the fungivores used in this study were well adapted to the defense system employed by the fungi. Therefore, 1-octen-3-ol seems to have become a kairomone for some animals that interact with mushrooms. Therefore, the behavior of a wider array of fungivores on 1-octen-3-ol deficient *C. cinerea* must be examined to further clarify the

ecophysiological role of 1-octen-3-ol. Tritrophic interactions among fungi, fungivores, and parasitoids have also been reported [48]. The involvement of 1-octen-3-ol in indirect defense to recruit predators/parasitoids to fungivores that actively feed on fungi should be examined.

2.4 Materials and Methods

Fungi

C. cinerea strain ku3-24 (*A43mutB43mut pab1-1 ΔCc.ku70(Flt^R)/a* progeny of ku70dfltF₂#92 × KF3#2) and strain 326 (*A43mutB43mut pab1-1*) were used in this study. Both strains were grown at 28 °C in the dark on yeast extract-malt extract-glucose (YMG) medium (3 g yeast extract, 3 g polypeptone, 3 g malt extract, 10 g glucose, and 20 g agar in 1 L distilled water), unless otherwise indicated. For the RT-PCR experiments, mycelia of *C. cinerea* strain 326 were inoculated into YMG liquid media (10 mL in a 100 mL flask) and cultured under static conditions at 28 °C in the dark.

Determination of Volatiles

C. cinerea (ku3-24) was grown on YMG agar for 5 days, after which 0.5 cm³ mycelia with the YMG agar were cut out and sealed in a glass vial (20 mL). Mycelia were subsequently frozen in liquid nitrogen for 2 min and thawed in a water bath at 35 °C for 10 min to disrupt the tissues. The volatiles formed were extracted from the headspace using an SPME fiber (50/30 μm DVB/CAR/PDMS, Merck) at 30 °C for 30 min. SPME-GCMS was performed on a QP-5050 (Shimadzu, Kyoto, Japan) instrument equipped with a 0.25 mm × 30 m DB-WAX column (film thickness 0.25 μm; Restek, Bellefonte, PA, USA). The SPME fiber was inserted into the injection port set at 200 °C for 10 min in the splitless mode. The sampling time was 1 min. The column temperature was initially set at 40 °C for 5 min, increased by 5 °C min⁻¹ to 200 °C, and then maintained at 200 °C for 2 min. The carrier gas (He) was supplied at a flow rate of 86.1 kPa. The injector and interface temperatures were maintained at 200 °C. The mass detector was operated in the electron impact mode with an ionization energy of 70 eV. 1-Octen-3-ol was assigned by comparing the MS profile and retention time of authentic 1-octen-3-ol (Tokyo Chemical Industry Co., Ltd., Tokyo, Japan) and quantified using an externally constructed calibration curve. When required, the fragment ion (*m/z* 72) was monitored to detect 1-octen-3-ol with high specificity. 3-Methyl-1-butanol, 3-octanone, and 1-octanol were identified by analyzing the MS profiles using the NIST08s database.

The volatiles were extracted with methyl *tert*-butyl ether (MTBE) and analyzed. After the freeze-thaw treatment, 1 mL of MTBE containing *n*-nonanyl acetate (internal

standard, 1 $\mu\text{g mL}^{-1}$) was added, and the mixture was centrifuged at $21,500 \times g$ for 10 min to collect the upper organic phase. The protein content was determined using a protein assay kit (Bio-Rad, Hercules, CA, USA). To examine the effect of reagents on the ability to form 1-octen-3-ol (Figs. 2C and 2D), mycelia grown on YMG agar were placed into a 2 mL microtube with 0.5 g glass beads (420-500 μm i.d.) and 400 μL of 50 mM Tris-HCl (pH 8.0) containing the reagent of interest. Subsequently, the mycelia were homogenized using a bead-homogenizer MS-100 (TOMY, Tokyo, Japan) at 3,500 rpm for 1 min. The volatiles formed were extracted by adding 1 mL MTBE containing the internal standard for GC-MS analysis. To examine the developmental changes in the ability to form 1-octen-3-ol in the mycelia grown in liquid culture, mycelia (strain 326) were collected every 4 days, washed with distilled water, and finally weighed. A portion of the mycelia was freeze-thaw treated (2 min in liquid N_2 and subsequently 10 min at 35 $^\circ\text{C}$) in a closed glass tube. 1-Octen-3-ol formed was extracted with MTBE containing an internal standard and subjected to GC-MS analysis, as described above.

Phylogenetic Analysis

Phylogenetic analysis was performed using the Maximum Likelihood method based on the LG model +G+I in MEGA X. Amino acid sequences were aligned using MAFFT v7.475 and Gblocks Server v0.91b. GenBank accession numbers of each protein used for phylogenetic analysis are listed in Table 2.

Recombinant Protein

Total RNA was extracted from the mycelium of *C. cinerea* strain 326 using the RNeasy Plant Mini kit (Qiagen, Hilden, Germany) and treated with a DNA-free kit (Thermo Fisher Scientific). cDNA was synthesized using the ReverTra Ace qPCR RT Master Mix (TOYOBO, Tokyo, Japan). The coding regions of *Ccdox1* and *Ccdox2* cDNA were amplified by PCR using PrimeSTAR Max DNA Polymerase (Takara Bio Inc., Shiga, Japan), and the primers listed in Table 4 were subcloned into the pA3hr5 vector (provided by Professor Kobayashi at Yamaguchi University) using the In-Fusion HD Cloning kit (Takara). Recombinant CcDOX proteins, with and without EGFP, were prepared. When only the N-terminal DOX domain of CcDOX1 was expressed, the 3D structural model of CcDOX1 predicted with AlphaFold2 was examined (Fig. 14). Based on the model structure, the junction between the N-terminal and C-terminal P450 domains of CcDOX1 was assigned as the site between Asn670 and Pro671. Accordingly, a protein sequence ranging from the initial Met to Asn670 was expressed as an EGFP fusion protein. Polyethyleneimine (4 µg) (Techno Chemical Co., Tokyo, Japan) in 100 µL of WakoVAC PSFM-J1 medium (serum-free medium; FUJIFILM Wako Pure Chemical Co., Osaka, Japan) was gently mixed with 2 µg of cDNA in the pA3hr5 vector dissolved in 100 µL of serum-free medium by pipetting, and the mixture was incubated at 25 °C for 15 min. BmN4 cells were poured into a plate (40 mm × 13.5 mm) and allowed to stand for at least 15 min to adhere to the bottom surface, after which the medium was carefully removed to prevent detachment. The plasmid DNA mixture was diluted with 800 µL serum-free medium and poured onto BmN4 cells on the plate. The plate was then sealed and incubated at 28 °C in the dark for four days.

Localization of CcDOX1 in Insect Cells

For insect cells, the medium was carefully removed from the plate (40 mm × 13.5 mm) and added 1 mL staining solution (mixed 0.5 µL NuclearMask™ Blue or ER-Tracker™ Red; Thermo Fisher Scientific in 1 mL serum-free medium). Incubated the cells for 30 min. Replaced the staining solution with fresh medium and viewed the cells using a fluorescence microscope (LAS AF-MZ16FA; Leica, Wetzlar, Germany).

Enzyme Assay and Product Analysis

The cells were harvested by centrifugation at $400 \times g$ for 10 min and washed with lysis buffer (50 mM potassium phosphate buffer (pH 7.4), 1 mM EDTA, 1 mM glutathione, 5% glycerol, 0.04% Tween 20). They were then suspended in 600 μL of lysis buffer and sonicated with an Ultrasonic Disrupter UD-201 (TOMY) three times with 5 s pulses while on ice. The cell-free lysate was collected after centrifugation at $15,000 \times g$ for 30 min at 4°C . In some experiments, the crude cell lysate supernatant was used as the enzyme source. The expressed protein fused with EGFP was immunoprecipitated with 10 μL Dynabead Protein G (Thermo Fisher Scientific) and 2 μg of anti-GFP monoclonal antibody (Fujifilm Wako Pure Chemicals). The beads were washed twice with lysis buffer and suspended in 147 μL lysis buffer for enzyme assay and SDS-PAGE analysis.

Recombinant CcDOX1 fused with EGFP was incubated with 10-500 μM linoleic acid, oleic acid, or α -linolenic acid for 30 min on ice. The reaction was terminated by adding three volumes of ethanol. After centrifugation at $15,000 \times g$ for 30 min at 4°C , the supernatant was filtered using a DISMIC-03JP (0.50 μm ; ADVANTEC, Tokyo, Japan). The clear supernatant was dried under N_2 gas flow, and the residue was dissolved in methanol containing 0.1 mM sodium acetate. The oxygenated fatty acids were analyzed with an HPLC-MS/MS system comprising a 3200 QTRAP (SCIEX, Tokyo, Japan) using an enhanced MS (EMS) scan mode with negative electrospray ionization (ion spray voltage, -4500 V at 300°C ; using nitrogen as both the curtain gas (set to 40 arbitrary units) and collision gas (set to "high"); collision energy, -10 V ; declustering potential, -10 V). The products were separated on a Mightysil RP18 column (5 μm , 2 mm inner diameter \times 150 mm, Kanto Chemical, Tokyo, Japan) using solvent A (water/formic acid, 100:0.1, v/v) and solvent B (acetonitrile/formic acid, 100:0.1, v/v). Elution conditions were as follows: 0–5.0 min, 20% B; 5.0–20.0 min, 20–60% B; 20.0–50.0 min, 60–65% B; 50.0–60.0 min, 65–100% B and 60.0–70.0 min, 100% B, with a flow rate of 0.2 mL min⁻¹. The [S]-v plot of recombinant CcDOX1 with linoleic acid was constructed by analyzing the peak area obtained by LC-MS/MS analysis in the negative ion mode. The largest peak obtained with 500 μM of linoleic acid was set to 100%. The data obtained were analyzed with Origin software (OriginPro 2022, OriginLab Co., Northampton, MA USA). To gain insight into the positional specificity of the oxygenation reaction, the hydroperoxides were reduced to the corresponding hydroxides by reacting with triphenylphosphine, and they were subjected to HPLC-MS/MS analysis with enhanced product ion (EPI) mode with a negative ion of m/z 295.30 or m/z 297.20, corresponding

to the hydroxide of linoleic acid ($C_{18}H_{32}O_3-H^+$) or hydroxide of oleic acid ($C_{18}H_{34}O_3-H^+$), as the parent ion. Elution conditions were as follows: 0–5.0 min, 20% B; 5.0–30.0 min, 20–60% B; 30.0–100.0 min, 60–65% B; 100.0–120.0 min, 65–100% B and 120.0–130.0 min, 100% B, with a flow rate of 0.2 mL min^{-1} . The fragment ion of m/z 183.1, or m/z 157.1, formed with a collision energy of -30 V , which followed the criteria for 10-hydroxide or 8-hydroxide of linoleic acid, respectively [49]. 10-Hydroxide or 8-hydroxide of oleic acid was tentatively assigned with the fragment ion of m/z 155.2, or m/z 157.1, respectively.

For complete structural determination and quantification, the HPLC-MS/MS system (4000 QTRAP quadrupole/linear ion trap tandem mass spectrometer (SCIEX, Tokyo, Japan)) in multiple reaction monitoring (MRM) mode with positive electrospray ionization after the addition of Na^+ ions was used [29]. An Inertsil ODS-3 column ($5\text{ }\mu\text{m}$, $2.1\text{ mm} \times 150\text{ mm}$, GL Sciences, Tokyo, Japan) was used with a column temperature of $40\text{ }^\circ\text{C}$. The mobile phases used were water/formic acid (99.9:0.1, v/v, solvent A) and methanol/formic acid (99.9:0.1, v/v, solvent B). Elution conditions were as follows: 0–5.0 min, 60% B; 5.0–15.0 min, 60–100% B; and 15.0–20.0 min, 100% B. The flow rate was maintained as follows: 0–5.0 min, 0.3 mL min^{-1} ; 5.0–20.0 min, 0.2 mL min^{-1} , 20.0–25.0 min, 0.3 mL min^{-1} . The injection volume was $10\text{ }\mu\text{L}$. The transitions used to identify each fatty acid hydroperoxide are listed in Table 3 [30]. The column eluent was mixed with methanol containing 2 mM sodium acetate, which was added at 0.01 mL min^{-1} . Each isomer of the fatty acid hydroperoxide was identified by the retention time and MS/MS profile of its Na^+ -adduct using a standard compound [30]. For the separation of the enantiomers [31], a CHIRALPAK ID ($2.1\text{ mm i.d.} \times 150\text{ mm}$, $5\text{ }\mu\text{m}$, Daicel, Osaka, Japan) column was used with a column temperature of $40\text{ }^\circ\text{C}$. Water/formic acid (99.9:0.1, v/v, solvent A) and methanol/formic acid (99.9:0.1, v/v, solvent B) were used as the mobile phases, and the elution conditions were as follows: 0–2.0 min, 60% B; 2.0–15.0 min, 60–90% B; 15.0–18.0 min, 90% B. The flow rate was 0.2 mL min^{-1} . The column eluent was mixed with methanol containing 2 mM sodium acetate, which was added at 0.01 mL min^{-1} .

The 10-hydroperoxide of linoleic acid was prepared using recombinant NpDOX protein expressed in *E. coli* cells. The codon usage of *Nostoc punctiforme* PCC73102 animal heme peroxidase (NpDOX) gene (GenBank: CP001037.1) was optimized for *E. coli*, the open reading frame was subcloned into the pET15b vector using the In-Fusion HD Cloning Kit (Takara Bio, Shiga, Japan), and *E. coli* BL21 Star (DE3) (Thermo Fisher Scientific) cells were transformed with the plasmid. The cells were grown in LB medium containing $100\text{ }\mu\text{g mL}^{-1}$ ampicillin at $37\text{ }^\circ\text{C}$ to an OD_{600} of 0.6–0.8. The expression of the

recombinant protein was induced by adding isopropyl- β -D-thiogalactopyranoside to a final concentration of 0.1 mM. After cultivation at 16 °C for 18 h, cells were harvested by centrifugation at 10,000 \times g for 10 min. They were then suspended in 5 mL of 50 mM Tris-HCl buffer (pH 8.75) and lysed by sonication with an Ultrasonic Disrupter UD-201 (TOMY) three times with 10 s pulses on ice. The cell lysate was centrifuged at 10,000 \times g for 30 min at 4 °C and the supernatant was collected. The supernatant was incubated with 5 mM of linoleic acid for 30 min on ice. The reaction mixture was acidified by adding diluted HCl and the product was extracted with ethyl acetate (3 mL). 10(*S*)HPODE was purified using preparative thin-layer chromatography.

To determine the substrate specificity, dioxygenase activity was monitored using a Clarktype oxygen electrode (Rank Brothers Ltd., Cambridge, UK) at 25 °C. The reaction was initiated by the addition of 6 μ L linoleic acid (18:2), oleic acid (18:1), or α -linolenic acid (18:3) at 50 mM in 294 μ L of lysis buffer containing purified CcDOX1 and stirred with a magnetic stirrer.

Expression of *Ccdoxs*

The mycelia of *C. cinerea* were inoculated into YMG liquid medium (10 mL in a 100 mL flask) and cultured under static conditions at 28 °C. Mycelia were collected every 4 days, washed with distilled water, and weighed. RNA was extracted from the mycelia using the RNeasy Plant Mini Kit (Qiagen) and treated with a DNA-free kit (Thermo Fisher). cDNA was constructed using ReverTra Ace RT Master Mix (Toyobo), and RT-qPCR was performed using SYBR Green (Kapa Biosystems). β -Tubulin (*CC1G_04743*) was used as the reference gene in the experiment. The primers used for RT-qPCR are listed in Table 4.

Disruption of *Ccdox1*

A genomic fragment containing *Ccdox1*, amplified using genomic DNA from *C. cinerea* ku3-24 as a template and the primer set SV13-SV14 (Table 4), was cloned into pBluescript II KS+ digested with *EcoRV*. Inverse PCR was performed with the resulting plasmid as a template and the primer set SV17-SV18. A DNA fragment containing the expression cassette for hygromycin resistance was also amplified by PCR using pTN2005 as the template and the primer set M13F-M13R. The two resulting DNA fragments were fused using the GeneArt Seamless Cloning and Assembly Kit (Thermo Fisher) to yield a plasmid containing the *Ccdox1*-disruption cassette [34]. Transformation was performed as described by Nakazawa et al. [50] using protoplasts prepared from mycelial cells.

Cleavage Reaction.

The mycelia of *C. cinerea* strains ku3-24 and $\Delta Ccdox1$ were cultivated at 28 °C for 12 days in YMG liquid medium. Mycelia were collected and washed with 100 mM Tris-HCl (pH 7.5). Mycelia (5 g) were suspended in 10 mL of 100 mM Tris-HCl (pH 7.5) and homogenized using a mortar and pestle on ice. The homogenate was centrifuged at $15,000 \times g$ for 30 min at 4 °C and then the supernatant was subsequently centrifuged at $138,000 \times g$ for 60 min at 4 °C. The collected microsome fraction was suspended in 400 μ L of 100 mM Tris-HCl (pH 7.5). Microsomes were incubated with 1.5 μ M 10(S)HPODE at 25 °C for 10 min. The products were extracted with 200 μ L of MTBE containing the internal standard for GC-MS analysis. Thermal denaturation was performed at 90 °C for 10 min.

Fungivores

The wild-type strain (Oregon R) of the fruit fly *D. melanogaster* was reared at 24 °C. *C. cinerea* ku3-24 and $\Delta Ccdox1$ strains were grown on YMG agar plates (90 mm diameter) until their mycelia covered the entire surface of the plate. Agar plugs with a diameter of 20 mm were removed from the middle of the region between the center and periphery of the plates using a cork borer and inserted into holes made at the periphery of the 90 mm chemotaxis plates (17 g agar, 1 mL 1 M CaCl₂, 1 mL 1 M MgSO₄, 5 mL 1 M KH₂PO₄, pH 6.0, in 1 L water) [39]. Ten third-instar larvae of *D. melanogaster* were placed at the center of the arena, and the number of larvae that reached the respective mycelia within 10 min was counted as those attracted to the agar plug. Agar plugs from plain YMG plates were used as the controls.

Individual larvae (7–10 mm) of the fungus gnat *N. dilatata* [40], reared on mycelial blocks of shiitake mushrooms (*L. edodes*) (Mori Co., Gunma, Japan), were placed on the surface of the mycelia of *C. cinerea* that fully covered the surface of YMG plates. The plate was kept for 24 h in the dark at 25 °C, and the area consumed by the fungivore was measured using the ImageJ software.

The fungal-feeding nematodes, *A. avenae*, *A. besseyi*, and *D. destructor*, were maintained on a *Botrytis cinerea* strain that lacks the ability to form spores as a food fungus. The strain was kept on a 5-fold diluted (1/5 ×) potato dextrose agar (PDA) plate (Eiken Chemical Co., Tokyo, Japan) [41]. Nematode propagation was compared using a 1/5 × PDA plate (9 cm diameter) seeded with the respective strains of *C. cinerea*. A 0.6 cm² piece of 1/5 × PDA with mycelia was inoculated on a fresh 1/5 × PDA plate and incubated at 20 °C for 2 weeks. Thereafter, 200 mixed-stage nematodes were inoculated on the plates. Four weeks after inoculation, nematodes were recovered from the plates using the Baermann method [41]. After repeated washing of the harvested nematodes with distilled water, protein content was determined using a BCA protein assay kit (Thermo Fisher Scientific). The population growth rate was calculated by dividing the protein content obtained after four weeks by the initial protein content of 200 nematode individuals.

Table 2. Proteins used to construct the phylogenetic tree shown in Fig. 4B.

Scientific name	Scientific classification	GenBank	RefSeq / protein_id	CDS / locus_tag	Products/Enzyme name
<i>Nostoc punctiforme</i> PCC 73102	Cyanobacteria	ACC83776.1	WP_012411722.1	NPUN_RS27670	10(S)-HPODE
<i>Podospira anserina</i>	Ascomycota	CAP61989.1	XP_001904211.1	PODANS_5_1240 (PaCOX2)	10-HODE/1-octen-3ol
<i>Fusarium oxysporum</i>	Ascomycota	EGU86021.1		FOXB_03425	10R-DOX-EAS
<i>Colletotrichum graminicola</i>	Ascomycota	EFQ36272.1	XP_008100292.1	GLRG_11417	7,8-LDS/8,11-dihydroxylinoleic acid
<i>Penicillium oxalicum</i> 114-2	Ascomycota	EPS31749.1		PDE_06706	7S,8S-DIHODE
<i>Aspergillus terreus</i>	Ascomycota	AGA95448.1	XP_001213170.1	ATEG_03992	5,8-LDS
<i>Aspergillus fumigatus</i> A1163	Ascomycota	EDP50447.1		AFUB_067850	5,8-LDS/PpoA
<i>Aspergillus nidulans</i>	Ascomycota	AAR88626.1			8-HODE/(5S,8R)-DIHODE/PpoA
<i>Penicillium chrysogenum</i>	Ascomycota	CAP97986.1	XP_002564723.1	PCH_Pc22g06980	8 R ,11 S -DIHODE/8-HODE
<i>Penicillium digitatum</i>	Ascomycota	EKV17116.1	XP_014535919.1	PDIP_33150	8-HODE
<i>Aspergillus luchuensis</i>	Ascomycota	GAT23542.1		RIB2604_01706810	PpoC (involved in 1-octen-3-ol formation)
<i>Aspergillus luchuensis</i>	Ascomycota	GAT25971.1		RIB2604_02005510	PpoA
<i>Aspergillus terreus</i>	Ascomycota	AFB71131.1		ATEG_04755	10(R)-DOX
<i>Aspergillus nidulans</i>	Ascomycota	AAT36614.1			10-HPODE/PpoC
<i>Aspergillus fumigatus</i> A1163	Ascomycota	EDP52540.1		AFUB_037060	(10R)-dioxxygenases/PpoC
<i>Penicillium marnieffii</i>	Ascomycota	EEA26582.1	XP_002147129.1	PMAA_076430	10(R)-DOX/PpoC
<i>Colletotrichum sublineola</i>	Ascomycota	KDN68726.1		CSUB01_04826	7,8-LDS/8,11-dihydroxylinoleic acid
<i>Colletotrichum graminicola</i>	Ascomycota	EFQ34869.1	XP_008098889.1	GLRG_10013	7,8-LDS/8,11-dihydroxylinoleic acid
<i>Magnaporthe oryzae</i>	Ascomycota	EHA52010.1	XP_003711817.1	MGG_13239	7,8-LDS
<i>Gaeumannomyces graminis</i>	Ascomycota	AAD49559.3		AAT_I	7,9-LDS
<i>Podospira anserina</i>	Ascomycota	CAP60153.1	XP_001912671.1	PODANS_1_4690 (PaCOX1)	10-HODE/1-octen-3ol
<i>Aspergillus nidulans</i>	Ascomycota	AA335769.1			PpoB
<i>Coccidioides immitis</i>	Ascomycota	EAS28473.3	XP_001240056.2	CIMG_09677	8R-DOX-AOS
<i>Zymoseptoria tritici</i>	Ascomycota	EGP83657.1	XP_003848681.1	MYCGRDRAFT_49830	8S-DOX-AOS
<i>Zymoseptoria tritici</i>	Ascomycota	EGP87976.1	XP_003853000.1	MYCGRDRAFT_71165	9R-DOX-AOS
<i>Aspergillus terreus</i>	Ascomycota	AGH14485.1	XP_001211214.1	ATEG_02036	9(R),10-epoxy-10,12(Z)-octadecadienoic acid
<i>Fusarium oxysporum</i>	Ascomycota	EGU88194.1		FOXB_01332	9S-DOX-AOS
<i>Glomerella graminicola</i>	Ascomycota	EFQ27323.1	XP_008091343.1	GLRG_01818	9S-DOX-AOS
<i>Fusarium oxysporum</i>	Ascomycota	EGU79548.1		FOXB_09952	9R-DOX
<i>Colletotrichum graminicola</i>	Ascomycota	EFQ36675.1	XP_008100695.1	GLRG_11821	9R-DOX
<i>Serpula lacrymans</i> var. <i>lacrymans</i>	Basidiomycota	EGO22364.1	XP_007320902.1	SERLADRAFT_416857	unkown
<i>Agaricus bisporus</i> var. <i>bisporus</i> H97	Basidiomycota	EKV46570.1	XP_006461894.1	AGABI2DRAFT_143643	unkown
<i>Coprinopsis cinerea</i>	Basidiomycota	EAU90460.2	XP_001831297.2	CC1G_00844 (CcCOX1)	10(S)-HPODE
<i>Fomitopsis pinicola</i>	Basidiomycota	EPT00655.1		FOMPIIDRAFT_99109	unkown
<i>Rickenella mellea</i>	Basidiomycota	TDL21822.1		BD410DRAFT_840230	unkown
<i>Rickenella mellea</i>	Basidiomycota	TDL21825.1		BD410DRAFT_279997	unkown
<i>Schizophyllum commune</i>	Basidiomycota	EFI97900.1	XP_003032803.1	SCHCODRAFT_11038	unkown
<i>Fomitopsis pinicola</i>	Basidiomycota	EPS97161.1		FOMPIIDRAFT_83073	unkown
<i>Agaricus bisporus</i> var. <i>bisporus</i> H97	Basidiomycota	EKV43127.1	XP_006456120.1	AGABI2DRAFT_195360	unkown
<i>Schizophyllum commune</i>	Basidiomycota	EFI91160.1	XP_003026063.1	SCHCODRAFT_114799	unkown
<i>Rickenella mellea</i>	Basidiomycota	TDL18561.1		BD410DRAFT_842735	unkown
<i>Coprinopsis cinerea</i>	Basidiomycota	EAU86789.2	XP_001835023.2	CC1G_09914 (CcCOX2)	unkown
<i>Pleurotus ostreatus</i> PC15	Basidiomycota	KDQ24228.1		PLEOSDRAFT_1085502	unkown
<i>Serpula lacrymans</i> var. <i>lacrymans</i>	Basidiomycota	EGO25105.1	XP_007317227	SERLADRAFT_414828	unkown
<i>Rickenella mellea</i>	Basidiomycota	TDL26424.1		BD410DRAFT_520610	unkown
<i>Fomitopsis pinicola</i>	Basidiomycota	EPS97159.1		FOMPIIDRAFT_95975	unkown
<i>Fomitopsis pinicola</i>	Basidiomycota	EPS97141.1		FOMPIIDRAFT_1052690	unkown
<i>Ustilago maydis</i>	Basidiomycota	AAL38020.1			unkown
<i>Serpula lacrymans</i> var. <i>lacrymans</i>	Basidiomycota	EGO22766.1	XP_007320006.1	SERLADRAFT_439529	unkown
<i>Rhizoctonia solani</i> 123E	Basidiomycota	KEP52552.1		V565_043610	unkown
<i>Rhizoctonia solani</i> 123E	Basidiomycota	KEP54849.1		V565_012270	unkown
<i>Rhizoctonia solani</i> 123E	Basidiomycota	KEP46854.1		V565_178510	unkown

Table 3. Condition for multiple reaction monitoring to identify each hydroperoxide of fatty acid.

	Precursor ion* [M+Na] ⁺ (m/z)	Product ion* (m/z)	DP (V)	EP (V)	CE (V)	CXP (V)	Curtain gas (psi)	Ion source gas 1 (psi)	Ion source gas 2 (psi)	Collision Gas (psi)
16-HPOTrE	333.2	287.1	56	10	22	16.5	20	40.0	40.0	4.0
15-HPOTrE	333.2	246.1	59	10	18.8	13.5	20	40.0	40.0	4.0
13-HPOTrE	333.2	247.1	54	10	19.3	13.5	20	40.0	40.0	4.0
13-HPOTrE	333.2	206.1	58	10	17.6	11.5	20	40.0	40.0	4.0
10-HPOTrE	333.2	207.1	61	10	20.7	10.8	20	40.0	40.0	4.0
9-HPOTrE	333.2	195.1	59	10	14.3	9.8	20	40.0	40.0	4.0
13-HPODE	335.2	247.1	56	10	19.5	16	20	40.0	40.0	4.0
12-HPODE	335.2	206.1	75	10	17.5	10	20	40.0	40.0	4.0
10-HPODE	335.2	207.1	75	10	19	10	20	40.0	40.0	4.0
9-HPODE	335.2	195.1	55	10	13	10	20	40.0	40.0	4.0
10-HPOME	337.2	195.1	80	10	19.5	10	20	40.0	40.0	4.0
9-HPOME	337.2	207.1	80	10	23.6	10	20	40.0	40.0	4.0

HPOTrE; hydroperoxide of linolenic acid (octadecatrienoic acid), HPODE; hydroperoxide of linoleic acid (octadecadienoic acid), HPOME; hydroperoxide of oleic acid (octadecenoic acid)
 Temperature: 600°C
 Ion spray voltage: 5500 V
 Source: Electrospray Ionization
 Ion polarity: Positive

*LC-MS/MS analysis was carried out in the presence of sodium ion; thus, [M+Na]⁺ was detected as the molecular ion. The product ion diagnostic to the identification of the position of the hydroperoxy group was chosen (Ito et al., 2015).

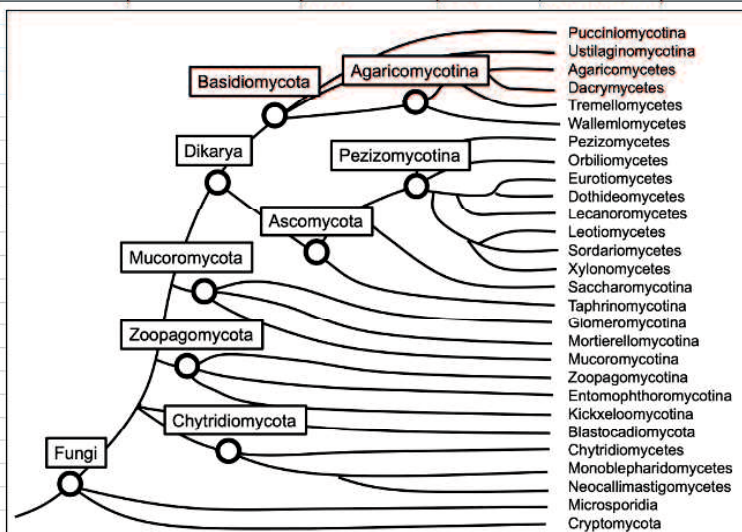
Reference: Ito, J., Mizuochi, S., Nakagawa, K., Kato, S., and Miyazawa, T. (2015) Tandem mass spectrometry analysis of linoleic acid and arachidonic acid hydroperoxides via promotion of alkali metal adduct formation. *Anal. Chem.* 87, 4980-4987

Table 4. Primers used in this study.

Primer	Sequence (5' --> 3')	Target gene	Gene ID	Usage
SV13	AAAGAAGCAGCCCTGGAGGAG	CcDOX1	CC1G_00844	Gene-disruption
SV14	TGACCTTCCATCTGACCCAC	CcDOX1	CC1G_00844	Gene-disruption
SV17	ACGTCGTGACTGGGAGCTTGATGGGGTCAGTGGGG	CcDOX1	CC1G_00844	Gene-disruption
SV18	CCTGTGTGAAATTGTATCCAAGCCCTCGTGTGTCG	CcDOX1	CC1G_00844	Gene-disruption
SV21	AGCCCGCTCGTATATCGCAC	CcDOX1	CC1G_00844	Gene-disruption
SV22	ATCCGAACCGCTGAAAACCC	CcDOX1	CC1G_00844	Gene-disruption
SV24	TGGAAGCAACAAGAGACGGTC	CcDOX1	CC1G_00844	Gene-disruption
TN40	ACCCTTTCCCCAAAATTTGGAAGC	pPHT1 (hph)		Gene-disruption
TN41	ACCTTCTGGCATGACCTTTTGTATGATCGC	pPHT1 (hph)		Gene-disruption
TN1009	TGGCTGAATGCACAATTACGG	CcDOX1	CC1G_00844	Gene-disruption
M13F	GTA AACGACGGCCAGT	pBluescript II		Gene-disruption
M13R	CAGGAACAGCTATGAC	pBluescript II		Gene-disruption
CcDOX1F	CCACCGGTCGCCACCATGTCGTCGAAGCAAGGTCAAGC	CcDOX1	CC1G_00844	Expression of recombinant protein
CcDOX1(+EGFP)R	GCCCTTGCTCACCATGGCAGCATCGTACAATACGGAA	CcDOX1	CC1G_00844	Expression of recombinant protein
CcDOX1(-EGFP)R	ACTTTGGCGGCCGCTTTAGGCAGCATCGTACAATACG	CcDOX1	CC1G_00844	Expression of recombinant protein
CcDOX2F	CCACCGGTCGCCACCATGTCCTCCATCCTTCGCAAGC	CcDOX2	CC1G_09914	Expression of recombinant protein
CcDOX2(+EGFP)R	GCCCTTGCTCACCATCGCAACCTGGTACTGCAGAATC	CcDOX2	CC1G_09914	Expression of recombinant protein
CcDOX2(-EGFP)R	ACTTTGGCGGCCGCTTCACGCAACCTGGTACTGCAGA	CcDOX2	CC1G_09914	Expression of recombinant protein
pA3vector(+EGFP)F	ATGGTGAGCAAGGGCCGAGGAGCTGT	pA3hr5		Expression of recombinant protein
pA3vector(-EGFP)F	AGCGGCCGCCAAAAGTTGTTTCTGAC	pA3hr5		Expression of recombinant protein
pA3vectorR	GGTGGCAGCCGGTGATCCTTGAAT	pA3hr5		Expression of recombinant protein
qPCR-b-tubulin-For	GTA ACTCCACCCGATCCAG	β-tubulin	CC1G_04743	RT-qPCR
qPCR-b-tubulin-Rev	GACCTCATCCTCGTATTACCC C	β-tubulin	CC1G_04743	RT-qPCR
qPCR-COXL1-For	CAACAGAGCCGTGAAGAGTC	CcDOX1	CC1G_00844	RT-qPCR
qPCR-COXL1-Rev	ATTAGGTGGTGTGTCGGTC	CcDOX1	CC1G_00844	RT-qPCR
qPCR-COXL2-For	GTCTGAACCCCTGCCATTCCA	CcDOX2	CC1G_09914	RT-qPCR
qPCR-COXL2-Rev	CAAGACCGCTCCTTCCCTTG	CcDOX2	CC1G_09914	RT-qPCR

Table 5. The domain structures of the proteins showing the highest homology to CcDOX1 within the respective class in the kingdom of fungi.

Sub-division	Class	Genus	Species	NCBI acc.no.	ref	E-value with CcCOX1	Interpro superfamily	
							Hem peroxidase sd	Cyt P450 sf
Basidiomycota	Pucciniomycotina	Leucosporidium	creatinivorum	ORY87519.1		0	+	+
	Ustilaginomycotina	Tilletia	indica	KAE8229188.1		0	+	+
	Agaricomycetes	Coprinopsis	cinerea	XP_001831297.2	this study	0	+	+
	Dacrymycetes	Dacryopinax	primogenitus	XP_040630007.1	PUBMED 22745431	0	+	+
	Tremellomycetes	Saitozyma	podzolica	RSH82924.1		5.00E-135	+	+
	Wallemiomycetes	Wallemia	hederase	TIA89457.1		1.00E-162	+	-
Ascomycota	Pezizomycetes	Morchella	conica	RPB15767.1	PUBMED 30420746	2.00E-163	+	+
	Orbiliomycetes	Arthrobotrys	flagrans	RVD83969.1	PUBMED 30917129	4.00E-173	+	+
	Eurotiomycetes	Aspergillus	terreus	AFB71132.1		0	+	+
	Dothideomycetes	Westerdykella	ornata	XP_033652023.1	DOI: 10.1016/j.simvco.2020.01.003	0	+	+
	Lecanoromycetes	Gomphillus	americanus	CAF9919921.1		7.00E-166	+	+
	Leotiomycetes	Pseudogymnoascus	s. VKM F-4519	KFZ07385.1	PUBMED 25994131	0	+	+
	Sordariomycetes	Metarhizium	robertsii	XP_007816192.1	PUBMED 25368161	0	+	+
	Xylonomycetes	Xylona	heveae	XP_018185456.1	PUBMED 26693682	5.00E-177	+	+
	Saccharomycotina	Trichomonascus	ciferrii	KAA8901464.1	PUBMED 31575637	2.00E-168	+	+
	Taphrinomycotina	Saitoella	complicata	GAO49361.1	PUBMED 24646756	3.00E-72	+	-
Mucoromycota	Glomeromycotina	Rhizophagus	clarus	GBC07128	https://doi.org/10.1186/s12864-018-4853-0	6.00E-138	+	-
	Mortierellomycotina	Entomortierella	beljakovae	KAF9432922.1	PUBMED 33364917	3.00E-90	+	-
	Mucoromycotina	Umbelopsis	isabelina	KAG2183470.1	DOI: 10.3389/fmicb.2021.636986	2.00E-99	+	-
Zoopagomycota	Zoopagomycotina	na	na	no hit		-	-	-
	Entomophthoromycotina	Basidiobolus	meristosporus	ORX79743.1		6.00E-108	+	-
	Kickxellomycotina	na	na	no hit		-	-	-
Blastocladiomycota	na	na	na	no hit		-	-	-
Chytridiomycota	Chytridiomycetes	Rhizoclostium	globosum	ORY30110.1		2.00E-77	+	-
	Monoblepharidomycetes	na	na	no hit		-	-	-
	Neocallimastigomycetes	na	na	no hit		-	-	-
Microsporidia	na	na	na	no hit		-	-	-
Cryptomycota	na	na	na	no hit		-	-	-
Genes showing a significant homology in the organisms other than fungi.								
Magnoliophyta	Magnoliopsida	Carpinus	fangiana	KAB8343050.1		1.00E-167	+	+
		Quercus	suber	XP_023877369.1		2.00E-161	+	+
Rotifera	Bdelloidea	Rotaria	magnacalcarata	CAF2064440.1		1.00E-113	+	-
		Adineta	steineri	CAF1363805.1		1.00E-113	+	-



The tree of fungi [adopted from the tree in MycoCosm (Grigoriev et al., 2014)]

2.5 References

1. Potter, C. J. H. (2014) Stop the biting: Targeting a mosquito's sense of smell. *Cell* **156**, 878-881
2. Takke, W., and Knols, B. G. J. (1999) Odor-mediated behavior of afrotropical malaria mosquitoes. *Annu. Rev. Entomol.* **44**, 131-157
3. Wurzenberger, M., and Grosch, W. (1982) The enzymic oxidative breakdown of linoleic acid in mushrooms (*Psalliota bispora*). *Z. Lebensm. Unters. Forsch.* **175**, 168-190
4. Wurzenberger, M., and Grosch, W. (1984) The formation of 1-octen-3-ol from the 10-hydroperoxide isomer of linoleic acid by a hydroperoxide lyase in mushrooms (*Psalliota bispora*). *Biochim. Biophys. Acta* **794**, 25-30
5. Wurzenberger, M., and Grosch, W. (1984) Stereochemistry of the cleavage of the 10-hydroperoxide isomer of linoleic acid to 1-octen-3-ol by a hydroperoxide lyase from mushrooms (*Psalliota bispora*). *Biochim. Biophys. Acta* **795**, 163-165
6. Akakabe, Y., Matsui, K., and Kajiwara, T. (2005) Stereochemical correlation between 10-hydroperoxyoctadecadienoic acid and 1-octen-3-ol in *Lentinula edodes* and *Tricholoma Matsutake* mushrooms. *Biosci. Biotechnol. Biochem.* **69**, 1539-1544
7. Garscha, U., and Oliw, E. H. (2007) Steric analysis of 8-hydroxy- and 10-hydroxyoctadecadienoic acids and dihydroxyoctadecadienoic acids formed from 8*R*-hydroperoxyoctadecadienoic acid by hydroperoxide isomerases. *Anal. Biochem.* **367**, 238-246
8. Tsitsigiannis, D. I., Kowieski, T. M., Zarnowski, R., and Keller, N. P. (2005) Three putative oxylipin biosynthetic genes integrate sexual and asexual development in *Aspergillus nidulans*. *Microbiology* **151**, 1809-1821
9. Tsitsigiannis, D. I., and Keller, N. P. (2007) Oxylipins as developmental and host-fungal communication signals. *Trend. Microbiol.* **15**, 109-118
10. Brodhun, F., and Feussner, I. (2011) Oxylipins in fungi. *FEBS J.* **278**, 1047-1063
11. Oliw, E. H. (2021) Fatty acid dioxygenase-cytochrome P450 fusion enzymes of filamentous fungal pathogens. *Fungal. Genet. Biol.* 10.1016/j.fgb.2021.103623
12. Brodowsky, I. D., Hamberg, M., and Oliw, E. H. (1992) A linoleic acid (8*R*)-dioxygenase and hydroperoxide isomerase of the fungus *Gaeumannomyces graminis*. *J. Biol. Chem.* **267**, 14738-14745
13. Brodhun, F., Schneider, S., Göbel, C., Hornung, E., and Feussner, I. (2010) PpoC from *Aspergillus nidulans* is a fusion protein with only one active haem. *Biochem. J.* **425**,

14. Ferrari, R., Lacaze, I., Le Faouder, P., Bertrand-Michel, J., Oger, C., Galano, J. M., Durand, T., Moularat, S., Chan Ho Tong, L., Boucher, C., Kilani, J., Petit, Y., Vanparis, O., Trannoy, C., Brun, S., Lalucque, H., Malagnac, F., and Sliar, P. (2018) Cyclooxygenase and lipoxygenase are used by the fungus *Podospora anserina* to repel nematodes. *Biochim. Biophys. Acta* **1862**, 2174-2182
15. Kataoka, R., Watanabe, T., Yano, S., Mizutani, O., Yamada, O., Kasumi, T., and Ogiwara, J. (2020) *Aspergillus luchuensis* fatty acid oxygenase ppoC is necessary for 1-octen-3-ol biosynthesis in rice koji. *J. Biosci. Bioeng.* **129**, 192-198
16. Huber, S. M. F. E., Lottspeich, F., and Kämper, J. (2002) A gene that encodes a product with similarity to dioxygenases is highly expressed in teliospores of *Ustilago maydis*. *Mol Genet. Genomics* **267**, 757-771
17. Oliw, E. H. (2018) Biosynthesis of oxylipins by *Rhizoctonia solani* with allene oxide and oleate 8S,9S-diol synthase activities. *Lipids* **53**, 527-537
18. Kües, U. (2000) Life history and developmental processes in the basidiomycete *Coprinus cinereus*. *Microbiol. Mol. Biol. Rev.* **64**, 316-353
19. Stajich, J. E., Wilke, S. K., Ahrén, D., and Pukkila, P. J. (2010) Insights into evolution of multicellular fungi from the assembled chromosomes of the mushroom *Coprinopsis cinerea* (*Coprinus cinereus*). *Proc. Natl. Acad. Sci. USA* **107**, 1889-11894
20. Inamdar, A. A., Morath, S., and Bennett, J. W. (2020) Fungal volatile organic compounds: more than just a funky smell? *Ann. Rev. Microb.* **74**, 101-116
21. Hörnsten, L., Su, C., Osbourn, A. E., Hellman, U., and Oliw, E. H. (2002) Cloning of the manganese lipoxygenase gene reveals homology with the lipoxygenase gene family. *Eur. J. Biochem.* **269**, 2690-2697
22. Grigoriev, I. V., Nikitin, R., Haridas, S., Kuo, A., Ohm, R., Otilar, R., Rilet, R., Salamiv, A., Zhao, X., Korzeniewski, F., Smirnova, T., Nordberg, H., Dubchak, I., and Shabalov, I. (2014) MycoCosm portal: gearing up for 1000 fungal genomes. *Nucleic Acids. Res.* **42**, D699–D704. 10.1093/nar/gkt1183
23. Marnett, L. J., Rowlinson, S. W., Goodwin, D. C., Kalgutkar, A. S., and Lanzo, C. A. (1999) Arachidonic acid oxygenation by COX-1 and COX-2. *J. Biol. Chem.* **274**, 22903-22906
24. Brodhun, F., Göbel, C., Hornung, E., and Feussner, I. (2009) Identification of PpoA from *Aspergillus nidulans* as a fusion protein of a fatty acid heme dioxygenase/peroxidase and a cytochrome P450. *J. Biol. Chem.* **284**, 11792-11805
25. Denisov, I. G., Makris, T. M., Sligar, S. G., and Schlichting, I. (2005) Structure and

- chemistry of cytochrome P450. *Chem. Rev.* **105**, 2253-2277
26. Oliw, E. H., Argó, M., Chen, Y., and Jernerén, F. (2016) A new class of fatty acid allene oxide formed by the DOX-P450 fusion proteins of human and plant pathogenic fungi, *C. immitis* and *Z. tririci*. *J. Lipid. Res.* **57**, 1518-1528
 27. Garscha, U. and Oliw, E. (2008a) *Pichia* expression and mutagenesis of 7,8-linoleate diol synthase change the dioxygenase and hydroperoxide isomerase. *Biochem. Biophys. Res. Commun.* **373**, 579-583
 28. Garscha, U. and Oliw, E. (2008b) Critical amino acids for the 8(*R*)-dioxygenase activity of linoleate diol synthase. A comparison with cyclooxygenases. *FEBS Lett.* **582**, 3547-3551
 29. Ito, J., Mizuochi, S., Nakagawa, K., Kato, S., and Miyazawa, T. (2015) Tandem mass spectrometry analysis of linoleic acid and arachidonic acid hydroperoxides via promotion of alkali metal adduct formation. *Anal. Chem.* **87**, 4980-4987
 30. Ito, J., Komuro, M., Parida, I. S., Shimizu, N., Kato, S., Meguro, Y., Ogura, Y., Kuwahara, S., Miyazawa, T., and Nakagawa, K. (2019) Evaluation of lipid oxidation mechanisms in beverages and cosmetics via analysis of lipid hydroperoxide isomers. *Sci. Rep.* **9**, 7387. 10.1038/s41598-019-43645-1
 31. Ito, J., Shimizu, N., Kobayashi, E., Hanzawa, Y., Otoki, Kato, S, Hirokawa, T., Kuwahara, S., Miyazawa, T., and Nakagawa, K. (2017) A novel chiral stationary phase LC-MS/MS method to evaluate oxidation mechanisms of edible oils. *Sci. Rep.* **7**, 10026. 10.1038/s41598-017-10536-2
 32. Brash, A. R., Niraula, N. P., Boeglin, W. E., and Mashhadi, Z. (2014) An ancient relative of cyclooxygenase in cyanobacteria is a linoleate 10*S*-dioxygenase that works in tandem with a catalase-related protein with specific 10*S*-hydroperoxide lyase activity. *J. Biol. Chem.* **289**, 13101-13111
 33. Jumper, J., Evans, R., Pritzel, A. et al. (2021) Highly accurate protein structure prediction with AlphaFold. *Nature* **596**, 583-589
 34. Nakazawa, T., and Honda, Y. (2015) Absence of a gene encoding cytosine deaminase in the genome of the agaricomycete *Coprinopsis cinerea* enables simple marker recycling through 5-fluorocytosine counterselection. *FEMS Microbiol. Lett.* **362**, fnv123. 10.1093/femsle/fnv123
 35. Senger, T., Wichard, T., Kunze, S., Göbel, C., Lerchl, J., Pohnert, G., and Feussner, I. (2005) A multifunctional lipoxygenase with fatty acid hydroperoxide cleaving activity form the moss *Physcomitrella patens*. *J. Biol. Chem.* **280**, 7588-7596
 36. Fisher, A. J., Grimes, H. D., and Fall, R. (2003) The biochemical origin of pentenol emissions from wounded leaves. *Phytochemistry* **62**, 159-163

37. Shen, J., Tieman, D., Jones, J. B., Taylor, M. G., Schmelz, E., Huffaker, A., Bies, D., Chen, K., and J. Klee, H. (2014) A 13-lipoxygenase, TomloxC, is essential for synthesis of C5 flavour volatiles in tomato. *J. Exp. Bot.* **65**, 419-428
38. Mochizuki, S., Sugimoto, K., Koeduka, T., and Matsui, K. (2016) Arabidopsis lipoxygenase 2 is essential for formation of green leaf volatiles and five-carbon volatiles. *FEBS Lett.* **590**, 1017-1027
39. Cevallos, J. A., Okubo, R. P., Perlman, S. J., and Hallem, E. A. (2017) Olfactory preferences of the parasitic nematode *Howardula aoronymphium* and its insect host *Drosophila falleni*. *J. Chem. Ecol.* **43**, 362-373
40. Sueyoshi, M. (2014) Taxonomy of fungus gnats allied to *Neoempheria ferruginea* (Brunetti, 1912) (Diptera: Mycetophilidae), with descriptions of 11 new species from Japan and adjacent areas. *Zootaxa* **3790**, 139-164. <http://dx.doi.org/10.11646/zootaxa.3790.1.6>
41. Haraguchi, S., and Yoshiga, T. (2020) Potential of the fungal feeding nematode *Aphelenchus avenae* to control fungi and the plant parasitic nematode *Ditylenchus destructor* associated with garlic. *Biol. Control* **143**, 104203. [10.1016/j.biocontrol.2020.104203](https://doi.org/10.1016/j.biocontrol.2020.104203)
42. Gokte, N., and Mathur, V. K. (1989) Reproduction and development of *Aphelenchoides besseyi*. *Phytoparasitica* **17**, 263-267
43. Bowers, W. S., Hoch, H. C., Evans, P. H., and Katayama, M. (1986) Thallophtyic allelopathy: isolation and identification of laetisaric acid. *Science*, **232**, 105-106
44. Combet, E., Henderson, J., Eastwood, D. C., and Burton, K. S. (2006) Eight-carbon volatiles in mushrooms and fungi: properties, analysis, and biosynthesis. *Mycosci.* **47**, 317-326
45. Tsitsigiannis, D., I., Zarnowski, R., and Keller, N. P. (2004) The lipid body protein, PpoA, coordinates sexual and asexual sporulation in *Aspergillus nidulans*. *J. Biol. Chem.* **279**, 11344-11353
46. Brodhun, F., Schneider, S., Göbel, C., Hornung, E., and Feussner, I. (2010) PpoC from *Aspergillus nidulans* is a fusion protein with only one active haem. *Biochem. J.* **425**, 553-565
47. Matsui, K. (2006) Green leaf volatiles: hydroperoxide lyase pathway of oxylipin metabolism. *Curr. Opin. Plant Biol.* **9**, 274-280
48. Mukai, H., and Kitajima, H. (2021) Laboratory evaluation of *Orthocentrus brachycerus* (Hymenoptera: Ichneumonidae), as a potential biological control agent in mushroom cultivation. *J. Appl. Entomol.* **145**, 348-357
49. Garscha, U., and Oliw, E. H. (2009) Leucine/valine residues direct oxygenation of

- linoleic acid by (10*R*)- and (8*R*)-dioxygenase. *J. Biol. Chem.* **284**, 13755-13765
50. Nakazawa, T., Tatsuta, Y., Fujita, T., Nakahori, K., and Kamada, T. (2010) Mutations in the *Cc.rmt1* gene encoding a putative protein arginine methyltransferase alter developmental programs in the basidiomycete *Coprinopsis cinerea*. *Curr. Genet.* **56**, 361-367

2.6 Acknowledgment

I wish to express my sincere thanks to Prof. Dr. Kenji Matsui, Department of Biological Chemistry, Faculty of Agriculture, Yamaguchi University for his kind guidance, suggestions and encouragement. I am also grateful to Researcher Risa Funai of Department of Biological Chemistry, Faculty of Agriculture, Yamaguchi University Japan, and Dr. Pattana Kakumyan of Bioscience to School of Science, Mae Fah Luang University, Thailand, for their helpful discussions and suggestions. I also thanks to Assistant Prof. Dr. Nakazawa Junya and Prof. Dr. Yoichi Honda of Graduate School of Agriculture, Kyoto University, Japan, for producing the $\Delta Ccdox1$ strain. I also thanks to Assistant Prof. Dr. Junya Ito and Prof. Dr. Kiyotaka Nakagawa of Food and Biodynamic Chemistry Laboratory, Graduate School of Agricultural Science, Tohoku University, Japan, for analyzing hydroperoxide of linoleic acid with LC-MS/MS. I also thanks to Prof. Dr. Toshihiko Utsumi and Prof. Dr. Ryutaro Murakami of Department of Biological Chemistry, Faculty of Agriculture, Yamaguchi University, Japan, Prof. Dr. Toyoshi Yoshiga of Department of Applied Biological Sciences, Faculty of Agriculture, Saga University, Japan, and Dr. Hiromi Mukai of Department of Forest Entomology, Forestry and Forest Products Research Institute, Japan, for providing BmN4 cells, *Drosophila melanogaster* larvae, *Neoempheria dilatate*, and *Aphelenchus avenae*, *Aphelenchoides besseyi*, and *Ditylenchus destructor*.

This works was supported by JSPS KAKENHI Grant Number 21J14407 (to T. Teshima).